PLATFORMS FOR BIOAFFINITY ASSAYS USING APTAMERS

DEVELOPING PLATFORMS FOR SOLID-PHASE BIOAFFINITY ASSAYS USING NUCLEIC ACID APTAMERS

By

CARMEN FELIZ CARRASQUILLA, B.Sc., M.Sc.

A Thesis Submitted to the School of Graduate Studies

in Partial Fulfillment of the Requirements for the Degree

Doctor of Philosophy

McMaster University

DOCTOR OF PHILOSOPHY (2017) McMaster University

(Chemical Biology) Hamilton, Ontario

TITLE: Developing Platforms for Solid-Phase Bioaffinity Assays Using Nucleic Acid Aptamers

AUTHOR: Carmen F. Carrasquilla, B.Sc. (University of Western Ontario), M.Sc. (McMaster University)

SUPERVISOR: Dr. John D. Brennan

NUMBER OF PAGES: xv, 133

ABSTRACT

This thesis focuses on devising strategies for immobilizing nucleic acid aptamers on or in solid supports that improve their stability, availability for binding interactions and compatibility with emerging solid-phase bioanalysis applications. The work begins with the entrapment of labile RNA-based aptamers within a sol-gel derived material for bio-immobilization without the need for extraneous binding molecules or complex conjugation procedures. A hybrid organic-inorganic material provided the best matrix environment not only for RNA functionality but protection from both nuclease attack and chemical degradation, enhancing long-term stability when compared to solution. To expand the application of aptamer/sol-gel biohybrids, rolling circle amplification was used to generate long DNA molecules containing concatemeric aptamer sequences. A high-throughput screen was used to identify materials with macropores that allowed for minimal leaching and high activity and of the entrapped concatemeric DNA aptamers. The optimal concatemer-entrapped material was used to make monolithic columns for flow-based detection of both small molecules and high molecular weight proteins, thus, broadening the range of analytes that can interact with sol-gel entrapped aptamers to include large macromolecules. To further expand the utility of concatemeric aptamers, these large molecules were inkjet-printed as "bioinks" on paper as an alternative means of producing paper-based sensing devices in a simple and inexpensive manner. The large structure of the concatemeric aptamer molecules allowed direct bio-immobilization through strong adsorption on cellulose without the need for surface conjugation or material entrapment. Although these concatemers remained immobilized after liquid elution over the printing area, they retained sufficient segmental

motion for target binding and signaling on the paper surface. Patterning letters/symbols to create internally-referenced and multiplexed assays for both qualitative and quantitative detection of small molecules and proteins, demonstrated a generic platform for on-demand printing of aptamer-based solid-phase assays in the emerging field of paper-based sensors for on-site detection applications.

ACKNOWLEDGEMENTS

I would like to express my sincere gratitude to my supervisor, Dr. John D. Brennan, for giving me the opportunity to conduct my graduate research in his lab. Thank you for allowing me independence and creativity in my work while providing guidance and support at the same time. The valuable knowledge and experience I have gained throughout the years is immeasurable. I would also like to thank the members of my supervisory committee, Dr. Yingfu Li and Dr. Michael A. Brook, for their advice and constructive feedback that has helped not only in directing my research but also in developing my scientific writing and presentation skills.

Thank you to all my colleagues in Dr. Brennan's lab and collaborating groups, both past and present, for sharing their experiences, scientific insight and enthusiasm that motivated me through the ups and downs of my graduate research. I am privileged for having worked with all of you as the relationships we have formed has made my time at McMaster most enjoyable. Furthermore, I would like to thank Tammy Feher, the Department of Chemistry & Chemical Biology and the scientific staff at the Biointerfaces Institute for providing administrative support and a great learning/working environment.

I thank my family for their constant encouragement, tireless support and unconditional love throughout my entire academic career. Mom – thank you for being a great role model in hard work and perseverance. To my dad – although no longer with us on this Earth to see me complete my PhD, I know he is proud of the accomplishment. Finally, I am eternally grateful to Dan Wagner, whose unwavering love and belief in me has helped me through some of the toughest times in my life and brought me so much happiness.

TABLE OF CONTENTS

LIST OF FIGURES

LIST OF TABLES

LIST OF ABBREVIATIONS

3-D	three-dimensional
µPAD	microfluidic paper analytical device
A	acceptor
ADA	adenosine deaminase
APTES	3-(aminopropyl)triethoxysilane
ATP	adenosine 5'-triphosphate
AuNPs	gold nanoparticles
BSA	bovine serum albumin
CNTs	carbon nanotubes
CTP	cytidine 5′-triphosphate
D	donor
DABCYL	4-(dimethylaminoazo)benzene-4-carboxylic acid
DGS	diglycerylsilane
DNA	deoxyribonucleic acid
DNase	deoxyribonuclease
dNTPs	2'-deoxyribonucleoside 5'-triphosphates
dPAGE	denaturing polyacrylamide gel electrophoresis
DTT	dithiothreitol
EGF	epidermal growth factor
FACS	fluorescence-activated cell sorting
FDNA	fluorophore-labeled DNA
FRET	fluorescence resonance energy transfer
GOs	graphene oxides
GOx	glucose oxidase
GTP	guanosine 5′-triphosphate
IGF-I	insulin-like growth factor I
HCl	hydrochloric acid
HPLC	high performance liquid chromatography
K_d	dissociation constant
LC	liquid chromatography
MSQ	methylsilsesquioxane
MTMS	methyltrimethoxysilane
MW	molecular weight
nt	nucleotide
NH-QDNA	‘no hybridization’ quencher-labeled DNA
OCA	optical contact angle
PAGE	polyacrylamide gel electrophoresis
PCR	polymerase chain reaction
PDGF	platelet-derived growth factor
PEG	(poly)ethylene glycol
pK_a	ionization constant
QDNA	quencher-labeled DNA

RCA	rolling circle amplification
RNA	ribonucleic acid
RNase	ribonuclease
SELEX	systematic evolution of ligands by exponential enrichment
SEM	scanning electron microscopy
SPR	surface plasmon resonance
SS	sodium silicate
T4 PNK	T4 polynucleotide kinase
TEOS	tetraethylorthosilicate
TMOS	tetramethylorthosilicate
TMP	thiamine monophosphate
TPP	thiamine pyrophosphate
UTP	uridine 5′-triphosphate

CHAPTER 1.

A GENERAL INTRODUCTION

1.1 Solid-Phase Bioaffinity Assays

1.1.1 Bioaffinity Interactions for Solid-Phase Assays

Numerous biological processes are driven by bioaffinity interactions such as specific binding between biomolecules (proteins, DNA, lipids, etc.) and/or small molecules (i.e. organic or inorganic chemical entities). Measuring bioaffinity interactions, however, remains notoriously difficult; as such, assays that can detect or probe these interactions have become essential for life science research. Many disciplines from drug discovery and optimization, biomedical diagnostics, environmental analysis, etc. also require the use of such assays.[1-3] Major bioaffinity interactions that have been exploited for assay purposes include nucleic acid hybridization in genomics, antibody-antigen immunoreactions for clinical chemistry, and lectin-carbohydrate interactions in cell physiology.[4,5]

Several advantages exist in moving bioaffinity assays from solution to the solid phase by immobilizing one or more assay components onto a solid support such as plastic, metal or glass. Mainly, solid phase assays make it possible to utilize a number of new miniaturized assay formats such as microarrays, capillary columns and microfluidic chips that can enhance sensitivity, reduce reagent consumption and increase assay throughput (Figure 1.1).[6] Solid-phase assays also facilitate the ability to perform wash steps or multi-step reactions that are not possible with homogenous solution-based assays. Moreover,

novel surface-dependent signal detection methods (surface plasmon resonance, total internal reflection fluorescence, etc.) are only accessible in the solid phase.[3]

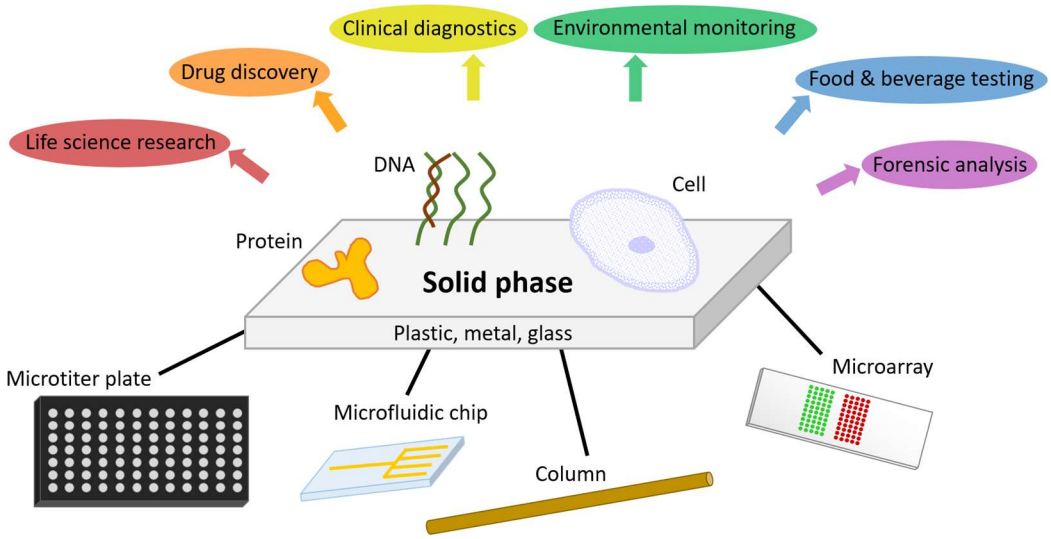

Figure 1.1. Overview of solid-phase bioaffinity assay applications. Biomolecules with binding interaction capabilities are immobilized to a solid support in order to be used in a various solid-phase assay formats. These assays serve as important biomolecular detection tools in numerous sectors of biotechnology.

While solid-phase bioaffinity assays have found utility in a wide range of areas, a large number of such assays have been reported for biosensing and other biodetection applications. This is because novel sensing designs that maintain the detection sensitivity and accuracy, while increasing speed, simplicity and cost-effectiveness are becoming more relevant as conventional diagnostics and molecular detection methodologies typically require hours to days for results and involve special laboratory equipment that necessitate trained personnel.

1.1.2 Biosensors

Biosensors are analytical devices that make use of a biological component to detect a target analyte. By incorporating the sensitivity and specificity of biology with physicochemical transducers, complex bioanalytical measurements can be performed in simple, easy-to-use formats.[7] Numerous biosensors have appeared in the literature over the past several decades with utility in areas such as medical diagnostics, environmental and food analysis, and even anti-terrorism screening.[8-10]

The biosensor was first conceived in 1962 when Leyland C. Clark immobilized glucose oxidase (GOx) enzymes on an electrode to measure the catalytic conversion of glucose to gluconic acid and hydrogen peroxide.[11] This electrochemical sensor system has since been used as a powerful analytical tool for monitoring blood glucose levels, which now benefits millions of people with diabetes worldwide, and has become the model upon which other enzyme-based electrochemical sensors have been developed for portable and low-cost sensing of small metabolites. Two decades after Clark's enzyme electrode discovery, optical transducers were coupled with antibodies as biorecognition molecules to create bioaffinity sensors – a new generation of biosensing technology.[7] These bioaffinity sensors for biomolecular binding have proven commercial success in home pregnancy (and ovulation) tests, have demonstrated utility in other lateral flow devices for biorecognition and have been applied to laboratory-based surface plasmon resonance (SPR) machines.[12] Thus, there has been increasing interest in finding new molecules that can replace antibodies, which are expensive to isolate and difficult to scale for mass production, to fulfill the demands of the rapidly growing biosensor sector. Among the different strategies

currently studied to identify antibody alternatives for bioaffinity sensors are nucleic acid aptamers.

1.2 Bioaffinity Assays Using Nucleic Acid Aptamers

1.2.1 Nucleic Acid Aptamers

Nucleic acid aptamers are short, single-stranded DNA or RNA oligonucleotides that can fold into stable, three-dimensional (3-D) sequence-dependent structures[13-15] in order to specifically bind to a wide variety of targets from small organic molecules to large proteins, viruses, and even cells.[16,17] The majority of these nucleic acids are artificially selected from large random-sequence or semi-rationally-designed libraries of DNA or RNA, containing up to 10^{16} unique molecules, using a technique known as SELEX (systematic evolution of ligands by exponential enrichment).[18-20] This process involves screening the DNA or RNA libraries using iterative cycles of *in vitro* selection and amplification in order to isolate sequences that exhibit the desired target-binding properties (Figure 1.2).[15,21-23]

Briefly, the library is incubated with the target of interest in order to allow binding with any oligonucleotides that have affinity towards the target. Bound molecules are extracted from the unbound fraction through column chromatography, gel electrophoresis or other biomolecular separation techniques. These very rare binding sequences are then amplified by polymerase chain reaction (PCR) in order to enrich the library. As shown in Figure 1.2, the resulting pool of sequences is then reintroduced to the target for a subsequent round of the selection/amplification process. Successive cycles, typically 10 – 15, are carried out until these binding molecules dominate the population and are

sequenced. It is also possible to adjust the selection stringency and include counter-selection steps (removing sequences that bind to molecules that are chemically-similar to targets but not of interest).

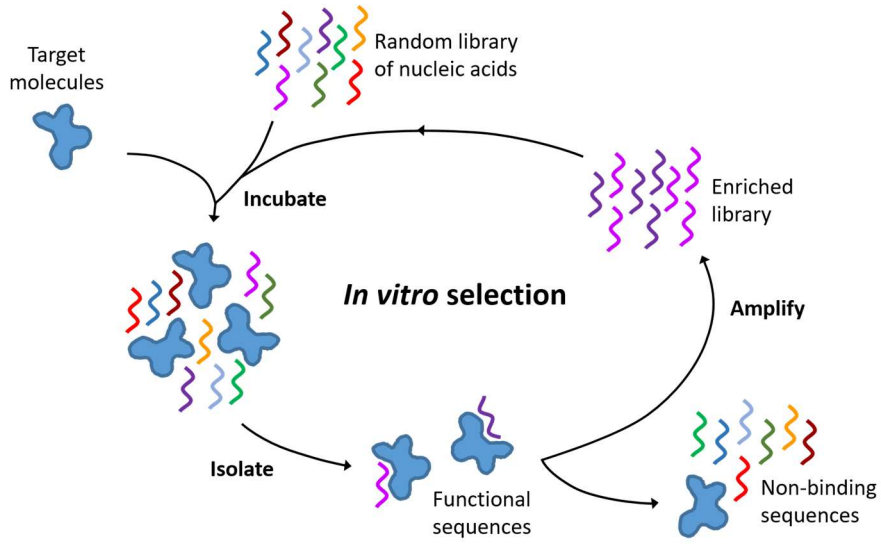

Figure 1.2. Generation of nucleic acid aptamers using *in vitro* selection or SELEX. A large library of nucleic acids is incubated with a target molecule to allow any functional sequences to bind. Bound sequences are isolated from the unbound pool then amplified by PCR. This process is repeated using the newly enriched library for multiple cycles until the binding nucleic acids dominate the population and are sequenced.

This *in vitro* selection process provides aptamers with impressive specificity and affinity for their target analytes. Indeed, efficient schemes for counter-selection have been performed to generate aptamers that demonstrate the ability to distinguish between variants, isoforms and even enantiomers of a given target molecule.[24] These remarkable molecular recognition properties can be attributed to the adaptive conformational transition associated with the aptamer-target formation. Nucleic acid aptamers bind their targets via an induced-fit mode by changing conformation from a disordered structure to a well-

defined binding structure that maximizes complementarity through tightly packed contacts in the binding pocket.[25,26] Various non-covalent driving forces, including hydrogen bonds, electrostatic interactions, aromatic stacking, van der Waals interactions, and hydrophobic effects may contribute to aptamer binding depending on the target. Therefore, aptamers for larger protein targets with more functional groups commonly have dissociation constant (K_d) values in the pico-nanomolar range while aptamers directed against small molecules are more often characterized with a micro-millimolar K_d.

1.2.2 Advantages of Aptamers in Biosensing

In addition to high specificity and picomolar to micromolar-range affinity, nucleic acid aptamers possess numerous advantages over protein-based antibodies.[27,28] First, in principle, *in vitro* selection provides the potential to isolate an aptamer for any given target of interest, including non-immunogenic toxins and small molecules that cannot be targeted by antibodies. Once selected, aptamers can be chemically synthesized with high reproducibility and purity from commercial sources, making it a reliable and cost efficient source for detection molecules. Moreover, the use of aptamers also eliminates the costly and time consuming need for cell lines or *in vivo* immunization of animals required for antibodies.

The main disadvantage to using nucleic acid aptamers in biosensing applications is their sensitivity to hydrolytic digestion by nucleases. This is particularly true for RNA molecules and, combined with their inherent chemical instability,[29-31] generally why their use in either solution or solid-phase biosensing is mostly avoided.[32-37] On the other hand,

DNA is still more chemically and thermally stable than both RNA and proteins, allowing for better long-term storage stability of fabricated biosensors, suitability in applications requiring harsh conditions (e.g. high temperature or extreme pH), and sensor reusability by reversible denaturation.[38-42]

Another key advantage of nucleic acids for solid-phase biosensing, is the ease of chemical modification for simpler labeling and tethering to the transduction interfaces.[43-45] Labeling the biorecognition molecules directly allows for the detection of free, unlabeled target analyte, making this method amenable to real-time detection with minimal preparation (post-capture labeling and washing) for the speed required of biosensors. The simple site-specific labeling of nucleic acids with dyes and redox-active moieties has made optical and electrochemical signaling prevalent methods used to monitor aptamer binding.[46,47]

1.2.3 Fluorescence-Based Signal Transduction

While developments in electrochemical biosensors have focused mainly on monitoring metabolites, bioaffinity sensing is principally carried out using optical techniques. Of these, fluorescence is one of the most sensitive methods to detect molecular interactions. This high sensitivity together with the ease of conjugating fluorophores to nucleic acids and the range of dyes available for molecular tagging have made fluorescence the preferred format for optical signal transduction using aptamers.[48,49]

The first aptamer-based sensor, reported in 1998,[50] made use of fluorescence anisotropy techniques to measure binding to the protein thrombin. In this study, the fluorophore-

labeled DNA aptamer molecules, covalently bound to a glass microscope cover slip, have a characteristic rotational diffusion rate that is reflected in a particular fluorescence anisotropy. Interaction with the protein target increases the size of the fluorescent complex and reduces free rotation of the fluorophore. The slower rotational diffusion results in an increase of the fluorescence anisotropy upon binding. The advantages of using fluorescence-labeled DNA aptamers as a biosensor platform were demonstrated with high selectivity, an apparent K_d of 47 nM, a response time of less than 10 minutes, and sensor reusability (by stripping thrombin with guanidinium hydrochloride followed by buffer re-equilibration).

While single fluorophore-labeled aptamer-based sensors for detecting alterations in fluorescence anisotropy or intensity are numerous, typically the change in signal can be quite small.[39] Thus, more recent studies have demonstrated a very ingenious use of fluorescence resonance energy transfer (FRET)-based probes that exploit the unique characteristic of aptamers to significantly change conformation and fold into diverse structures for fluorescence signal transduction. The FRET mechanism can be applied to a fluorescent donor (D) and nearby acceptor (A) with overlapping emission and excitation spectra, respectively. Since the efficiency of FRET is inversely proportional to the sixth power of intermolecular separation,[51] the D-A pair must be located in very close proximity (1-5 nm).

When a fluorophore donor and its corresponding non-emitting acceptor (or a quencher) are used as the D-A pair, the fluorophore emission is negated by the presence of the nearby quencher.[52,53] A classic example is based on the "molecular beacon" strategy[54-57] in which the sequence that makes up the aptamer is placed in a stem-loop hairpin structure through strand self-complementation and dual-labeled with a fluorophore and a quencher on either end. The binding of the target disrupts the stem hybridization, which separates the fluorophore and quencher from one another, leading to an increase in fluorescence via a dequenching mechanism.[58] These aptamer beacons can be extended to fiber-optic sensing as exemplified by Yu and co-workers who were able to detect a target-dependent increase in emission intensity using thrombin-binding aptamers interfaced to optical fibers by affinity interactions.[59]

Nutiu and Li[60,61] modified this scheme by placing the aptamers in a tripartite complex with two short, complementary DNA sequences: one labeled with a fluorophore (FDNA) and one with a quencher (QDNA). The aptamer and quencher strands are elegantly designed such that binding the target forces the dissociation of the QDNA, which is accompanied by an increase in fluorescence (Figure 1.3). This structure-switching/fluorescence-signaling approach can be adapted to both DNA and RNA-based aptamers by strategic placement and hybridization strength optimization of the QDNA strand.[62]

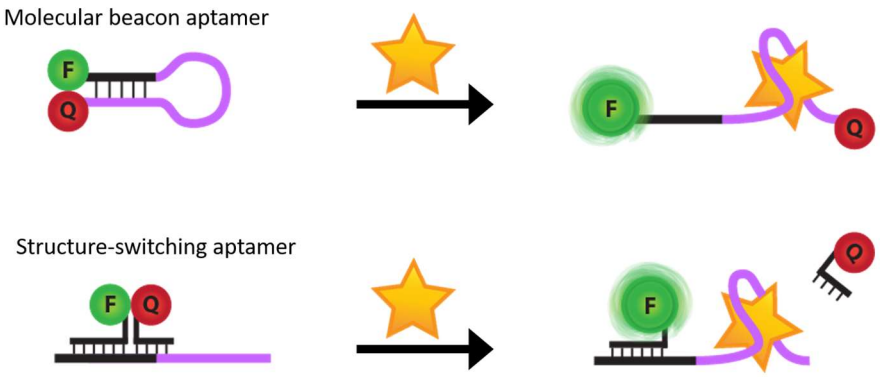

Figure 1.3. Fluorescence-based signaling aptamers using FRET dequenching mechanisms. In both the molecular beacon and structure-switching aptamer design, a quencher (Q) is placed in close proximity to the fluorophore (F), reducing its fluorescence signal. Upon target binding, spatial separation between the F and Q leads to an increase in fluorescence.

Fluorescence signal enhancement by energy transfer or dequenching mechanisms can also be achieved using polymers, nanoparticles or nanomaterials. Indeed, signaling platforms based on graphene oxides (GOs)[63,64] and carbon nanotubes (CNTs)[65,66] have recently emerged due to their unique interaction with nucleic acids in different conformational states. For example, single-stranded fluorophore-labeled aptamers adsorb to both CNTs and GO through electrostatic interactions and π-stacking. The interaction with the surface results in fluorescence quenching. However, when the aptamer binds its target and folds into a defined tertiary structure, the aptamer dissociates from the material, allowing an increase in fluorescence signal to be measured.

In another example, fluorescence quenching occurs when a polythiophene polymer is complexed with DNA aptamers in an array format.[67] In binding its protein target, thrombin, the aptamer adopts a different structure which leads to a significant enhancement

in polythiophene emission. Efficient energy transfer of this emission to the Cy-3 labeled aptamers immobilized with the polymer via covalent attachment to an aldehyde surface, results in significant and selective fluorescence signaling. However, despite the inherent sensitivity of these fluorescence-signaling aptamer-based assay formats, additional steps may still be required to obtain suitable detection limits for targets that may only be present at very low levels, particularly in complex molecular mixtures.

1.2.4 Signal Amplification

To improve the sensitivity and lower detection limits of bioaffinity assays, various methods can be used to amplify the signal generated from target binding. Although PCR was the first and remains the most widespread amplification technology for detecting low-abundance nucleic acids, several isothermal amplification methodologies have emerged as promising alternatives. Isothermal amplification allows rapid and efficient nucleic acid amplification at a constant temperature without the thermocycling required in PCR.[68] Owing to its high amplification efficiency and operational simplicity, rolling circle amplification (RCA) has become a popular isothermal amplification technique for bioanalytical detection applications.[69]

In RCA, a small circular DNA strand acts as template for the generation of a long single-stranded DNA chain that can contain up to thousands of nucleotides.[70-72] When this circular template is hybridized with a short primer, the presence of a DNA polymerase enzyme and deoxyribonucleoside triphosphates (dNTPs) extends the primer with repeating sequence units complementary to the circle (Figure 1.4). The length of newly synthesized

RCA product is mainly dependent on the type of the polymerase. Highly processive DNA polymerases, such as ϕ29 DNA polymerase, remain bound to the circular DNA template longer leading to larger RCA products.[73] Studies initiating the RCA process by specific target binding have already demonstrated how a single molecular recognition event can be amplified to improve sensitivities for biosensing.[74-77] Generally, multiple labeling of each tandem repeating unit with DNA probes affixed with a fluorescence dye allows for greater signal generation.[72,74,77]

Figure 1.4. Schematic illustration of the RCA process. First, a circular DNA template hybridizes with a short primer sequence. This primer is then continuously extended as a DNA polumerase adds nucleotides to the primer by copying the circular template. Highly processive ϕ29 DNA polymerase can generate a long single-stranded DNA chain containing up to thousands of nucleotides.

An example study by Di Giusto *et al.*[75] involved the use of two different aptamers that bind thrombin in separate locations, one acting as the primer and the other as the circular template for RCA. Both aptamer sequences were modified in such a way that they can form a very weak duplex together. Without thrombin, this duplex is unstable and cannot form; however, the presence of thrombin forces duplex formation when both aptamers engage one thrombin molecule to trigger the RCA process. This amplification reaction can

be monitored in real time with the use of fluorophore-labeled complementary DNA probes for multiple labeling of the long DNA polymer that results in a large detectable signal.

By encoding the circular template with the complement of an aptamer sequence, the resulting single-stranded RCA product can be comprised of multiple aptamers in tandem repeating order. Zhao *et al.* designed a network of such RCA-based multi-aptamer molecules on a microfluidic device for the capture of cancer cells.[78] The long chains of repeating aptamers extended farther from the surface than single aptamer molecules, increasing their accessibility to and frequency of interactions with target cells. Another multivalent aptamer system synthesized by RCA and intercalated with chemotherapy agents has also demonstrated to be more effective than single aptamer-drug species in targeting and killing leukemia cells due to enhanced binding and cell internalization.[79] Similarly, Tan and co-workers have optimized self-assembled aggregates of functional RCA products (termed nanoflowers due to their unique petal-like structure) to incorporate aptamer sequences, drug loading sequences and fluorophore-labeled nucleotides for selective cancer cell bioimaging and targeted drug delivery.[80,81]

1.3 Platforms for Aptamer Immobilization

1.3.1 Immobilization Techniques Overview

The sensitivity and signal output of any solid-phase assay also depends on the method by which biomolecules are immobilized on or in the solid support.[10] This is because several factors such as the density, orientation and stability of the immobilized species affects its ability to access and interact with the target analyte. Typical methods used for bio-

immobilization are either based on attachment through physical adsorption, covalent binding and affinity interactions to the surface or entrapment within hydrogels, semi-permeable membranes, or porous inorganic materials.[82-87]

Physical adsorption functions through weak, non-specific interactions such as hydrogen bonding, hydrophobic interactions, or electrostatic interactions between the biomolecule and the surface. Therefore, biomolecules lay on the surface in a random orientation and can easily dissociate with changes in conditions (pH, temperature, ionic strength, etc.). The random orientation may alter the native conformation to undergo undesirable changes that reduce the activity of biomolecules or make them inaccessible to the analyte.[84]

Covalent attachment makes use of coupling agents to chemically link biomolecules to a surface in order to achieve more specific and stronger binding. As such, this is the most prevalent immobilization method for nucleic acids. Generally, this implies chemical modification of the aptamer at its 3′ or 5′ end to incorporate reactive functional groups or molecules that facilitate linkage to the surface, allowing certain control over the density of immobilized nucleic acids.[85,88] However, drawbacks include heterogeneous populations of nucleic acid molecules in addition to the potential need for complex conjugation procedures.

The most widely used affinity interactions involve the use of a biotin-streptavidin bridge to link biotinylated biomolecules to a solid support. This bioaffinity interaction

offers the greatest control over orientation as DNA or RNA molecules can be specifically labeled with biotin at any location in the nucleic acid strand,[86,88] however, any advantage achieved by aptamers in terms of robustness or reproducibility are negated by the presence of a more easily denatured protein-based linker.

Thus, optimization of the immobilization components become crucial. Not only do binding conditions need to be optimized but also the length and chemical composition of spacer arms, which keep biomolecules far enough from the surface to reduce steric hindrance and non-specific binding to the solid support in order to function properly. The lengthy optimization of these parameters is an additional drawback to any surface-attachment methodology.[87,89,90]

An alternative route for bio-immobilization involves the entrapment of biomolecules within a 3-D polymeric matrix. Typical matrices include organic polymers such as nylon or polyacrylamide,[82,91] and inorganic materials such as sol-gel derived silica.[92] Using this entrapment technique, biomolecules are encapsulated within the pores of the cross-linked matrix. Smaller analyte molecules diffuse into the porous matrix while larger species are retained through size exclusion (Figure 1.5). However, disadvantages of entrapment within organic polymers include the potential for biomolecular degradation by the harsh chemical polymerization conditions or biomolecules leaching out of the polymer due to swelling when in contact with aqueous solutions.[91,93]

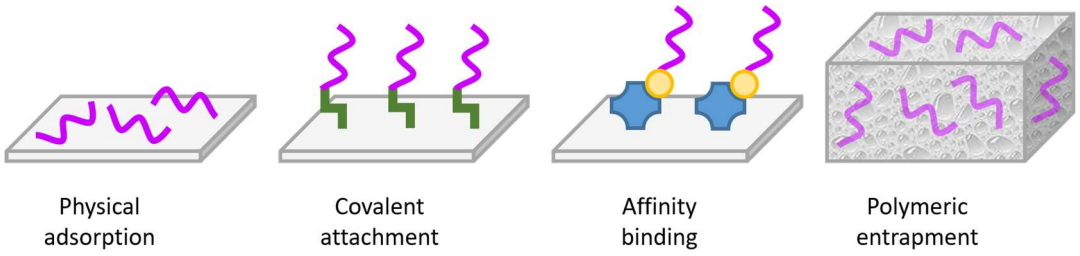

Figure 1.5. Comparison of different DNA immobilization methods. Nucleic acid aptamers can be attached to a solid support via physical adsorption, covalent attachment, affinity binding or entrapment within a polymeric matrix.

1.3.2 Aptamer Entrapment Using the Sol-Gel Process

Another entrapment technique makes use of a low temperature sol-gel process for creating porous networks of inorganic silica materials around the biosensing molecules.[94,95] Typically, this simple two-step process begins with the formation of an aqueous sol through acid or base catalyzed hydrolysis of a silane precursor, such as tetraethylorthosilicate (TEOS) or tetramethylorthosilicate (TMOS). The harsh hydrolysis step is then followed by condensation (and polycondensation) that can be performed at physiological pH using buffered solution containing the biomolecule as well as any additives for aiding bimolecular stability or modifying the material.[96,97] The sudden change to a more neutral pH results in the formation of siloxane bonds that entrap the biomolecules within the nanoscale pores of the cross-linking gel matrix. The speed of the condensation reaction depends upon the pH and ionic strength of the sol as well as the types of additives present, resulting in gelation times of seconds to days. As the hydrated silica gel ages, polycondensation continues, releasing water and causing shrinkage and rigidity of the material (Figure 1.6).

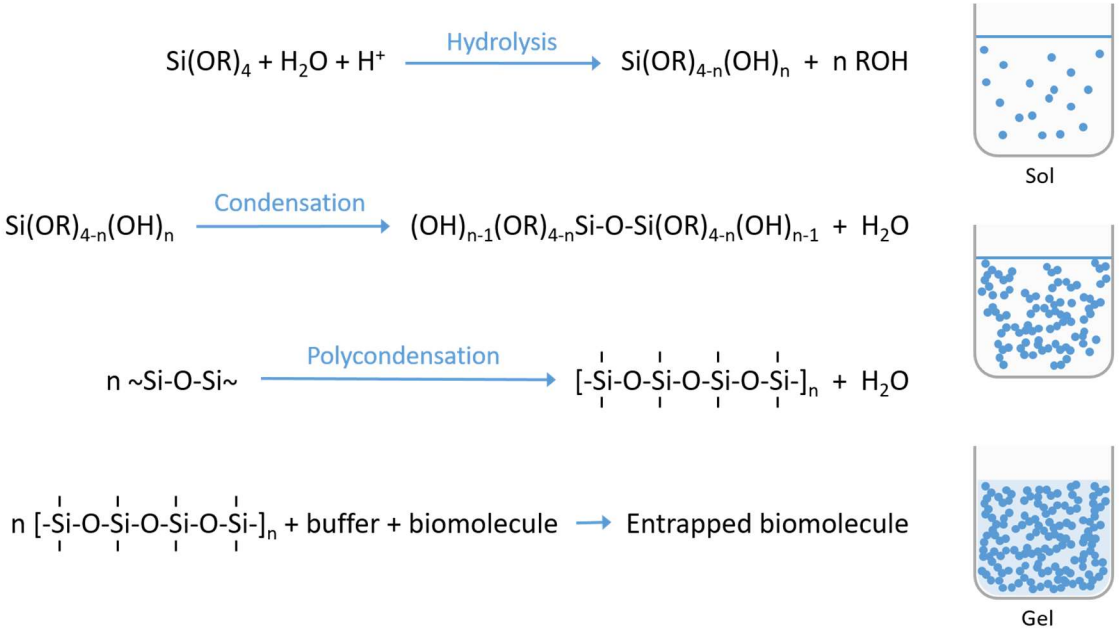

Figure 1.6. The sol-gel process for tetraalkoxysilanes. Biomolecules can be entrapped within inorganic, organic or hybrid porous materials (depending on the R group) through this two-step process of hydrolysis and (poly-)condensation. The condensation reaction can be accelerated with the addition of buffer at a neutral pH. Biomolecules added to the condensing sol become entrapped within the nanoscale pores of the cross-linking gel matrix. Note: the bonds to Si are denoting further Si-O bonds.

While the majority of early entrapment studies involving the sol-gel process have used TEOS or TMOS precursors,[92,95] these alkoxysilanes liberate large amounts of alcohol that may denature the entrapped biomolecule, particularly proteins. Thus, the use of more biocompatible precursors, such as sodium silicate (SS) or diglyceryl silane (DGS),[98] or modified processes, such as evaporation of residual alcohol,[99] have been employed more recently for biomolecular entrapment. The properties of the silica material, such as polarity and porosity, can be further tuned by varying the condensation conditions through changes in pH and ionic strength or through the addition of poragens with the addition of various

modified silanes and polymers. This versatility in the matrix environment allows for materials that can be tailored to specific biomolecules and for use in various applications, including immobilization of specific biomolecules in bioanalytical applications.[100-103] For example, material compositions with added (poly)ethylene glycol (PEG) undergo phase separation of the cross-linking silica from solution just prior to gelation, resulting in a bimodal pore size distribution. These meso/macroporous materials have found great use in the fabrication of monolithic protein-doped capillary columns in affinity chromatography or as enzyme reactors.[104,105] The larger macropores (greater than 50 nm)[106] allow eluent containing substrate and/or inhibitor molecules to flow through the column with low backpressure, while the smaller mesopores retain the protein receptor or enzyme of interest in the stationary phase.

Although the sol-gel process has been widely used to entrap proteins, such as antibodies and enzymes, its use in the field of nucleic acid immobilization has been much narrower since the utility of nucleic acids for small molecule interactions is a relatively recent discovery. To date only a few reports in the literature describe the entrapment of nucleic acids within sol-gel derived materials, with the first report on DNA hybridization within silica using biotinylated DNA molecular beacons presented in 2001.[107] Rupcich *et al.* was the first to report on the entrapment of a functional DNA aptamer within a sol-gel derived matrix.[108] In this study, biotinylated structure-switching signaling aptamers for binding ATP were complexed with streptavidin (to increase their physical size) and entrapped within the porous silica material with minimal leaching. When entrapped in a polar material using a sodium silicate precursor, the DNA aptamer was able to retain its ability

to change conformation and produce a fluorescence signal upon binding ATP, similar to that free in solution. However, the key advantage, when comparing entrapment to affinity-immobilization or solution-based platforms, was the protection from DNase degradation that enhances the biosensor long-term stability.

Further studies by Brennan and co-workers involved the co-entrapment of a DNA aptamer a protein enzyme, adenosine deaminase (ADA). The aptamer for binding ATP was used as a fluorescent reporter of the catalytic conversion of adenosine to inosine in the solid-phase.[109] Inhibition of ADA leads to high adenosine concentrations that induce fluorescence signaling of the aptamer reporter. It was found that separate material layers with the enzyme on top of the aptamer layer provided more accurate IC_{50} and K_I values as compared to when these species compete for the same substrate in single phase co-immobilization. This study demonstrates the ability to create layered structures not only so that assays may occur sequentially in the vertical direction but also for spatial separation of multiple types of biomolecules – of particular advantage when these species are incompatible or require different environments to function.

1.3.3 Immobilization for Paper-Based Devices

These previous studies involving the entrapment of DNA aptamers have demonstrated the advantages of combining sol-gel processing with emerging nucleic acid technologies. For sensing purposes, this combination has allowed for higher sensitivity, protection from degradation for longer sensor lifetimes, and better customization than other immobilization platforms. Another method for employing the adaptability of sol-gel materials for solid-

phase assay development involves aerosol spraying or ink-jet printing sols containing biomolecules as "bioinks" on emerging paper-based biosensing platforms.[110]

The need for portable, affordable and rapid detection assays for on-site health and environmental monitoring in resource-limited settings has sparked research interest in the burgeoning field of paper-based biosensors.[111-117] Although nitrocellulose and plastic have been used since the 1970s for solid-based bioaffinity assays,[114] cellulose-based paper has recently emerged as an attractive solid-phase platform because it is abundant, inexpensive and biodegradable. Moreover, it can be sterile, easily printed/coated on and its porous structure facilitates liquid transport via capillary action with no need for external pumps or power.[112,115]

The first microfluidic paper analytical device (μPAD)[118] exploited the intrinsic capillary fluidics of paper to drive an aqueous sample through channels created on the hydrophilic paper surface by patterning hydrophobic barriers with photoresist polymer. Wicking a sample through these flow channels resulted in directed passive transport of an analyte to the detection zone(s), wherein reagents for glucose and protein assays were deposited by simple adsorption. While many early μPAD studies focused on creating hydrophobic barriers using traditional microfluidic chip fabrication technologies, such as photolithography, plasma treatment or screen printing,[112-114] Abe *et al.* made use of the method most amenable to a paper-based platform: inkjet printing.[119,120] By etching hydrophobic polymer deposited on the paper surface using an inkjet printer, they developed 550-μm-wide channels wherein the assay reagents could also be printed using the same inkjet printer.

Inkjet printing has now emerged as a preferred method for creating hydrophobic barriers due to its simplicity (ease of use), low cost (especially when using standard office inkjet printers), speed (for scaling production) and control in deposition (both volume and position). Printing and subsequent heating of solid wax is the dominant technique for applying a material that can be melted into paper in order to create the hydrophobic barriers that define microfluidic channels.[117,121] However, some surfactants and organic solvents necessary in certain assays can leak through wax barrier walls causing loss of sample and poor detection capability. Thus, alternative barrier materials, such as organic polymers or silicones, have been demonstrated.[122-124]

Since is a heterogeneous material composed mainly of cellulose fibers, there are few functional groups available on the surface for direct attachment of biomolecules,[111,115,116] some studies have been directed at the chemical modification of paper fibres for such applications.[125-128] Su *et al.* compared the physical adsorption of ATP-binding aptamers with covalent coupling to a cellulose dialysis membrane that was oxidized to generate aldehyde groups on the surface. Physical adsorption was found to be too weak to attach the short oligonucleotides to cellulose as all the aptamer molecules were removed after washing with buffer. While the covalently-coupled aptamer demonstrated activity and specificity, the coupling efficiency to the cellulose membrane was found to be only about 25%.[126] Therefore, other strategies used to immobilize biomolecules on paper include entrapment within sol-gel derived inks or conjugation to larger colloidal particles that can be applied to paper. Although entrapping enzymes within layers of printed sol-gel derived silica materials demonstrated advantages in the function and long-term stability of paper-

based sensor strips for pesticide detection, the dynamic nature of material polymerization presents challenges during the printing process such as clogging of printheads or cartridges.[129,130]

Paper-based bioaffinity assays using aptamer molecules have thus focused on carrier-mediated immobilization by linking the biomolecules to nanoparticles or microbeads for specific localization on paper (Figure 1.7). In one such example, microgel-based ink modified either with an antibody or a DNA aptamer were printed on paper. This study found that the large microgel particles remain stationary and sufficiently hydrophilic to be wetted during sample flow on the paper to expose the bioaffinity probes to their targets. The aptamer binding signal functioned using a fluorescence-based structure-switching approach while antigen detection made use of a yellow-producing peroxidase reaction. Although the sensitivity using either detection methods was poor, this study demonstrated the ability of both the antibody and aptamer to retain some recognition capabilities when coupled to microgel on paper.[131] Zhao *et al.* made use of gold nanoparticles (AuNPs) as both the immobilization and colorimetric signal carrier for aptamer-based ATP sensing on paper.[132] In this proof-of-concept study, the use of AuNPs allowed for visible detection of changes in color from blue/purple to red (or vice versa) upon AuNP dispersion (or aggregation), eliminating the need for detection instrumentation.[133] DNA aptamers cross-linked to AuNP aggregates were spotted on either hydrophobic or hydrophilic paper such that deposition of ATP in buffer resulted in redispersion of the AuNP aggregates on the paper surface causing a blue-to-red shift in color.

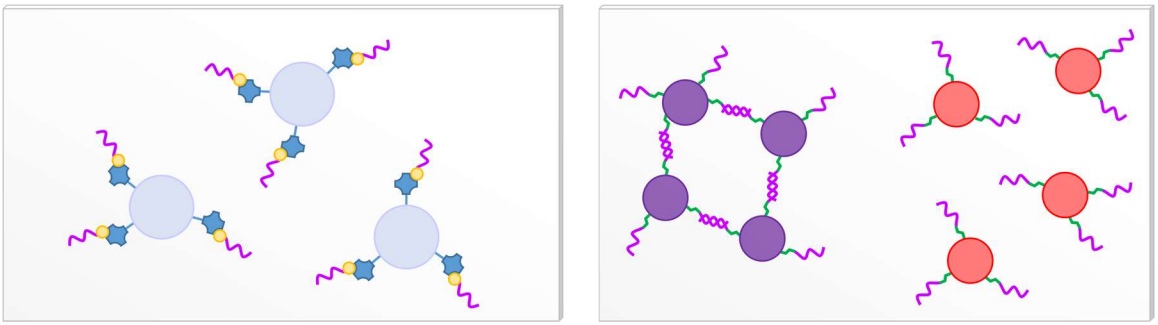

Figure 1.7. Immobilization of nucleic acids on paper. Aptamers are typically conjugated to larger microbeads or nanoparticles (such as AuNPs) in order to localize these biomolecules on the surface of cellulose-based paper.

Liu *et al.* developed a 3-D aptamer-based µPAD with only a single sheet of patterned paper using the principles of origami (paper folding).[134] The 3-D origami-based device was generated using wax printing to outline channels and detection reservoirs for sample flow, while screen printing was used to create electrodes as a separate layer. When the paper is folded, the electrodes contact the end of two fluidic channel where they recombine at the detection reservoirs to form an electrochemical cell. In one channel, an aptamer immobilized on polystyrene microbeads binds to the target, adenosine, and releases a GOx-labeled DNA strand that flows towards the cell. The current generated with increasing GOx concentration, due to increasing adenosine binding, can be measured by simply connecting the 3-D µPAD to a breadbox.

These examples demonstrate how the advantages of paper-based sensors over other solid-phase assay formats have led to various studies related to fabrication methods, detection techniques and intricate configurations. Indeed, a number of paper-based assay have been designed to detect pH value, urine metabolites, blood glucose, liver function,

hormones, infectious agents, etc.[116,117] Still, challenges in their development exist in that they are subject to the same considerations of other solid-phase assay formats as their performance depends on a number of factors: mainly the nature of the biorecognition molecules and the method of immobilization.

1.4 Thesis Goals and Outline

While there are many advantages in utilizing nucleic acid aptamers for developing solid-phase bioaffinity assays, combining these biorecognition molecules with conventional immobilization methodologies still limit the potential of such assays in regards to biomolecule stability, performance and compatibility with emerging applications. The research in this thesis aims to address this by employing principles from materiomics[135] to design, develop and optimize both the nucleic acid biomaterials for analyte recognition and the solid support materials for immobilization in a systematic and high-throughput manner. The projects described in the subsequent chapters exemplify solid-phase bioaffinity assays that employ direct aptamer immobilization without the need for extraneous binding molecules, complex conjugation procedures or spacer arm optimization.

Chapter two describes the entrapment of structure-switching/fluorescence-signaling RNA aptamers into porous sol-gel derived silica and organosilane materials in wells of a microtiter plate. These materials were investigated for the purpose of finding a solid-phase platform that can stabilize labile RNA molecules against degradation while immobilizing these species in a solid support. In evaluating the leaching, stability, resistance to nuclease

attack and signaling capabilities relative to solution, the data clearly show that being entrapped within the pores of a hybrid organic-inorganic sol-gel derived material protected the RNA from both nuclease and chemical degradation, providing the long-term stability required of a robust RNA aptamer-based biosensor. Thus, this sol-gel entrapment scheme for immobilization expands the use of nucleic acid aptamers to include relatively unexplored RNA aptamer species for solid-phase biosensing applications. However, limitations of this method still exist in that it is only amenable to the detection of small molecules that can enter the matrix pores to interact with the entrapped aptamer. Thus, new strategies for binding larger macromolecules must still be devised.

Therefore, Chapter three describes the entrapment of long RCA products containing tandem-repeating aptamer sequences in macroporous sol-gel derived materials that can accommodate accessibility to large macromolecular targets. A high-throughput material screening approach was used to identify and optimize materials with a macroporous morphology that allows for high activity and minimal leaching of the extremely large biorecognition molecules, termed concatemeric DNA aptamers, entrapped within. The optimal concatemeric aptamer-doped material was used to produce monolithic columns for pressure-driven flow-based biorecognition devices. These columns were amenable to the detection of not only small molecules but also high molecular weight proteins, thus, expanding the range of analytes that can interact with entrapped biomolecules to include large macromolecules.

In order to demonstrate the versatility of such “long-chain DNA aptamers” for emerging applications, Chapter four then presents a simple and effective approach for

patterning paper sensors by inkjet printing these biorecognition molecules on filter paper. Optimization of the fluorescence signaling capabilities was first performed in solution followed by testing on paper. It was found that the concatemeric aptamer reporters remain immobilized at the point of printing after liquid elution over the area through strong adsorption and retain sufficient segmental motion required for target binding and signaling on the paper surface. The convenience of inkjet printing allows for patterning internally-referenced and multiplexed assay designs for both qualitative and quantitative detection of small molecule and protein targets. This strategy provides a generic platform for on-demand printing of sensors for environmental, food safety, and clinical applications in remote locations.

Finally, Chapter five recapitulates the major achievements and conclusions drawn from the research projects outlined above and recommends future directions for the continuation of this work.

1.5 References

(1) Hanninen, P.; Soini, A.; Meltola, N.; Soini, J.; Soukka, J.; Soini, E. *Nat. Biotechnol.* **2000**, *18*, 548-50.
(2) Soini, J. T.; Waris, M. E.; Hanninen, P. E. *J. Pharm. Biomed. Anal.* **2004**, *34*, 753-60.
(3) Forsberg, E. M.; Sicard, C.; Brennan, J. D. *Annu. Rev. Anal. Chem.* **2014**, *7*, 337-59.
(4) Ziegler, C.; Gopel, W. *Curr. Opin. Chem. Biol.* **1998**, *2*, 585-91.
(5) Guijt, R. M.; Baltussen, E.; van Dedem, G. W. K. *Electrophoresis* **2002**, *23*, 823-35.
(6) Templin, M. F.; Stoll, D.; Schrenk, M.; Traub, P. C.; Vohringer, C. F.; Joos, T. O. *Trends Biotechnol.* **2002**, *20*, 160-6.
(7) Turner, A. P. F. *Chem. Soc. Rev.* **2013**, *42*, 3184-96.
(8) Cooper, M. A. *Nat. Rev. Drug Discovery* **2002**, *1*, 515-28.
(9) Mascini, M.; Tombelli, S. *Biomarkers* **2008**, *13*, 637-57.
(10) Scheller, F. W.; Wollenberger, U.; Warsinke, A.; Lisdat, F. *Curr. Opin. Biotechnol.* **2001**, *12*, 35-40.
(11) Newman, J. D.; Tigwell, L. J.; Turner, A. P. F.; Warner, P. J. *Biosensors: A Clearer View*; Cranfield University: Swindon, UK, 2004.
(12) Bahadir, E. B.; Sezginturk, M. K. *Anal. Biochem.*, *478*, 107-20.
(13) Ellington, A. D.; Szostak, J. W. *Nature* **1990**, *346*, 818-22.
(14) Tuerk, C.; Gold, L. *Science* **1990**, *249*, 505-10.
(15) Wilson, D. S.; Szostak, J. W. *Annu. Rev. Biochem.* **1999**, *68*, 611-47.
(16) Lee, J. F.; Hesselberth, J. R.; Meyers, L. A.; Ellington, A. D. *Nucleic Acids Res.* **2004**, *32*, D95-D100.
(17) Liu, J.; Cao, Z.; Lu, Y. *Chem. Rev.* **2009**, *109*, 1948-98.
(18) Bock, L. C.; Griffin, L. C.; Latham, J. A.; Vermaas, E. H.; Toole, J. J. *Nature* **1992**, *355*, 564-6.
(19) Klug, S. J.; Famulok, M. *Mol. Biol. Rep.* **1994**, *20*, 97-107.
(20) Breaker, R. R. *Curr. Opin. Chem. Biol.* **1997**, *1*, 26-31.
(21) Osborne, S. E.; Ellington, A. D. *Chem. Rev.* **1997**, *97*, 349-70.
(22) Joyce, G. F. *Annu. Rev. Biochem.* **2004**, *73*, 791-836.
(23) Famulok, M.; Mayer, G.; Blind, M. *Acc. Chem. Res.* **2000**, *33*, 591-9.
(24) Mairal, T.; Cengiz Ozalp, V.; Lozano Sanchez, P.; Mir, M.; Katakis, I.; O'Sullivan, C. K. *Anal. Bioanal. Chem.* **2008**, *390*, 989-1007.
(25) Patel, D. J. *Curr. Opin. Chem. Biol.* **1997**, *1*, 32-46.
(26) Hermann, T.; Patel, D. J. *Science* **2000**, *287*, 820-5.
(27) Jayasena, S. D. *Clin. Chem.* **1999**, *45*, 1628-50.
(28) Iliuk, A. B.; Hu, L.; Tao, W. A. *Anal. Chem.* **2011**, *83*, 4440-52.
(29) Oivanen, M.; Kuusela, S.; Lonnberg, H. *Chem. Rev.* **1998**, *98*, 961-90.
(30) Li, Y.; Breaker, R. R. *J. Am. Chem. Soc.* **1999**, *121*, 5364-72.
(31) Soukup, G. A.; Breaker, R. R. *RNA* **1999**, *5*, 1308-25.
(32) Clark, S. L.; Remcho, V. T. *Anal. Chem.* **2003**, *75*, 5692-6.

(33) Minunni, M.; Tombelli, S.; Gullotto, A.; Luzi, E.; Mascini, M. *Biosens. Bioelectron.* **2004**, *20*, 1149-56.
(34) Cho, E. J.; Collett, J. R.; Szafranska, A. E.; Ellington, A. D. *Anal. Chim. Acta* **2006**, *564*, 82-90.
(35) Min, K.; Cho, M.; Han, S.-Y.; Shim, Y.-B.; Ku, J.; Ban, C. *Biosens. Bioelectron.* **2008**, *23*, 1819-24.
(36) Ferapontova, E. E.; Olsen, E. M.; Gothelf, K. V. *J. Am. Chem. Soc.* **2008**, *130*, 4256-8.
(37) Lee, H. S.; Kim, K. S.; Kim, C. J.; Hahn, S. K.; Jo, M. H. *Biosens. Bioelectron.* **2009**, *24*, 1801-5.
(38) Brody, E. N.; Gold, L. *J. Biotechnol.* **2000**, *74*, 5-13.
(39) McCauley, T. G.; Hamaguchi, N.; Stanton, M. *Anal. Biochem.* **2003**, *319*, 244-50.
(40) Tombelli, S.; Minunni, M.; Mascini, M. *Biosens. Bioelectron.* **2005**, *20*, 2424-34.
(41) Navani, N. K.; Li, Y. F. *Curr. Opin. Chem. Biol.* **2006**, *10*, 272-81.
(42) Cho, E. J.; Lee, J. W.; Ellington, A. D. *Annu. Rev. Anal. Chem.* **2009**, *2*, 241-64.
(43) Clark, S. L.; Remcho, V. T. *Electrophoresis* **2002**, *23*, 1335-40.
(44) Hamula, C. L. A.; Guthrie, J. W.; Zhang, H.; Li, X.-F.; Le, X. C. *TrAC, Trends Anal. Chem.* **2006**, *25*, 681-91.
(45) Sefah, K.; Phillips, J. A.; Xiong, X.; Meng, L.; Van Simaeys, D.; Chen, H.; Martin, J.; Tan, W. *Analyst* **2009**, *134*, 1765-75.
(46) Tombelli, S.; Minunni, M.; Mascini, M. *Biomol. Eng.* **2007**, *24*, 191-200.
(47) Famulok, M.; Mayer, G. *Acc. Chem. Res.* **2011**, *44*, 1349-58.
(48) Song, S. P.; Wang, L. H.; Li, J.; Zhao, J. L.; Fan, C. H. *TrAC, Trends Anal. Chem.* **2008**, *27*, 108-17.
(49) Li, D.; Song, S.; Fan, C. *Acc. Chem. Res.* **2010**, *43*, 631-41.
(50) Potyrailo, R. A.; Conrad, R. C.; Ellington, A. D.; Hieftje, G. M. *Anal Chem* **1998**, *70*, 3419-25.
(51) Lakowicz, J. *Principles of Fluorescence Spectroscopy*; Second ed.; Kluwer Academic/Plenum Publishers: New York, Boston, Dordrecht, London, Moscow, 1999.
(52) Jhaveri, S. D.; Kirby, R.; Conrad, R.; Maglott, E. J.; Bowser, M.; Kennedy, R. T.; Glick, G.; Ellington, A. D. *J. Am. Chem. Soc.* **2000**, *122*, 2469-73.
(53) Marras, S. A. E.; Kramer, F. R.; Tyagi, S. *Nucleic Acids Res.* **2002**, *30*, e22.
(54) Tyagi, S.; Kramer, F. R. *Nat. Biotech.* **1996**, *14*, 303-8.
(55) Fang, X. H.; Liu, X. J.; Schuster, S.; Tan, W. H. *J. Am. Chem. Soc.* **1999**, *121*, 2921-2.
(56) Radi, A. E.; Sanchez, J. L. A.; Baldrich, E.; O'Sullivan, C. K. *J. Am. Chem. Soc.* **2006**, *128*, 117-24.
(57) Yamamoto, R.; Baba, T.; Kumar, P. K. *Genes Cells* **2000**, *5*, 389-96.
(58) Hamaguchi, N.; Ellington, A.; Stanton, M. *Anal. Biochem.* **2001**, *294*, 126-31.
(59) Yu, S.; Cai, X.; Tan, X.; Zhu, Y.; Lu, B. *Proc.SPIE Int. Soc. Opt. Eng.* **2001**, *4414*, 35-7.
(60) Nutiu, R.; Li, Y. *J. Am. Chem. Soc.* **2003**, *125*, 4771-8.
(61) Nutiu, R.; Li, Y. *Chemistry* **2004**, *10*, 1868-76.

(62) Lau, P. S.; Coombes, B. K.; Li, Y. *Angew. Chem. Int. Ed.* **2010**, *49*, 7938-42.
(63) Lu, C.-H.; Yang, H.-H.; Zhu, C.-L.; Chen, X.; Chen, G.-N. *Angew. Chem. Int. Ed.* **2009**, *48*, 4785-7.
(64) Ping, J.; Zhou, Y.; Wu, Y.; Papper, V.; Boujday, S.; Marks, R. S.; Steele, T. W. J. *Biosens. Bioelectron.* **2015**, *64*, 373-85.
(65) Zheng, M.; Jagota, A.; Semke, E. D.; Diner, B. A.; McLean, R. S.; Lustig, S. R.; Richardson, R. E.; Tassi, N. G. *Nat. Mater.* **2003**, *2*, 338-42.
(66) Yang, R.; Jin, J.; Chen, Y.; Shao, N.; Kang, H.; Xiao, Z.; Tang, Z.; Wu, Y.; Zhu, Z.; Tan, W. *J. Am. Chem. Soc.* **2008**, *130*, 8351-8.
(67) Béra Abérem, M.; Najari, A.; Ho, H. A.; Gravel, J. F.; Nobert, P.; Boudreau, D.; Leclerc, M. *Adv. Mater.* **2006**, *18*, 2703-7.
(68) Zhao, Y.; Chen, F.; Li, Q.; Wang, L.; Fan, C. *Chem. Rev.* **2015**, *115*, 12491-545.
(69) Ali, M. M.; Li, F.; Zhang, Z.; Zhang, K.; Kang, D. K.; Ankrum, J. A.; Le, X. C.; Zhao, W. *Chem. Soc. Rev.* **2014**, *43*, 3324-41.
(70) Fire, A.; Xu, S. Q. *Proc. Natl. Acad. Sci. U.S.A.* **1995**, *92*, 4641-5.
(71) Liu, D. Y.; Daubendiek, S. L.; Zillman, M. A.; Ryan, K.; Kool, E. T. *J. Am. Chem. Soc.* **1996**, *118*, 1587-94.
(72) Zhao, W. A.; Ali, M. M.; Brook, M. A.; Li, Y. F. *Angew. Chem. Int. Ed.* **2008**, *47*, 6330-7.
(73) Rodriguez, I.; Lazaro, J. M.; Blanco, L.; Kamtekar, S.; Berman, A. J.; Wang, J. M.; Steitz, T. A.; Salas, M.; de Vega, M. *Proc. Natl. Acad. Sci. U.S.A.* **2005**, *102*, 6407-12.
(74) Cho, E. J.; Yang, L. T.; Levy, M.; Ellington, A. D. *J. Am. Chem. Soc.* **2005**, *127*, 2022-3.
(75) Di Giusto, D. A.; Wlassoff, W. A.; Gooding, J. J.; Messerle, B. A.; King, G. C. *Nucleic Acids Res.* **2005**, *33*, e64.
(76) Lizardi, P. M.; Huang, X. H.; Zhu, Z. R.; Bray-Ward, P.; Thomas, D. C.; Ward, D. C. *Nat. Genet.* **1998**, *19*, 225-32.
(77) Yang, L. T.; Fung, C. W.; Cho, E. J.; Ellington, A. D. *Anal. Chem.* **2007**, *79*, 3320-9.
(78) Zhao, W.; Cui, C. H.; Bose, S.; Guo, D.; Shen, C.; Wong, W. P.; Halvorsen, K.; Farokhzad, O. C.; Teo, G. S.; Phillips, J. A.; Dorfman, D. M.; Karnik, R.; Karp, J. M. *Proc. Natl. Acad. Sci. U.S.A.* **2012**, *109*, 19626-31.
(79) Zhang, Z.; Ali, M. M.; Eckert, M. A.; Kang, D.-K.; Chen, Y. Y.; Sender, L. S.; Fruman, D. A.; Zhao, W. *Biomaterials* **2013**, *34*, 9728-35.
(80) Zhu, G.; Hu, R.; Zhao, Z.; Chen, Z.; Zhang, X.; Tan, W. *J. Am. Chem. Soc.* **2013**, *135*, 16438-45.
(81) Hu, R.; Zhang, X.; Zhao, Z.; Zhu, G.; Chen, T.; Fu, T.; Tan, W. *Angew. Chem. Int. Ed.* **2014**, *53*, 5821-6.
(82) O'Driscoll, K. F. *Methods Enzymol.* **1976**, *44*, 169-83.
(83) Scouten, W. H. *Methods Enzymol.* **1987**, *135*, 30-65.
(84) Andrade, J. D.; Hlady, V.; Wei, A. P. *Pure Appl. Chem.* **1992**, *64*, 1777-81.
(85) Weetall, H. H. *Appl. Biochem. Biotechnol.* **1993**, *41*, 157-88.
(86) Ramsay, G. *Nature Biotechnol.* **1998**, *16*, 40-4.

(87) Balamurugan, S.; Obubuafo, A.; Soper, S. A.; Spivak, D. A. *Anal. Bioanal. Chem.* **2008**, *390*, 1009-21.
(88) Zhu, H.; Snyder, M. *Curr. Opin. Chem. Biol.* **2003**, *7*, 55-63.
(89) Petrovykh, D. Y.; Kimura-Suda, H.; Whitman, L. J.; Tarlov, M. J. *J. Am. Chem. Soc.* **2003**, *125*, 5219-26.
(90) Du, F.; Guo, L.; Qin, Q.; Zheng, X.; Ruan, G.; Li, J.; Li, G. *TrAC, Trends Anal. Chem.* **2015**, *67*, 134-46.
(91) Maleki, A.; Kjoniksen, A. L.; Knudsen, K. D.; Nystrom, B. *Polym. Int.* **2006**, *55*, 365-74.
(92) Bhatia, R. B.; Brinker, C. J.; Gupta, A. K.; Singh, A. K. *Chem. Mater.* **2000**, *12*, 2434-41.
(93) Livshits, M. A.; Mirzabekov, A. D. *Biophys.J.* **1996**, *71*, 2795-801.
(94) Braun, S.; Rappoport, S.; Zusman, R.; Avnir, D.; Ottolenghi, M. *Mater. Lett.* **1990**, *10*, 1-5.
(95) Avnir, D.; Braun, S.; Lev, O.; Ottolenghi, M. *Chem. Mater.* **1994**, *6*, 1605-14.
(96) Brinker, C. J.; Scherer, G. W. *Sol-Gel Science*; Academic Press: New York, 1990.
(97) Jin, W.; Brennan, J. D. *Anal. Chim. Acta* **2002**, *461*, 1-36.
(98) Brook, M. A.; Chen, Y.; Guo, K.; Zhang, Z.; Jin, W.; Deisingh, A.; Cruz-Aguado, J.; Brennan, J. D. *J. Sol-Gel Sci. Technol.* **2004**, *31*, 343-48.
(99) Ferrer, M. L.; del Monte, F.; Levy, D. *Chem. Mater.* **2002**, *14*, 3619-21.
(100) Avnir, D.; Coradin, T.; Lev, O.; Livage, J. *J. Mater. Chem.* **2006**, *16*, 1013-30.
(101) Brennan, J. D. *Acc. Chem. Res.* **2007**, *40*, 827-35.
(102) Gupta, R.; Chaudhury, N. K. *Biosens. Bioelectron.* **2007**, *22*, 2387-99.
(103) Monton, M. R. N.; Forsberg, E. M.; Brennan, J. D. *Chem. Mater.* **2011**, *24*, 796-811.
(104) Hodgson, R. J.; Chen, Y.; Zhang, Z.; Tleugabulova, D.; Long, H.; Zhao, X. M.; Organ, M.; Brook, M. A.; Brennan, J. D. *Anal. Chem.* **2004**, *76*, 2780-90.
(105) Besanger, T. R.; Hodgson, R. J.; Green, J. R.; Brennan, J. D. *Anal. Chim. Acta* **2006**, *564*, 106-15.
(106) Rouquerol, J.; Avnir, D.; Fairbridge, C. W.; Everett, D. H.; Haynes, J. H.; Pernicone, N.; Ramsay, J. D. F.; Sing, K. S. W.; Unger, K. K. *Pure Appl. Chem.* **1994**, *66*, 1739-58.
(107) Li, J.; Tan, W. H.; Wang, K.; Yang, X.; Tang, Z. W.; He, X. X. *Proc. SPIE Int. Soc. Opt. Eng.* **2001**, *4414*, 27-30.
(108) Rupcich, N.; Nutiu, R.; Li, Y. F.; Brennan, J. D. *Anal. Chem.* **2005**, *77*, 4300-7.
(109) Rupcich, N.; Nutiu, R.; Li, Y. F.; Brennan, J. D. *Angew. Chem. Int. Ed.* **2006**, *45*, 3295-9.
(110) Di Risio, S.; Yan, N. *Macromol. Rapid Commun.* **2007**, *28*, 1934-40.
(111) Pelton, R. *TrAC, Trends Anal. Chem.* **2009**, *28*, 925-42.
(112) Martinez, A. W.; Phillips, S. T.; Whitesides, G. M.; Carrilho, E. *Anal. Chem.* **2010**, *82*, 3-10.
(113) Liana, D. D.; Raguse, B.; Gooding, J. J.; Chow, E. *Sensors* **2012**, *12*, 11505-26.
(114) Yetisen, A. K.; Akram, M. S.; Lowe, C. R. *Lab Chip* **2013**, *13*, 2210-51.
(115) Then, W. L.; Garnier, G. *Rev. Anal. Chem.* **2013**, *32*, 269-94.

(116) Mahadeva, S. K.; Walus, K.; Stoeber, B. *ACS Appl. Mater. Interfaces* **2015**, *7*, 8345-62.
(117) Yang, Y.; Noviana, E.; Nguyen, M. P.; Geiss, B. J.; Dandy, D. S.; Henry, C. S. *Anal. Chem.* **2017**, *89*, 71-91.
(118) Martinez, A. W.; Phillips, S. T.; Butte, M. J.; Whitesides, G. M. *Angew. Chem. Int. Ed.* **2007**, *46*, 1318-20.
(119) Abe, K.; Suzuki, K.; Citterio, D. *Anal. Chem.* **2008**, *80*, 6928-34.
(120) Abe, K.; Kotera, K.; Suzuki, K.; Citterio, D. *Anal. Bioanal. Chem.* **2010**, *398*, 885-93.
(121) Carrilho, E.; Martinez, A. W.; Whitesides, G. M. *Anal. Chem.* **2009**, *81*, 7091-5.
(122) Sameenoi, Y.; Nongkai, P. N.; Nouanthavong, S.; Henry, C. S.; Nacapricha, D. *Analyst* **2014**, *139*, 6580-8.
(123) Rajendra, V.; Sicard, C.; Brennan, J. D.; Brook, M. A. *Analyst* **2014**, *139*, 6361-5.
(124) Jahanshahi-Anbuhi, S.; Pennings, K.; Leung, V.; Kannan, B.; Brennan, J. D.; Filipe, C. D. M.; Pelton, R. H. *ACS Appl.Mater. Interfaces* **2015**, *7*, 25434-40.
(125) Araujo, A. C.; Song, Y.; Lundeberg, J.; Stahl, P. L.; Brumer, H., 3rd *Anal. Chem.* **2012**, *84*, 3311-7.
(126) Su, S.; Nutiu, R.; Filipe, C. D.; Li, Y.; Pelton, R. *Langmuir* **2007**, *23*, 1300-2.
(127) Filpponen, I.; Kontturi, E.; Nummelin, S.; Rosilo, H.; Kolehmainen, E.; Ikkala, O.; Laine, J. *Biomacromolecules* **2012**, *13*, 736-42.
(128) Yu, A.; Shang, J.; Cheng, F.; Paik, B. A.; Kaplan, J. M.; Andrade, R. B.; Ratner, D. M. *Langmuir* **2012**, *28*, 11265-73.
(129) Hossain, S. M. Z.; Luckham, R. E.; Smith, A. M.; Lebert, J. M.; Davies, L. M.; Pelton, R. H.; Filipe, C. D. M.; Brennan, J. D. *Anal. Chem.* **2009**, *81*, 5474-83.
(130) Hossain, S. M. Z.; Luckham, R. E.; McFadden, M. J.; Brennan, J. D. *Anal. Chem.* **2009**, *81*, 9055-64.
(131) Su, S.; Ali, M. M.; Filipe, C. D. M.; Li, Y.; Pelton, R. *Biomacromolecules* **2008**, *9*, 935-41.
(132) Zhao, W.; Ali, M. M.; Aguirre, S. D.; Brook, M. A.; Li, Y. *Anal. Chem.* **2008**, *80*, 8431-7.
(133) Zhao, W.; Brook, M. A.; Li, Y. *ChemBioChem* **2008**, *9*, 2363-71.
(134) Liu, H.; Xiang, Y.; Lu, Y.; Crooks, R. M. *Angew. Chem. Int. Ed.* **2012**, *51*, 6925-8.
(135) Cranford, S. W.; de Boer, J.; van Blitterswijk, C.; Buehler, M. J. *Adv. Mater.* **2013**, *25*, 802-24.

CHAPTER 2.

STABILIZING STRUCTURE-SWITCHING SIGNALING RNA APTAMERS BY ENTRAPMENT IN SOL-GEL DERIVED MATERIALS FOR SOLID-PHASE ASSAYS

Author's Preface:

The following chapter was published in the *Journal of the American Chemical Society* under the citation:

Carrasquilla C, Lau PS, Li Y and Brennan JD. Stabilizing Structure-Switching Signaling RNA Aptamers by Entrapment in Sol–Gel Derived Materials for Solid-Phase Assays. *J. Am. Chem. Soc.* **2012** 134: 10998-11005.

I was responsible for all experimental design, execution and analysis included in this chapter. Pui Sai Lau provided the RNA aptamers and fluorophore-labeled DNA used in this study. I wrote the first draft of the manuscript. Dr. Li and Dr. Brennan provided editorial input to generate the final draft of the paper.

2.1 Abstract

Structure-switching, fluorescence-signaling DNA and RNA aptamers have been reported as highly versatile molecular recognition elements for biosensor development. While structure-switching DNA aptamers have been utilized for solid-phase sensing, equivalent RNA aptamers have yet to be successfully utilized in solid-phase sensors due to their lack of chemical stability and susceptibility to nuclease attack. In this study, we examined entrapment into sol-gel derived organic-inorganic composite materials as a platform for immobilization of structure-switching fluorescence-signaling RNA aptamer reporters, using both the synthetic theophylline- and naturally occurring thiamine pyrophosphate-binding RNA aptamers as test cases. Structure-switching versions of both aptamers were entrapped into a series of sol-gel derived composites, ranging from highly polar silica to hydrophobic methylsilsesquioxane-based materials, and the target-binding and signaling capabilities of these immobilized aptamers were assessed relative to solution. Both immobilized aptamers demonstrated sensitivity and selectivity similar to that of free aptamers when entrapped in a composite material derived from 40% (v/v) methyltrimethoxysilane/tetramethoxysilane. This material also conferred protection from nuclease degradation and imparted long-term chemical stability to the RNA reporter systems. Given the versatility of sol-gel entrapment for development of biosensors, microarrays, bioaffinity columns and other devices, this entrapment method should provide a useful platform for numerous solid-phase RNA aptamer-based devices (Figure 2.1).

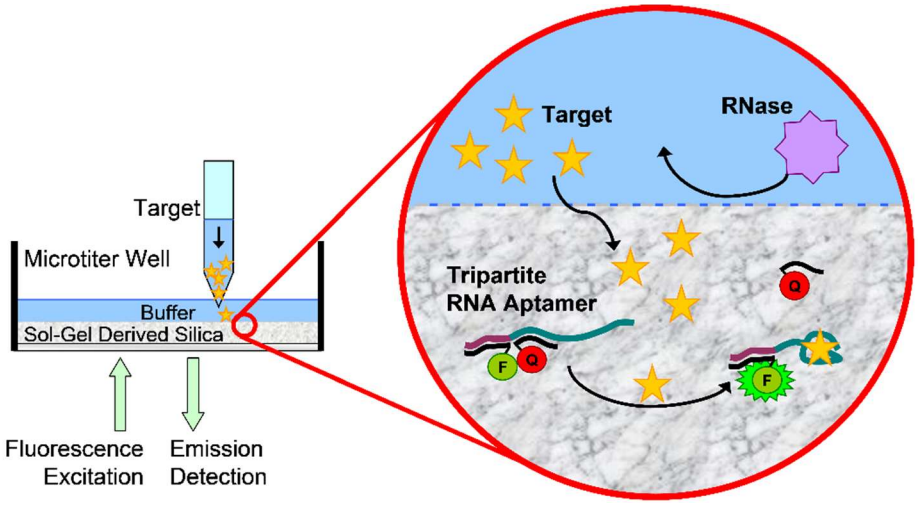

Figure 2.1. Schematic illustration of RNA aptamer reporter entrapment in sol-gel derived materials (TOC figure).

2.2 Introduction

Aptamers are single-stranded nucleic acids commonly generated through *in vitro* selection that can function as receptors for small molecules, proteins or even cells, due to their ability to fold into distinct three-dimensional structures[1-3] that possess specificity and affinity for their target ligands comparable to, if not surpassing, that of antibodies.[4] These features, combined with their chemical stability and ease of modification, have seen DNA aptamers emerge as promising biological recognition elements in analytical and diagnostic applications.[5-9] However, the limited range of analytes for DNA aptamers (with only 12 small-molecule and 9 protein targets as of 2009)[10] and the lack of known naturally-evolved DNA aptamers limit their potential for widespread use in sensing applications.

RNA aptamers, by contrast, can fold into more complex structures in order to provide a greater diversity of potential analytes as demonstrated by over 90 unique RNA aptamers

for various small-molecule and protein targets.[10-12] Moreover, RNA aptamers have recently been derived from natural sources (i.e. riboswitches).[13-15] However, reports on the use of RNA-based aptamers in solution or solid-phase biosensing applications are still relatively limited, mostly due to their inherent chemical instability[16-18] and susceptibility to nuclease attack,[19] combined with their lack of intrinsic signal-development capabilities. Several studies have focused on increasing the stability of functional RNA, usually by substituting the highly reactive hydroxyl group at the 2'-position of nucleotides containing pyrimidines, to make them nuclease-resistant.[20-24] However, chemical modification of RNA aptamers may alter their selectivity and binding affinity[25] without a significant increase in stability if the aptamer is purine rich. Studies involving *in vitro* selections using a combinatorial library with modified bases[26] or Spiegelmers[27-29] (mirror-image nucleotides) have generated families of aptamers with distinctly dissimilar minimal sequences compared to conventional RNA aptamers, providing completely different molecules and making these methods of limited use for unmodified RNA aptamers that are naturally-occurring or have already been selected in the past twenty years.

Recently, the Li group addressed the signaling ability of RNA aptamers by developing a structure-switching/fluorescence-signaling approach similar to that described previously for DNA aptamers.[30] The synthetic theophylline-binding aptamer (33 nt, 100 nM K_d)[31] and the naturally-occurring thiamine pyrophosphate (TPP)-binding aptamer (87 nt, 0.85 nM K_d)[32] were converted to reporter systems by designing complementary fluorophore-labeled DNA (FDNA) and quencher-labeled DNA (QDNA) strands to assemble a tripartite signaling duplex such that a conformational change from a RNA/DNA duplex to a

RNA/target complex was coupled to a fluorescence-dequenching mechanism, generating a fluorescence signal upon target binding. While the structure-switching reporters retained the same specificity as the original aptamers, the affinities of both aptamers were observed to be 10-fold poorer than the original K_d values (1 μM and 0.1 μM, respectively), with maximal signal enhancements of ~6–fold and 3.5–fold for the theophylline-binding and TPP-binding aptamer, respectively.[33]

To extend the utility of signaling RNA aptamers for diagnostic applications, it is generally necessary to immobilize these species onto or within a suitable surface while maintaining chemical stability and structure-switching abilities.[34] At this time, very few studies have examined immobilized RNA aptamers for solid-phase biosensing devices,[35-41] and none have examined the immobilization of structure-switching signaling RNA aptamers. In this report, we investigate the use of a low temperature sol-gel process for entrapment of structure-switching RNA aptamers into porous silica and organosilane materials.[42,43] This simple immobilization process has been shown to be "biofriendly" and applicable to the entrapment of a variety of viable biomolecules,[44-49] including structure-switching DNA aptamers[50] and DNA enzymes,[51] suggesting that the method should be useful for the development of solid-phase RNA aptamer biosensors. However, the entrapment of functional RNA aptamers requires a material that can stabilize these labile molecules against degradation by both intramolecular transesterification and external nuclease attack. Therefore, structure switching variants of both an *in vitro* selected RNA aptamer and a naturally-occurring aptamer were entrapped in a variety of sol-gel processed composite materials (polar, anioinic, cationic, hydrophobic) and the leaching, stability,

resistance to nuclease attack and signaling capabilities were evaluated relative to these species in solution. The data clearly show that the optimal materials for entrapment of RNA aptamers are very different from those that stabilize proteins, and demonstrate the versatility of the sol-gel immobilization method to expand solid-phase sensing through the utilization of relatively unexplored RNA aptamer species.

2.3 Results and Discussion

Characterization of Sol-Gel Derived Materials. Sol-gel derived materials were prepared from two previously reported biofriendly precursors (sodium silicate (SS) and diglyceryl silane (DGS) with and without 3-aminopropyltriethoxysilane (APTES) (to produce a cationic surface), along with tetramethylorthosilicate (TMOS) derived composites containing up to 80% methyltrimethoxysilane (MTMS) to produce a gradient of polarity, and methylsilsesquioxane (MSQ) materials derived from pure MTMS to examine whether aptamers could be entrapped into highly hydrophobic materials. Prior to performing studies focused on the leaching of tripartite RNA aptamers from the various sol-gel materials, the polarity (as judged by contact angle) and morphology of all materials were assessed. Table S2.1 showed that all silica-based materials, with or without added APTES, had contact angles in the range of 16 – 28 degrees, indicative of highly polar, hydrophilic materials. Addition of MTMS caused a non-linear increase in contact angle, with only moderate increases in contact angle up to 40% MTMS (49 degrees), followed by a large increase in contact angle to 91 degrees at 60% MTMS and 120 degrees for MSQ, indicative of a highly hydrophobic material. The morphology of the materials was also highly

dependent on composition, with high surface areas and namometer scale pores, indicative of mesoporous materials, being observed up to 60% MTMS, followed by a sudden change to low surface area macroporous materials at 80% MTMS and above (see scanning electron microscopy images of all materials in Table S2.2). These data show that the switchover from predominantly silica to predominantly MSQ-based materials resulted in a loss of mesopores and a tendency toward phase separation to generate macropores.[42]

Leaching of Aptamers from Sol-Gel Derived Materials. The extent of leaching of the entrapped aptamer was evaluated for each material, as indicated in Figure 2.2. Leaching ranged from a low of ~5% in SS materials to ~30% in materials containing up to 80% MTMS, and then increased to 60-80% in pure MSQ materials, depending on the aptamer, demonstrating the general trend of increased leaching with increased hydrophobicity and increased pore size. Leaching was generally higher for the anti-TPP aptamer relative to the anti-theophylline aptamer, and typically occurred predominantly during the first washing step. The very large extent leaching in pure MSQ materials is likely reflective of the lack of mesopores, which would be expected to retain the small aptamers while macropores would not. The MSQ materials also are unlikely to be able to template around the RNA aptamers to aid in retention, as has been reported for some proteins entrapped in silica.[51]

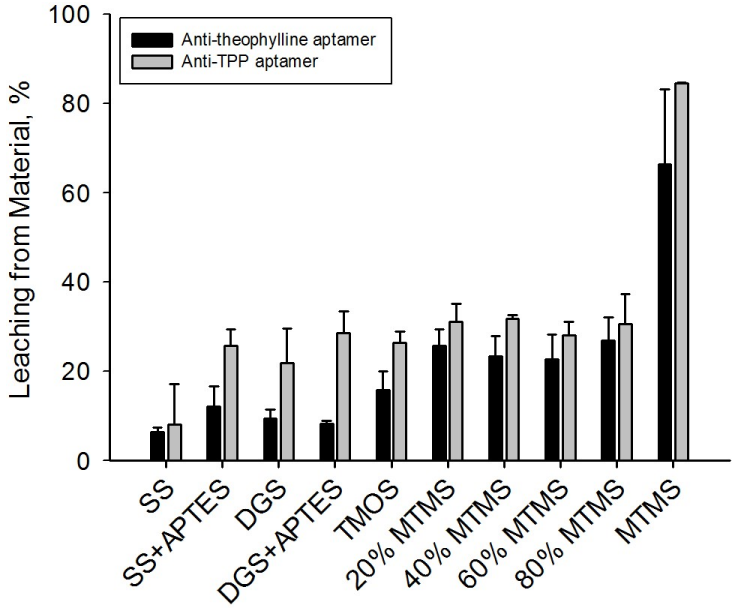

Figure 2.2. Leaching of the anti-theophylline and anti-TPP RNA aptamer reporter constructs from various sol-gel derived materials.

The overall degree of leaching is relatively high compared proteins, but is similar to that of DNA aptamers entrapped in polar silica monoliths.[50] This previous study found that the attachment of a bulky streptavidin protein to biotinylated DNA, used to enlarge the molecular complex, did not improve leaching within error. Use of steptavidin would also be incompatible with the use of hydrophobic composites, and thus this strategy was not examined in this study. It is important to note that since fluorescence intensity measurements are used to determine the amount of leaching, the FDNA cannot be distinguished from the FDNA-aptamer complex. However, given that the FDNA is essential for signaling target binding in the tripartite design, measuring leaching of these short 20-nt oligonucleotide components is of equal importance for this reporter system.

Signal generation from entrapped RNA aptamer reporters. A key requirement for entrapped structure-switching signaling aptamers is the ability to undergo conformational changes upon binding of ligands and to subsequently release the QDNA strand to elicit a fluorescence response. Experiments were performed to assess the degree of signal enhancement upon target binding for each RNA aptamer entrapped in the full series of sol-gel derived materials. All materials were first washed to remove leachable aptamers, followed by addition of either 1 mM theophylline or 100 μM TPP to the appropriate RNA reporter system. Figure 2.3 shows relative fluorescence enhancement and rate of signal development for each of the RNA aptamers when in solution and entrapped in the various sol-gel derived materials. Consistent with the previous findings,[33] full signal development required a longer time for the anti-TPP aptamer relative to the anti-theophylline aptamer, even in solution. When entrapped, both aptamer reporter systems were able to structure-switch and produce a fluorescence signal in all materials, however, the signal enhancements and rates of signal development were highly dependent on the type of sol-gel derived material used for entrapment.

Composite MTMS/TMOS materials always produced higher signal enhancements than polar silica materials (SS, DGS) or nonpolar MSQ materials. Previous studies have shown that only a small fraction (~10%) of biomolecules entrapped in polar materials are inaccessible to external analytes,[50,52136,137] thus the loss of signal in polar materials likely reflects electrostatic aptamer backbone-silica interactions that prevented structure switching of the aptamer. The high silica content of polar materials may also be detrimental

to the chemical stability of RNA by promoting hydrolysis reactions, which cause cleavage of the phosphodiester linkages to degrade the aptamer.[16]

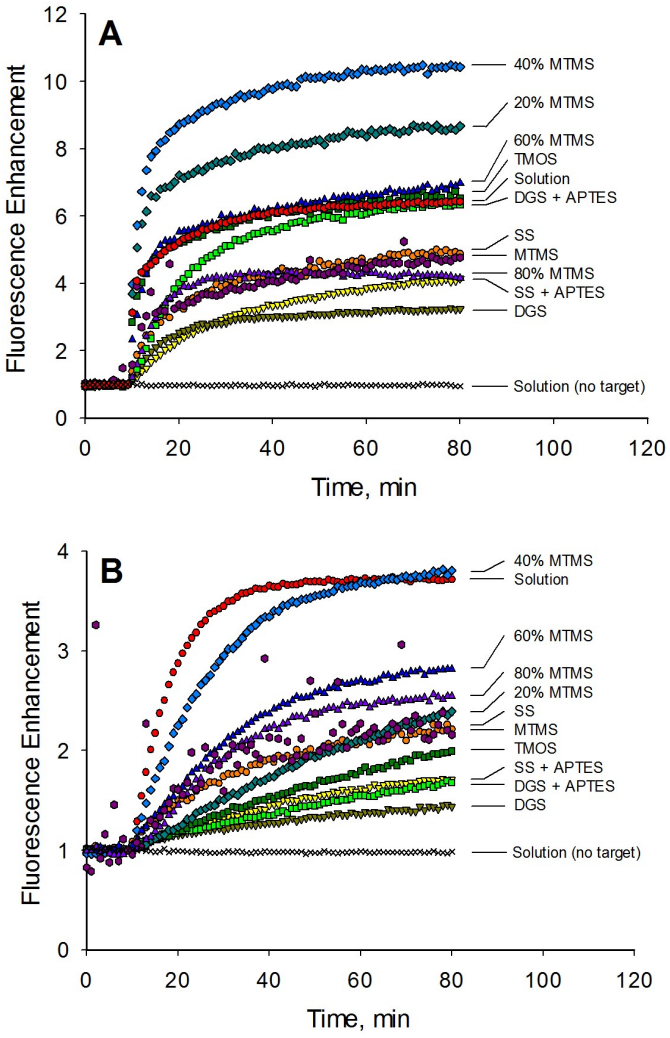

Figure 2.3. Fluorescence signaling ability of RNA aptamer reporters in solution and in various sol-gel derived materials. Target-induced response of the (A) theophylline-binding aptamer and (B) TPP-binding aptamer upon exposure to 1 mM theophylline and 100 µM TPP, respectively, after 10 min baseline incubation.

DGS derived materials demonstrated the lowest enhancement for both aptamers, which is not surprising since it has been suggested that glycerol modifies electrostatic interactions between polynucleotides[53] and destabilizes double-stranded DNA.[54] Thus, this byproduct of DGS condensation, though proven as a stabilizer of proteins, appears to destabilize the double-stranded structure required for the intact RNA aptamer reporter complex, causing higher background fluorescence and a poorer signal enhancement. Interestingly, both reporters showed decreased signal enhancements when entrapped in SS+APTES (compared to SS materials) while the addition of APTES to DGS improved the signal generation, particularly for the anti-theophylline aptamer. The inconsistent results related to the addition of APTES are not fully understood, but suggest that this species may be located in different environments in SS relative to DGS derived materials or the strength of its electrostatic effects differ in materials with varied porosity and pore size, as suggested by previous studies entrapping DNA in cationic hydrogels.[55] The low signal enhancement and high variability in pure MSQ materials is most likely due to the significant leaching of the reporters from this particular matrix.

The best overall performance for both aptamers (highest signal enhancement and fastest signal development) was observed using an organic-inorganic hybrid material composed of 40% MTMS and 60% TMOS (v/v), suggesting that this material had the best balance of polarity and surface charge that minimized analyte- and/or RNA-surface interactions while retaining enough conformational flexibility to allow for structure-switching and signaling to occur. When compared to the signal enhancement obtained in solution, the entrapped theophylline-binding RNA generated a greater enhancement, up to 10-fold (compared to

6-fold in solution). The signal enhancement of the TPP-binding aptamer was comparable to that of the solution, with almost a 4-fold enhancement. The high signal enhancements observed for both aptamers using this material may also be due to alterations in the local pH of the microenvironment around the aptamers or restriction of RNA backbone mobility caused by entrapment in the pores of a partially hydrophobic composite matrix.

Indeed, under neutral or alkaline pH conditions (in the presence of alkali metals and alkali-earth metals), the dominant pathway for RNA chemical degradation is the internal phosphoester transfer reaction via an S_N2 mechanism wherein the 2'-oxygen attacks the adjacent phosphorus center.[56] The protonation state of this 2'-oxygen largely dictates this rate of transesterification, which is enhanced by specific base catalysis through deprotonation of the 2'-hydroxyl group to the more nucleophilic 2'-oxyanion group.[57] Thus, in solution, constant bombardment with hydroxide ions increases the fraction of these reactive 2'-oxyanion group to promote RNA cleavage. However, when entrapped in a sol-gel derived matrix, the RNA species interacts with only a few hydroxide ions present in the thin solution layer between the biomolecule and the material surface,[58] effectively decreasing the hydroxide-dependent degradation rate. Moreover, previous studies[59] have shown that the apparent pK_a of pH sensitive dyes increases when entrapped in organic-inorganic composites, demonstrating that the pH within the composites is less basic that in the surrounding solution (i.e., a probe with a pK_a of 6.0 in solution has an apparent pK_a of 8.3 in materials composed of MTES/TEOS).

The physical restriction of RNA mobility may also stabilize the secondary structure of the entrapped RNA aptamers, promoting FDNA/QDNA hybridization for a lower

background signal and preventing sampling of in-line geometries that induce intramolecular cleavage.[18] These effects would be more evident using the smaller theophylline-binding aptamer, which has a larger amount of its sequence hybridized to DNA and a shorter flexible single-stranded region that is less likely to sample conformations susceptible to spontaneous cleavage, producing the significant improvement in signaling that was observed for this particular aptamer. Nevertheless, additional experimentation is currently underway to better examine the specific effects of entrapment in inorganic materials that chemically stabilize RNA.

Sensitivity and selectivity of entrapped RNA aptamer reporters. Figure 2.4A and 2.4B show the target concentration-dependent signal enhancements of the anti-theophylline and anti-TPP aptamers, respectively, when entrapped in the 40% MTMS material and in solution. The anti-theophylline RNA reporter demonstrated a similar detection limit and dynamic range to that reported in solution (1-1000 μM) while the anti-TPP aptamer had a detection limit of 1 μM, which was 10-fold worse than the value in solution, and an upper concentration range of 100 μM, which was similar to the value in solution.[33] The poorer detection limit may be due to the exclusion of the anionic TPP from the hydrophobic matrix, which would require a higher external concentration to reach a sufficient internal concentration to produce signaling. Interestingly, the use of initial rate data provided a broader dynamic range for TPP sensing while maintaining the detection limit of 1 μM (Figure 2.4B, inset).

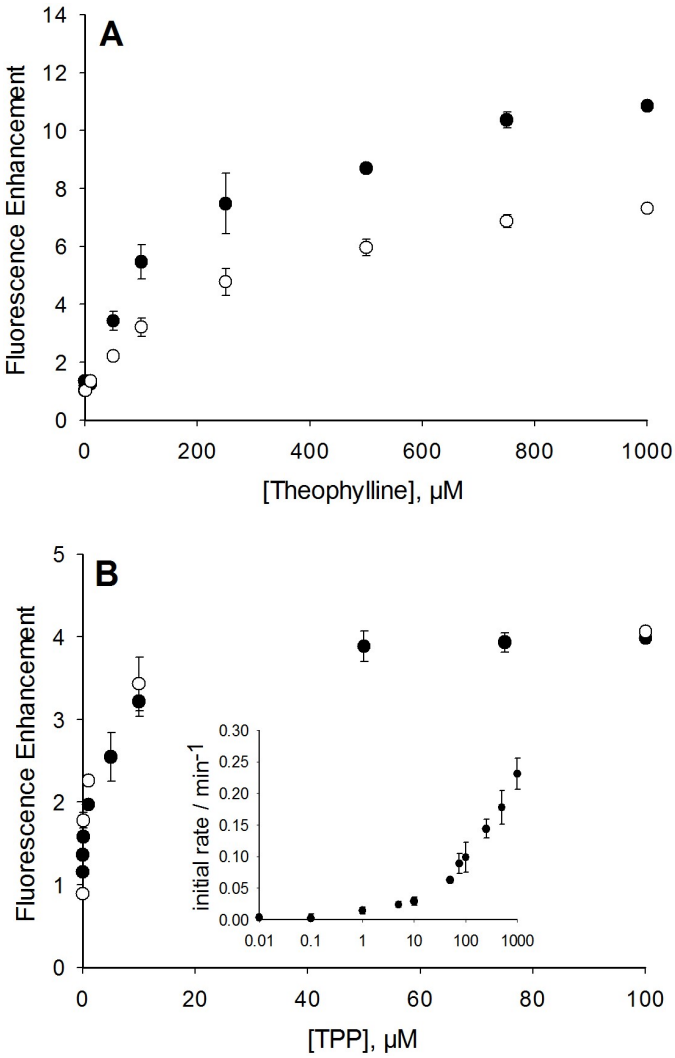

Figure 2.4. Sensitivity of the sol-gel entrapped RNA aptamer reporters. Response curve of the (A) theophylline-binding aptamer to increasing theophylline concentrations and (B) TPP-binding aptamer to increasing TPP concentrations, either entrapped in the 40% MTMS material (●) or in solution (○). Inset (B): Change in initial signaling rate of the entrapped TPP-binding aptamer when exposed to increasing TPP concentrations.

The selectivity of entrapped RNA reporters was assessed using molecules that were chemically similar to their targets. These included caffeine and theobromine for the theophylline-binding aptamer and thiamine monophosphate (TMP), thiamine and

oxythiamine for the TPP-binding aptamer. Mutant versions of each RNA aptamer were also entrapped and subjected to either theophylline or TPP at concentrations of 1 mM and 100 μM, respectively. Selectivity was maintained for both entrapped aptamer systems, with little to no change in signal when using structural derivatives of targets or mutant constructs (Figure S2.1).

RNA aptamer sensitivity to ribonucleases. Previous studies have shown that entrapping DNA aptamers within a polyacrylamide hydrogel[60] or silica matrix[50] can provide a steric barrier to digestive enzymes, such as DNase I. To assess the protective effects of entrapment in MTMS/TMOS composites on the RNA reporters, the stability of free (solution) and entrapped aptamers towards digestion by two different ribonucleases was compared. RNase A was chosen since it is abundant in biological fluids and is pyrimidine-specific,[138] while RNase H is known to degrade the RNA from RNA/DNA hybrids[139] such as the tripartite reporter complex in this work. Degradation by either ribonuclease can be monitored by an increase in fluorescence as the distance between the fluorescein and dabcyl moieties increases due to release of the QDNA, FDNA or both from the digested RNA aptamer strand. As shown in Figure 2.5, the addition of RNase A or RNase H to either RNA aptamer reporter in solution resulted in an increase in fluorescence of greater than 20-fold and 4-fold, respectively. In the case of the aptamers entrapped in the 40% MTMS sol-gel derived material, less than 4-fold and 2-fold fluorescence enhancements were observed upon addition of RNase A or RNase H, respectively.

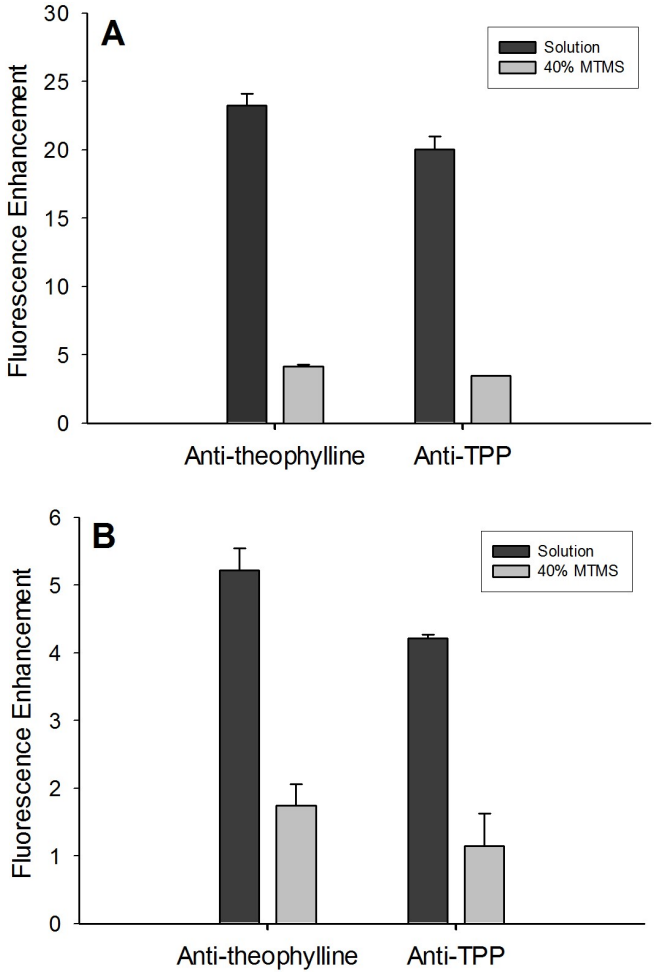

Figure 2.5. Changes in emission intensity of RNA aptamer reporters upon exposure to RNase A or RNase H. Fluorescence measurements 2 hrs after addition of 3 units of (A) RNase A or (B) RNase H to the theophylline-binding and TPP-binding reporter constructs in solution or entrapped within the sol-gel derived material.

These results indicate that both ribonucleases are unable to enter the material and access the entrapped RNA aptamers, producing 80% less digestion with RNase A and 70% less digestion when using RNase H. The small amount of degradation is likely due to the digestion of aptamer molecules that reside very close to the surface of the small silica disks (less than 1 mm thickness) that have a much higher surface area-to-volume ratio than

typical large bulk monoliths, which is more representative of a biosensor design that minimizes target diffusion time. Overall, these results indicate that the entrapped RNA was not accessible to the RNase enzymes and thus was well-protected from digestion when entrapped in the mesoporous matrix.

Effects of long-term storage on RNA aptamer activity. We examined the long-term stability of the RNA reporters entrapped in the 40% MTMS material and compared it to that of the RNA reporters in solution. Figure 2.6 demonstrates that when in solution, the activity of the theophylline-binding aptamer after 1 week is not much lower than in a freshly prepared solution, while that of the 1 week old TPP-binding aptamer is at almost half the original activity. This is consistent with the hypothesis that the larger anti-TPP aptamer undergoes greater intrinsic cleavage due to in-line nucleophilic attack. However, after 1 month of storage, both RNA aptamer reporters show relatively low signal enhancements upon target addition with about 2-fold increase for the anti-theophylline aptamer and 1.5-fold enhancement with the anti-TPP aptamer. This loss in signal is due to higher fluorescence backgrounds as the RNA is degraded over time, releasing the fluorescent moiety from its close interaction with its quencher prior to introduction of their cognate targets.

When these aptamers were entrapped in the 40% MTMS material and then stored up to 1 month, the signal enhancements were maintained above 8-fold and 2.5-fold for the theophylline-binding and TPP-binding aptamers, respectively. The observed loss of activity (~20-30 %) likely reflects continued evolution of the sol-gel matrix, which could

lead to pore shrinkage and subsequent restriction of dynamic motion or restriction of access for the entrapped RNA[42,63] (currently under investigation).

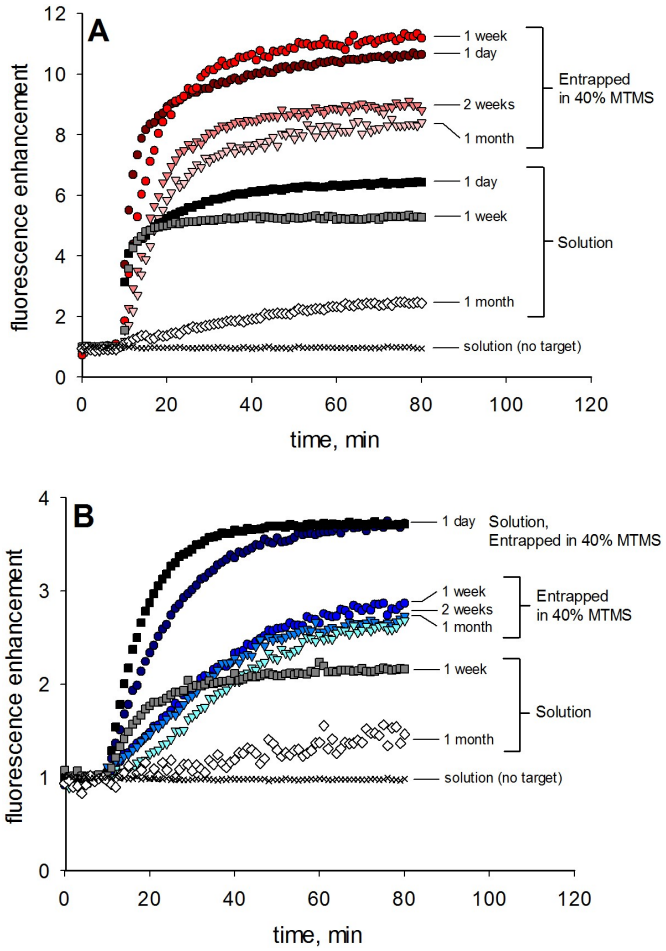

Figure 2.6. Structure-switching and signaling ability of RNA aptamer reporters after different storage time. Target-induced fluorescence signaling ability of solution-based or entrapped RNA aptamer reporters after increasing storage time at 4 °C of the (A) theophylline-binding aptamer using 1mM theophylline and (B) TPP-binding aptamer using 100 µM TPP, after 10 min baseline incubation.

Initial fluorescence levels of all aged materials (1 week to 1 month) were slightly lower than those of newly-prepared composites, indicating that the entrapped aptamers were not being degraded upon storage, although further leaching of surface-proximal RNA during the longer storage periods may have contributed to the observed loss in activity (fluorescence intensity values provided in Table S2.3). The ability to remove leached FDNA or degraded aptamer so as to lower background signals highlights another benefit of entrapment over solution-based studies. In general, although the signal enhancements of both aptamers are slightly reduced over the first 1-2 weeks, the signaling ability is maintained over an extended storage time, highlighting the ability of the matrix to protect the RNA aptamers from both intrinsic chemical instability and external enzymatic degradation, and leading to a more robust solid-phase sensor.

2.4 Conclusions

A simple and general approach for improving the stability of RNA aptamers is demonstrated based on their entrapment in a sol-gel derived composite material. Two different RNA aptamer reporters retained maximum sensitivity and selectivity when entrapped in an organic-inorganic composite material prepared by co-hydrolysis and condensation of 40% MTMS and 60% TMOS (v/v). Since the RNA reporter system was entrapped in the pores of the sol-gel derived matrix, it was relatively well protected from nuclease degradation and, perhaps more importantly, the composite material also reduced the extent of in-line chemical degradation, providing the long-term stability required of a robust biosensor. As such, this immobilization scheme expands the use of functional

nucleic acids from the limited number of DNA aptamers to the much broader range of relatively unexplored RNA aptamer species.

Importantly, sol-gel derived materials possess significant versatility in that they are amenable to many configurations, including microarrays, bioaffinity columns or thin-film coatings for interfacing to various analytical devices.[43,64103,140] Although the current study focuses on fluorescence signaling in monolithic materials, the use of the sol-gel method for biomolecular entrapment has been utilized in both colorimetric and electrochemical sensors[141] and thus presents a broadly applicable platform for preparing solid-phase RNA aptamer sensors. Such biosensors may find wide appeal in environmental and clinical analysis, particularly for the detection of small metabolites, an area where elicitation of monoclonal antibodies is difficult.

2.5 Experimental

2.5.1 Materials. All DNA oligonucleotides were synthesized using standard phosphoramidite chemistry by Integrated DNA Technologies (Coralville, IA) and purified by 10% denaturing PAGE prior to use. Fluorescently-labeled DNA oligonucleotides were purified by HPLC as described elsewhere.[30] Theophylline, theobromine, caffeine, thiamine pyrophosphate (TPP), thiamine monophosphate (TMP), thiamine, oxythiamine, tetramethylorthosilicate (TMOS), methyltrimethoxysilane (MTMS), 3-(aminopropyl)triethoxysilane (APTES) and Dowex 50×8-100 cation exchange resin were obtained from Sigma-Aldrich (Oakville, ON). Ribonuclease A (RNase A) and ribonuclease H (RNase H) were purchased from Fermentas Life Sciences (Burlington,

ON). Sodium silicate solution (SS solution, ultrapure grade, ~14% Na_2O, ~29% silica) was purchased from Fisher Scientific (Pittsburg, PA). Diglycerylsilane (DGS) was prepared from TMOS as described elsewhere.[66,67] Water was purified with a Milli-Q Synthesis A10 water purification system and autoclaved. Buffer salt solutions were autoclaved after preparation and all other chemicals and solvents were of analytical grade and were used as received.

2.5.2 Methods.

Preparation of RNA aptamers and reporter constructs. Polymerase chain reaction of the DNA templates for the theophylline and TPP aptamer, as well as RNA transcription of these RNA aptamers, was performed as described elsewhere.[33] The specific DNA template sequences used in this work were as follows.

DNA template for the theophylline reporter: 5'-GAATT CTAAT ACGAC TCACT ATAGG CCTGC CACGC TCCGA CGCTA TCACT CTATG GGCGA TACCA GCCGA AAGGC CCTTG GCAGC GTCCA ACACA TCG-3' (in the mutant **1** template, C_{64} and A_{83} were mutated to A_{64} and T_{83}; in the mutant **2** template, $C_{63}C_{64}$ were replaced with $G_{63}A_{64}$)

Theophylline aptamer template forward primer: 5'-GAATT CTAAT ACGAC TCACT ATA-3'

Theophylline aptamer template reverse primer: 5'-CGATG TGTTG GACGC-3'

DNA template for the TPP reporter: 5'-GAATT CTAAT ACGAC TCACT ATAGG CCTGC CACGC TCCGA CGCTA TCACT CTATG CCACT AGGGG TGCTT GTTGT

GCTGA GAGAG GAATA ATCCT TAACC CTTAT AACAC CTGAT CTAGG TAATA CTAGC GAAGG GAAGT GG-3' (mutant **1** template was made by replacing G_{60}, G_{74}, G_{76}, A_{77} and G_{126} with C_{60}, C_{74}, T_{66}, T_{67}, T_{126}, while in the mutant **2** template, G_{60}, T_{73},G_{74}, G_{76}, A_{77}, C_{125}, G_{126}, G_{131}, A_{132} were mutated to C_{60}, C_{73}, C_{74}, T_{66},T_{67}, A_{125}, T_{126}, C_{131}, G_{132})

TPP aptamer template forward primer: 5'-GAATT CTAAT ACGAC TCACT ATA-3'

TPP aptamer template reverse primer: 5'-GCTTC TGTTC CCACT-3'

The tripartite complexes of these RNA aptamer reporters were prepared by combining 80 nM of the extended RNA aptamer with 40 nM of FDNA and 120 nM of QDNA in 50 mM Tris·HCl (pH 7.5) with 20 mM $MgCl_2$. This mixture was first heated at 65 °C for 2 min, cooled at room temperature for 10 min, and then stored at 4 °C until analysis. The sequences of the fluorescein-labeled (FDNA) and DABCYL-labeled (QDNA) oligonucleotides were as follows.

Theophylline/TPP aptamer FDNA: 5'-**F**TAGCG TCGGA GCGTG GCAGG-3'

Theophylline aptamer QDNA: 5'-TATCG CCCAT AGAGT G**Q**-3'

TPP aptamer QDNA: 5'-CTAGT GGCAT AGAGT G**Q**-3'

Entrapment of aptamers within sol-gel derived materials. Silane and organosilane precursors were used to prepare the sols for aptamer entrapment studies, including SS, DGS, TMOS, APTES and MTMS. Sodium silicate sols were prepared as described elsewhere[68] by diluting 2.6 g of a stock SS solution to 10 mL with water, mixing the solution with 5.5 g DOWEX to bring the pH of the SS solution to ~4, and then filtering this solution through a Büchner funnel to remove the resin followed by further filtration

through a 0.45 μM membrane syringe filter to remove any particulates in the solution. The DGS precursor sol was prepared by grinding DGS to a fine powder and dissolving 0.5 g in 1 mL of water, followed by 15 min sonication in ice-cold water and filtering the solution through a 0.2 μM membrane syringe filter. Materials containing 0.1% (v/v) APTES in either SS or DGS were also tested, with the APTES added to the sol prior to addition of aptamer solutions. To make TMOS and MTMS sols, 700 μL of water and 50 μL HCl (0.1 N) were added to 2.25 mL TMOS or MTMS and then sonicated for 20 min in ice-cold water as described elsewhere.[51] The TMOS-MTMS mixtures were prepared by proportionally dividing the 2.25 mL of silane using volume percentages of 20 - 80 % MTMS in TMOS, mixing with water and acid and co-hydrolyzing in a sonicator as described above.

Tripartite aptamer complexes (in a 1:2:3 FDNA:RNA:QDNA molar ratio) for entrapment were prepared at double the concentration of typical solutions in 100 mM Tris·HCl (pH 7.5) with 40 mM $MgCl_2$ and heated at 65 °C for 2 min, cooled at room temperature for 10 min, then stored at 4 °C until mixing in a 1:1 volume ratio with a freshly-prepared silica sol at room temperature. The aptamer-sol mixtures were deposited into 96-well microtiter plates at a volume of 50 μL per well and allowed to gel. These plates were then left to age at 4 °C for at least 4 hrs and then overlayed with 100 μL of 50 mM Tris·HCl (pH 7.5) with 20 mM $MgCl_2$ prior to washing and analysis.

Characterization of sol-gel derived silica morphology. Larger monoliths (3 mL total volume of 1:1 sol-gel precursor:buffer, v:v) of the various sol-gel derived materials

described above were prepared without entrapped aptamer. After gelation, all monoliths were cured in air for 4-6 h at 20 °C prior to aging for 5 days in sealed vials. Water contact angle measurements were performed using a Krüss drop shape analyzer system (DSA10, Dataphysics) at 25 ºC by applying conventional sessile drops on the material surface. Average contact angle was calculated from three values obtained from different areas of each sample. These monoliths were then desiccated for another 7 days, crushed and outgassed for 8 – 12 h to remove air and residual water from the surface prior to performing porosimetry measurements. Nitrogen porosimetry and mercury intrusion analyses were carried out as described in detail elsewhere.[69] Samples for SEM imaging were aged for 10 days before analysis and coated with 5 nm of platinum under vacuum to improve conductivity. Imaging was performed at 5 kV using a JEOL JSM 7000F Scanning Electron Microscope.

Leaching studies. Prior to any fluorescence measurements, the various sol-gel derived materials containing the reporter complexes were washed three times with 100 μL buffer at room temperature to remove any un-encapsulated RNA from the material surface. Leaching of entrapped aptamers from the materials was determined by comparing the total fluorescence intensity prior to any washing to that of washed materials, as well as the fluorescence intensity of the wash solutions for all three washes.

Target-binding assays. All fluorescence assays were performed at 37 °C using a Tecan M1000 platereader. Both solution and sol-gel entrapped aptamer samples were excited at

490 nm and emission was collected at 520 nm using a 5-nm bandpass for both excitation and emission with a 0.5 s integration time using the bottom-read setting. Analytes (3 μL at the appropriate concentration) were either added directly to solution samples or the overlaying buffer of material samples after measuring initial baseline fluorescence for 10 min (stock analyte solutions were heated at 90 °C for 5 min and cooled to room temperature for 10 min prior to addition to ensure no contaminant RNase was introduced). Fluorescence emission was measured every 1 min for both baseline measurements and after target addition for a total of 80 min. Samples were corrected for light scattering by blank subtraction of signals originating from the materials or buffer without RNA reporters present. All fluorescence measurements are reported as fluorescence enhancement or F/F_o where F is the endpoint fluorescence intensity and F_o is the initial fluorescence intensity prior to target addition. Time-dependent measurements are represented by the average values of three independent experiments (with less than 10% variability), while error bars indicate the standard deviation of three independent experiments in endpoint bar graphs.

RNase protection assays. Either three (Kunitz) units of RNase A or three units of RNase H was added directly to solution samples or the overlaying buffer of material samples after measuring initial baseline fluorescence for 10 min, and fluorescence emission was measured every 1 min for 120 min using the same settings as were used for the target-binding fluorescence measurements.

Storage stability studies. The 40% MTMS materials containing the tripartite aptamer complexes were prepared and aged as described above. These materials were overlayed with 150 μL buffer and the microwell plates were covered with lids and wrapped in Parafilm to prevent evaporation upon storage. Plates were stored for 1 week, 2 weeks or 1 month at 4 °C in the dark prior to target-binding measurements, and were compared to materials that had been aged for 1 day. Solutions containing the tripartite aptamer complexes were prepared in microcentrifuge tubes and stored for up to 1 month at 4 °C prior to target-binding measurements.

2.6 Acknowledgements

The authors thank the Natural Sciences and Engineering Research Council of Canada (NSERC) and the SENTINEL Bioactive Paper Network for funding this work. The authors also thank the Canada Foundation for Innovation and the Ontario Innovation Trust for support of this work. YL holds the Canada Research Chair in Directed Evolution of Nucleic Acids. JDB holds the Canada Research Chair in Bioanalytical Chemistry and Biointerfaces.

2.7 References

(1) Wilson, D. S.; Szostak, J. W. *Annu. Rev. Biochem.* **1999**, *68*, 611-47.
(2) Ellington, A. D.; Szostak, J. W. *Nature* **1990**, *346*, 818-22.
(3) Tuerk, C.; Gold, L. *Science* **1990**, *249*, 505-10.
(4) Jayasena, S. D. *Clin. Chem.* **1999**, *45*, 1628-50.
(5) Clark, S. L.; Remcho, V. T. *Electrophoresis* **2002**, *23*, 1335-40.
(6) Hamula, C. L. A.; Guthrie, J. W.; Zhang, H.; Li, X.-F.; Le, X. C. *TrAC-Trends Anal. Chem.* **2006**, *25*, 681-691.
(7) Song, S. P.; Wang, L. H.; Li, J.; Zhao, J. L.; Fan, C. H. *TrAC-Trends Anal. Chem.* **2008**, *27*, 108-117.
(8) Sefah, K.; Phillips, J. A.; Xiong, X.; Meng, L.; Van Simaeys, D.; Chen, H.; Martin, J.; Tan, W. *Analyst* **2009**, *134*, 1765-75.
(9) Liu, J.; Cao, Z.; Lu, Y. *Chem. Rev.* **2009**, *109*, 1948-98.
(10) Silverman, S. K. In *Functional Nucleic Acids for Analytical Applications*; Li, Y., Yi, L., Eds.; Springer New York, 2009; pp 47-108.
(11) Klug, S. J.; Famulok, M. *Mol. Biol. Rep.* **1994**, *20*, 97-107.
(12) Marshall, K. A.; Ellington, A. D. *Methods Enzymol.* **2000**, *318*, 193-214.
(13) Winkler, W. C.; Breaker, R. R. *Chembiochem* **2003**, *4*, 1024-32.
(14) Mandal, M.; Breaker, R. R. *Nat. Rev. Mol. Cell Biol.* **2004**, *5*, 451-63.
(15) Montange, R. K.; Batey, R. T. *Annu. Rev. Biophys.* **2008**, *37*, 117-33.
(16) Oivanen, M.; Kuusela, S.; Lonnberg, H. *Chem. Rev.* **1998**, *98*, 961-990.
(17) Li, Y.; Breaker, R. R. *J. Am. Chem. Soc.* **1999**, *121*, 5364-5372.
(18) Soukup, G. A.; Breaker, R. R. *RNA* **1999**, *5*, 1308-25.
(19) Famulok, M.; Mayer, G.; Blind, M. *Acc. Chem. Res.* **2000**, *33*, 591-599.
(20) Pieken, W. A.; Olsen, D. B.; Benseler, F.; Aurup, H.; Eckstein, F. *Science* **1991**, *253*, 314-7.
(21) Cummins, L. L.; Owens, S. R.; Risen, L. M.; Lesnik, E. A.; Freier, S. M.; McGee, D.; Guinosso, C. J.; Cook, P. D. *Nucleic Acids Res.* **1995**, *23*, 2019-24.
(22) Kubik, M. F.; Bell, C.; Fitzwater, T.; Watson, S. R.; Tasset, D. M. *J. Immunol.* **1997**, *159*, 259-67.
(23) Kujau, M. J.; Wolfl, S. *Nucleic Acids Res.* **1998**, *26*, 1851-3.
(24) Kusser, W. *J Biotechnol* **2000**, *74*, 27-38.
(25) Jellinek, D.; Green, L. S.; Bell, C.; Lynott, C. K.; Gill, N.; Vargeese, C.; Kirschenheuter, G.; McGee, D. P.; Abesinghe, P.; Pieken, W. A. *Biochemistry* **1995**, *34*, 11363-72.
(26) Burmeister, P. E.; Lewis, S. D.; Silva, R. F.; Preiss, J. R.; Horwitz, L. R.; Pendergrast, P. S.; McCauley, T. G.; Kurz, J. C.; Epstein, D. M.; Wilson, C.; Keefe, A. D. *Chem. Biol.* **2005**, *12*, 25-33.
(27) Klussmann, S.; Nolte, A.; Bald, R.; Erdmann, V. A.; Furste, J. P. *Nat. Biotechnol.* **1996**, *14*, 1112-5.
(28) Leva, S.; Lichte, A.; Burmeister, J.; Muhn, P.; Jahnke, B.; Fesser, D.; Erfurth, J.; Burgstaller, P.; Klussmann, S. *Chem. Biol.* **2002**, *9*, 351-9.
(29) Eulberg, D.; Klussmann, S. *ChemBioChem* **2003**, *4*, 979-83.

(30) Nutiu, R.; Li, Y. *J. Am. Chem. Soc.* **2003**, *125*, 4771-8.
(31) Jenison, R. D.; Gill, S. C.; Pardi, A.; Polisky, B. *Science* **1994**, *263*, 1425-9.
(32) Welz, R.; Breaker, R. R. *RNA* **2007**, *13*, 573-82.
(33) Lau, P. S.; Coombes, B. K.; Li, Y. *Angew. Chem. Int. Ed.* **2010**, *49*, 7938-42.
(34) Potyrailo, R. A.; Conrad, R. C.; Ellington, A. D.; Hieftje, G. M. *Anal. Chem.* **1998**, *70*, 3419-3425.
(35) Clark, S. L.; Remcho, V. T. *Anal. Chem.* **2003**, *75*, 5692-6.
(36) McCauley, T. G.; Hamaguchi, N.; Stanton, M. *Anal. Biochem.* **2003**, *319*, 244-250.
(37) Minunni, M.; Tombelli, S.; Gullotto, A.; Luzi, E.; Mascini, M. *Biosens. Bioelectron.* **2004**, *20*, 1149-56.
(38) Cho, E. J.; Collett, J. R.; Szafranska, A. E.; Ellington, A. D. *Anal. Chim. Acta* **2006**, *564*, 82-90.
(39) Min, K.; Cho, M.; Han, S. Y.; Shim, Y. B.; Ku, J.; Ban, C. *Biosens. Bioelectron.* **2008**, *23*, 1819-24.
(40) Lee, H. S.; Kim, K. S.; Kim, C. J.; Hahn, S. K.; Jo, M. H. *Biosens. Bioelectron.* **2009**, *24*, 1801-5.
(41) Ferapontova, E. E.; Olsen, E. M.; Gothelf, K. V. *J. Am. Chem. Soc.* **2008**, *130*, 4256-8.
(42) Brinker, C. J.; Scherer, G. W. *Sol-Gel Science*; Academic Press: New York, 1990.
(43) Brennan, J. D. *Acc. Chem. Res.* **2007**, *40*, 827-835.
(44) O'Driscoll, K. F. *Methods Enzymol.* **1976**, *44*, 169-83.
(45) Avnir, D.; Braun, S.; Lev, O.; Ottolenghi, M. *Chem. Mater.* **1994**, *6*, 1605-1614.
(46) Braun, S.; Rappoport, S.; Zusman, R.; Avnir, D.; Ottolenghi, M. *Mater. Let.* **1990**, *10*, 1-5.
(47) Bhatia, R. B.; Brinker, C. J.; Gupta, A. K.; Singh, A. K. *Chem. Mater.* **2000**, *12*, 2434-2441.
(48) Jin, W.; Brennan, J. D. *Anal. Chim. Acta* **2002**, *461*, 1-36.
(49) Pierre, A. C. *Biocatal. Biotransform.* **2004**, *22*, 145-170.
(50) Rupcich, N.; Nutiu, R.; Li, Y.; Brennan, J. D. *Anal. Chem.* **2005**, *77*, 4300-7.
(51) Shen, Y. T.; Mackey, G.; Rupcich, N.; Gloster, D.; Chiuman, W.; Li, Y. F.; Brennan, J. D. *Anal. Chem.* **2007**, *79*, 3494-3503.
(52) Sui, X.; Cruz-Aguado, J. A.; Chen, Y.; Zhang, Z.; Brook, M. A.; Brennan, J. D. *Chem. Mater.* **2005**, *17*, 1174-1182.
(53) Del Vecchio, P.; Esposito, D.; Ricchi, L.; Barone, G. *Int. J. Biol. Macromol.* **1999**, *24*, 361-9.
(54) Bonner, G.; Klibanov, A. M. *Biotechnol. Bioeng.* **2000**, *68*, 339-44.
(55) Joseph, K. A.; Dave, N.; Liu, J. *ACS Appl. Mater. Interfaces* **2011**, *3*, 733-39.
(56) Oivanen, M.; Kuusela, S.; Lonnberg, H. *Chem. Rev.* **1998**, *98*, 961-90.
(57) Li, Y.; Breaker, R. R. *J. Am. Chem. Soc.* **1999**, *121*, 5364-72.
(58) Frenkel-Mullerad, H.; Avnir, D. *J. Am. Chem. Soc.* **2005**, *127*, 8077-8081.
(59) Gulcev, M. D.; Goring, G. L. G.; Rakic, M.; Brennan, J. D. *Anal. Chim. Acta* **2002**, *457*, 47-59.

(60) Dave, N.; Chan, M. Y.; Huang, P.-J. J.; Smith, B. D.; Liu, J. *J. Am. Chem. Soc.* **2010**, *132*, 12668-73.
(61) Raines, R. T. *Chem. Rev.* **1998**, *98*, 1045-1066.
(62) Donis-Keller, H. *Nucleic Acids Res.* **1979**, *7*, 179-92.
(63) Keeling-Tucker, T.; Brennan, J. D. *Chem. Mater.* **2001**, *13*, 3331-3350.
(64) Monton, M. R. N.; Forsberg, E. M.; Brennan, J. D. *Chem. Mater.* **2011**, *24*, 796-811.
(65) Avnir, D.; Coradin, T.; Lev, O.; Livage, J. *J. Mater. Chem.* **2006**, *16*, 1013-1030.
(66) Brook, M. A.; Chen, Y.; Guo, K.; Zhang, Z.; Brennan, J. D. *J. Mater. Chem.* **2004**, *14*, 1469-1479.
(67) Brook, M. A.; Chen, Y.; Guo, K.; Zhang, Z.; Jin, W.; Deisingh, A.; Cruz-Aguado, J.; Brennan, J. D. *J. Sol-Gel Sci. Technol.* **2004**, *31*, 343-348.
(68) Carrasquilla, C.; Li, Y.; Brennan, J. D. *Anal. Chem.* **2011**, *83*, 957-65.
(69) Besanger, T. R.; Hodgson, R. J.; Guillon, D.; Brennan, J. D. *Anal. Chim. Acta* **2006**, *561*, 107-118.

2.8 Supplementary Information

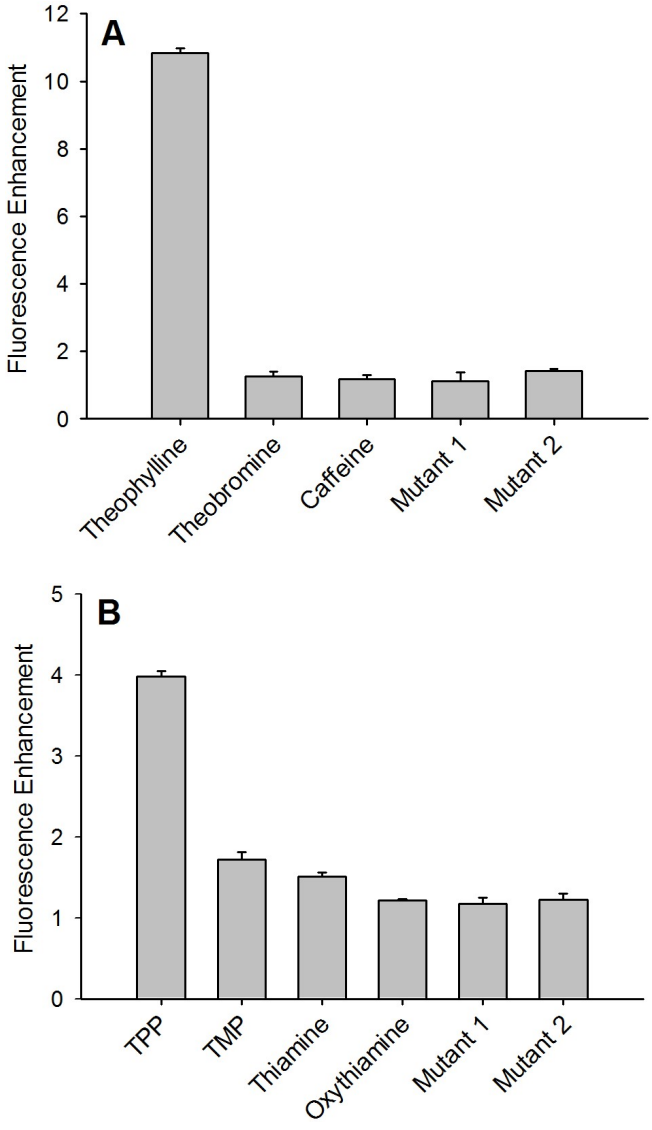

Figure S2.1. Selectivity of the sol-gel entrapped RNA aptamer reporters. Final signal enhancements of the (A) theophylline-binding aptamer and (B) TPP-binding aptamer to structurally similar molecules or using mutant aptamer constructs with the appropriate target.

Table S2.1. Contact angle (θ) and morphology of the sol-gel derived materials used for entrapment of RNA aptamer reporters.

Sample	Mean θ, °	BET surface area, $m^2\ g^{-1}$	Median pore diameter, nm	Total intruded volume, $cm^3\ g^{-1}$	Bulk particle density, $g\ cm^{-3}$	Porosity, %
Glass	25.51 ± 0.03	N/A	N/A	N/A	N/A	N/A
SS	16.3 ± 0.2	209.79	23.6	0.525	0.9755	51.22
SS+APTES	22 ± 1	206.97	8.1	0.229	1.2693	36.54
DGS	23.7 ± 0.2	508.20	16.0	0.245	1.4340	28.30
DGS+APTES	25 ± 2	506.85	6.5	0.185	1.4608	26.96
TMOS	28.7 ± 0.2	540.31	19.8	0.332	1.3826	30.87
20% MTMS	35.9 ± 0.1	600.03	7.7	0.185	1.1965	40.18
40% MTMS	49 ± 5	601.13	18.3	0.403	1.0839	45.80
60% MTMS	91 ± 1	499.46	15.0	0.320	1.0214	48.92
80% MTMS	105 ± 9	39.87	96.8	0.284	1.2749	36.26
MTMS	120 ± 13	36.95	172.8	0.407	1.3395	54.55

Table S2.2. Scanning electron microscopy (SEM) images of the various sol-gel derived materials used for RNA aptamer entrapment, 5000 x (bar = 1 μm).

SS 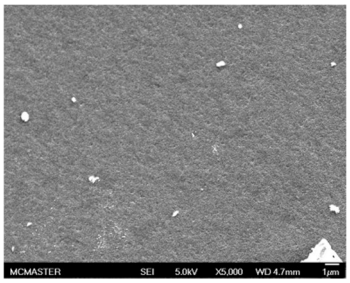	SS+APTES 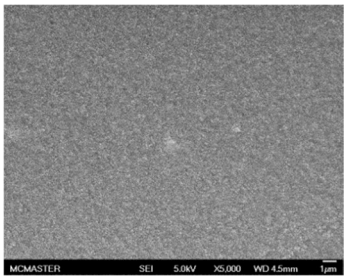
DGS 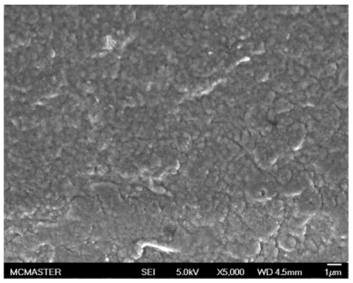	DGS+APTES 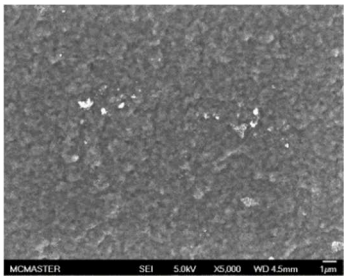
TMOS 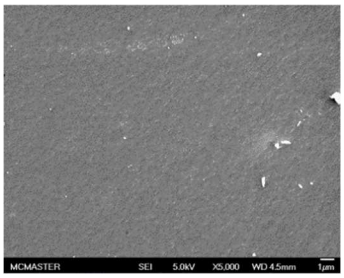	20% MTMS 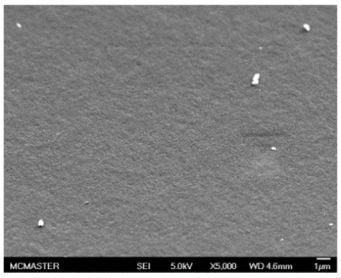
40% MTMS 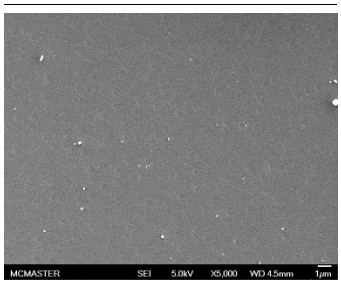	60% MTMS 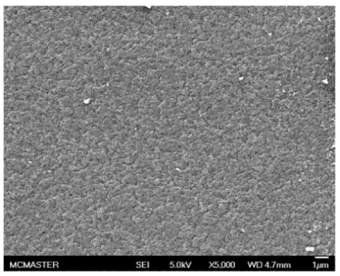
80% MTMS 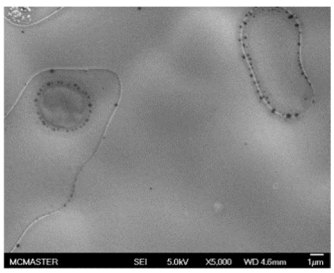	MTMS 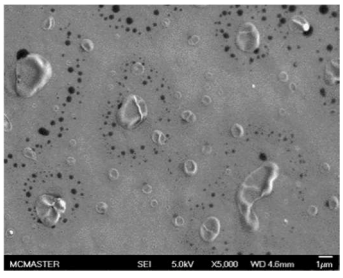

Table S2.3. Fluorescence intensity values in relative fluorescence units (RFU) of RNA aptamer reporters used in storage stability studies (1 day versus 1 month).

		Before Target	After Target	Before Target	After Target
		1 day (RFU)		1 month (RFU)	
Theophylline-binding aptamer	Solution	820 ± 20	5260 ± 200	1230 ± 40	3010 ± 70
	Entrapped	460 ± 10	4900 ± 180	350 ± 30	2930 ± 50
TPP-binding aptamer	Solution	3410 ± 90	12720 ± 180	5180± 120	7580 ± 220
	Entrapped	2040 ± 60	7620 ± 80	1390 ± 40	3720 ± 80

CHAPTER 3.

SOL-GEL DERIVED BIOHYBRID MATERIALS INCORPORATING LONG-CHAIN DNA APTAMERS

Author's Preface:

The work presented in the following chapter has been accepted for publication in the journal *Angewandte Chemie International Edition* with the citation:

Carrasquilla C, Kapteyn E, Li Y and Brennan JD. Sol-Gel Derived Biohybrid Materials Incorporating Long-Chain DNA Aptamers. *Angew. Chem. Int. Ed.* **2017** DOI: 10.1002/anie.201702859 and 10.1002/ange.201702859.

I was responsible for the experimental design, data analysis and interpretation. I performed a majority of the experiments with SEM imaging executed by Emily Kapteyn. I wrote the first draft of the manuscript. Dr. Brennan provided editorial revisions with input from Dr. Li to generate the final draft.

3.1 Abstract

Sol-gel derived bio/inorganic hybrid materials have been examined for diverse applications, including biosensing, affinity chromatography and drug discovery. However, such materials have mostly been restricted to the interaction between entrapped biorecognition elements and small molecules, owing to the requirement for nanometer-scale mesopores in the matrix to retain entrapped biorecognition elements. Herein, we report on a new class of macroporous bio/inorganic hybrids, engineered through a high-throughput materials screening approach, that entrap micron-sized concatemeric DNA aptamers. We demonstrate that the entrapment of these long-chain DNA aptamers allows their retention within the macropores of the matrix, so that aptamers can interact with high molecular weight targets such as proteins. Our approach overcomes the major limitation of conventional sol-gel derived biohybrid materials by enabling molecular recognition for targets beyond small molecules.

3.2 Introduction

The sol-gel process has been employed as a means of immobilizing biomolecules by entrapment in a porous material matrix for use in various solid-phase bioassay designs,[1-7] including bulk monolithic materials, thin films, microarrays, and capillary-scale monolithic columns. However, in all cases the retention of entrapped biomolecules is based on size exclusion, with proteins or nucleic acids entrapped in mesopores with diameters of under 10 nm. As such, these bio/inorganic hybrid materials are restricted to interactions with small molecules (usually under 2 kDa),[8] since larger targets are unable to access the recognition elements retained within the mesopores.[9-15]

To extend the molecular weight range of potential targets that can be analyzed using sol-gel derived biohybrid materials, it is necessary to produce materials with macroporous morphologies. To prevent leaching of biomolecules from such materials, it is possible to immobilize biomolecules to the surface of the material using covalent or affinity based interactions.[16-20] However, these methods require multiple processing steps, which are time consuming and can lead to issues with biomolecule denaturation, and have lower loading capability compared to sol-gel entrapment. An alternative method, which has never been reported before, is the entrapment of biomolecular species that are large enough to remain immobilized even in micron-sized pores. In such a case, these micron-size biomolecules should become accessible to a range of analytes, including proteins, allowing for a major expansion in the range of targets that can be analyzed by sol-gel derived biohybrids. This led us to investigate the entrapment of concatemeric DNA aptamers,

which can be easily produced by rolling circle amplification (RCA), as the molecular recognition element.

RCA is a biochemical reaction in which a DNA polymerase makes round-by-round copies of a circular single-stranded DNA template to produce very large single-stranded DNA amplicons that contain a repetitive DNA sequence.[21,22] Depending on the conditions used, these amplicons can reach megadalton molecular weights (MW) and then undergo a self-assembly process to form compact flower-like structure.[23,24] When the circular DNA template is designed to contain the complementary sequence of a DNA aptamer, its RCA reaction will generate long strands of DNA containing tandem repeats of an aptamer sequence,[25] which are referred to as concatemeric DNA aptamers in this report. Herein, we demonstrate that these MDa assemblies of concatemeric aptamers can be entrapped into specially-designed macroporous sol-gel derived composites with high target-binding activity and minimal leaching, allowing for fabrication of flow-through biosensors for targets ranging from small molecules to proteins.

Our initial goal was to identify an appropriate porous material for entrapping concatemeric aptamers. The morphology of sol-gel materials is affected by a number of parameters, including the silane precursors, buffer type and ionic strength (which control gelation time), the type, concentration and molecular weight of porogen (which control the timing and extent of phase separation), and reaction pH (controlling both gelation and phase separation times).[9,11,26] For this reason, we used a previously reported hierarchical screening approach,[26] wherein we synthesized and evaluated a range of sol-gel derived material formulations, to identify compositions with a pore structure that could: 1) retain

functional concatemeric aptamers with minimal leaching, 2) allow concatemer accessibility to both small molecule and protein targets, 3) produce self-supporting monolithic capillary columns, and 4) allow pressure-driven flow through a capillary column with low backpressure.

3.3 Results and Discussion

A total of 140 formulations were prepared from four different silica precursors – sodium silicate (SS), tetramethylorthosilicate (TMOS), methyltrimethoxysilane (MTMS) or 40% MTMS in TMOS – as these have previously been shown to be suitable for the entrapment of functional aptamers (see Supporting Information for further experimental detail).[27] Each of these was combined with seven different molecular weights of poly(ethylene glycol) (PEG), ranging from 600 – 10,000 Da, at varying concentrations (0, 1.25, 2.5, 5, 10 % w/v). Macroporosity was assessed by measuring the transmittance of each material at 400 nm, which decreases owing to increased light scattering as materials become more macroporous (Figure S3.1). We selected a cutoff of 20% transmittance, below which materials are considered to be macroporous.[26] Figure 3.1 demonstrates that transmittance (and hence morphology) can be carefully controlled by adjusting the precursor and porogen properties. Many materials comprised of SS, TMOS or 40% MTMS in TMOS with variable amounts of PEG demonstrated transmittance values indicative of macroporosity and formed self-supporting monoliths without flocculation, and thus were further investigated.

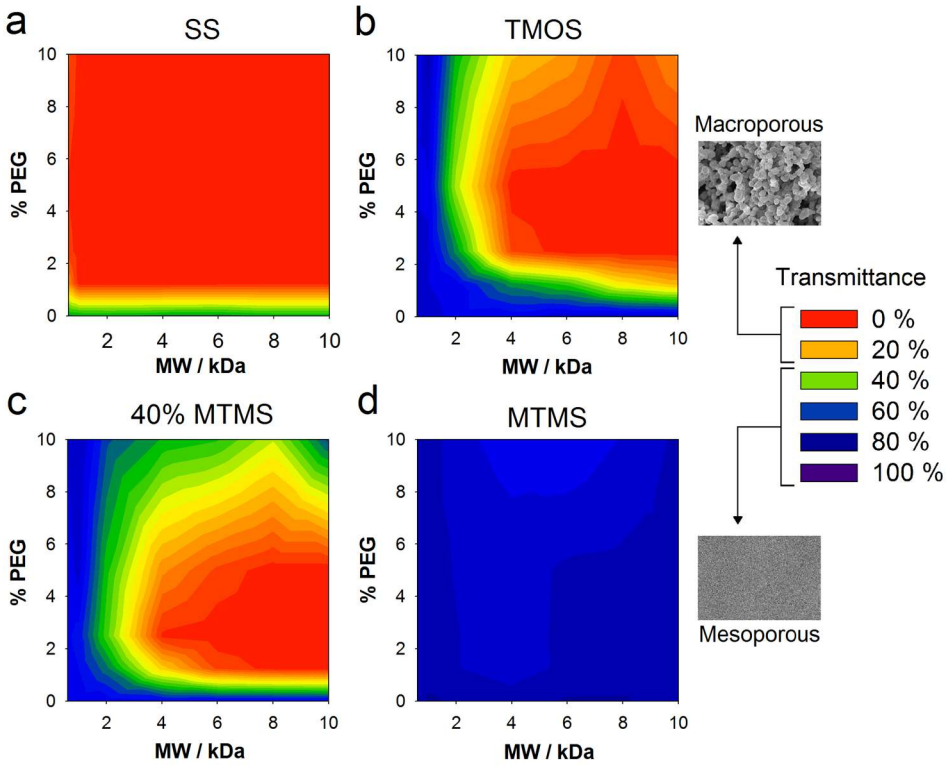

Figure 3.1. Opacity plots of sol-gel derived materials. Percent transmittance of a) SS, b) TMOS, c) 40% MTMS (in TMOS), and d) MTMS sols mixed in assay buffer with 0 – 10 kDa PEG at various concentrations after 3 h gelation at room temperature. Materials with transmittance ≤ 20 % are considered to be macroporous.

To monitor the effects of entrapment on the performance of aptamers (e.g. leaching, target-binding ability), two structure-switching DNA signaling aptamers were selected, one for ATP, and another for the platelet-derived growth factor (PDGF) protein[28,29] (Table S3.1 lists the DNA sequences used).[30-32] In this design, fluorophore and quencher-labeled DNA strands (FDNA and QDNA, respectively) hybridize to the each aptamer sequence (monomeric or concatemeric aptamers) to form a quenched aptamer/DNA duplex. Upon binding its target molecule, this duplex undergoes a conformational change to dissociate

the QDNA and produce a target concentration-dependent fluorescence signal enhancement. Dynamic light scattering measurements monomeric and concatemeric aptamers in solution (Figure S3.2) demonstrated that the average hydrodynamic diameter of the concatemeric aptamers was ~1.5 μm, with a relatively high polydispersity, likely due to the variation in amplicon length obtained using RCA. This value was substantially higher that the size of monomers, which would have a maximum length of ~20 nm if fully extended. The small peak at ~100 nm in the concatemeric aptamer samples were identified as the circular DNA template for RCA, which is difficult to remove due to complementarity to the repeating aptamer units.

Prior to entrapment, we examined the effect of PEG on the structure-switching capabilities of aptamers in solution, as previous studies have shown that high levels of PEG can interfere with hybridization, and thus formation of the FDNA and QDNA complexes with the aptamers.[33,34] Figure S3.3 demonstrates that reduced signal enhancement occurs with increasing PEG concentrations and MW. Therefore, a subset of 24 macroporous materials with low to intermediate MWs and concentrations of PEG, were chosen for aptamer entrapment (Table S3.2).

Figure 3.2 shows the extent of leaching of monomeric aptamers and amplicons entrapped into monolithic materials formed in 96-well plates, as determined by the fluorescence intensity of the supernatant used to wash the monoliths. Monomeric aptamers demonstrated extensive leaching from both mesoporous and macroporous materials (50 % and 90 %, respectively). Conversely, concatemeric aptamer amplicons demonstrated significantly lower leaching from all materials (20% or less), and

fluorescence polarization studies demonstrated that the intensity arose from dehybridized FDNA rather than loss of concatemeric aptamers from the materials (Table S3.3), indicating efficient entrapment of concatemeric aptamers even in macroporous materials. Based on these results, further studies focused on a small subset of three macroporous materials: SS with 5% of 0.6 kDa PEG (Macro SS), TMOS with 5% 6 kDa PEG (Macro TMOS), and 40 % MTMS with 5 % 6 kDa PEG (Macro 40% MTMS).

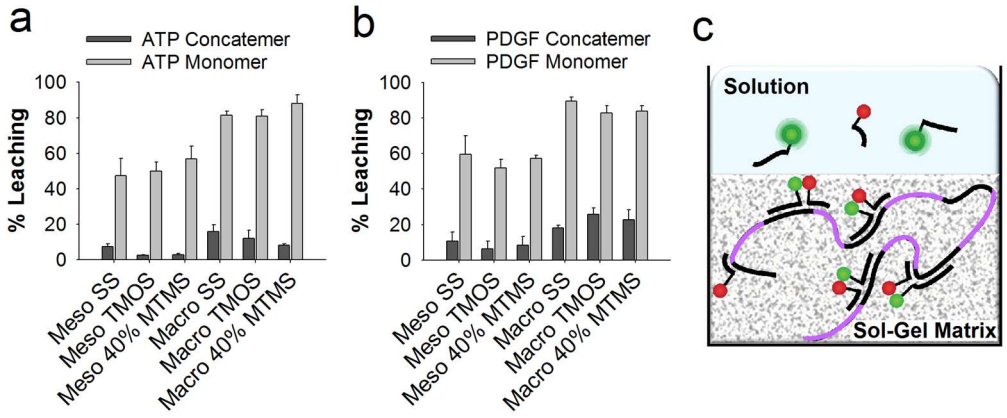

Figure 3.2. Aptamer reporter leaching from sol-gel derived materials. The percent leaching of a) ATP concatemers versus monomers and b) PDGF concatemers versus monomers entrapped in various mesoporous or macroporous sol-gel derived materials. C) schematic of concatemers entrapped within a macroporous matrix.

We next evaluated the signal response of the entrapped monomeric and concatemeric aptamers when exposed to their cognate targets (either 2 mM ATP or 200 nM PDGF, see Figure 3), which will depend on both access of the analyte to the entrapped aptamer and the ability of the aptamer construct (monomer or concatemer) to retain structure-switching ability.

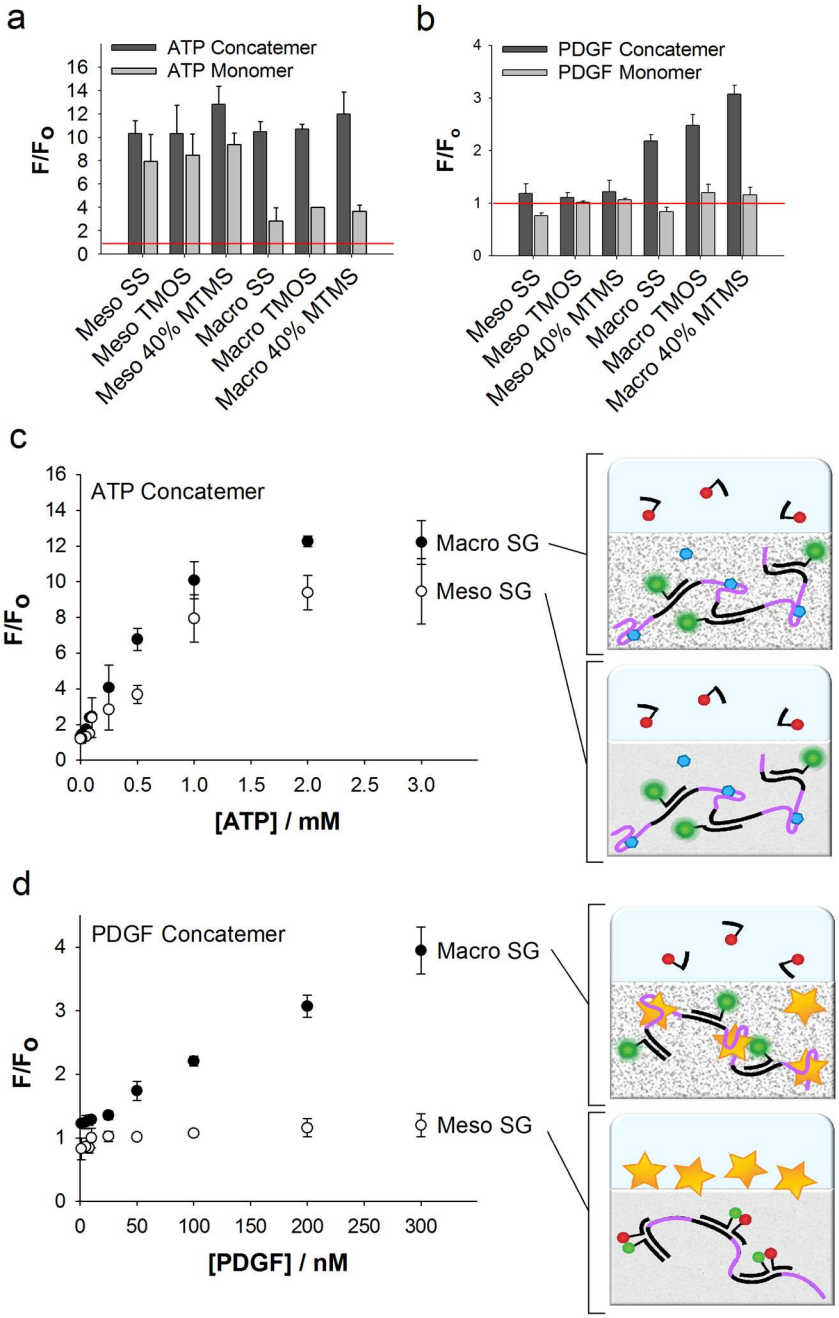

Figure 3.3. Signal response comparison of aptamer reporters. Fluorescence signal from a) ATP monomer and concatemer with 2 mM ATP or b) PDGF monomer and concatemer with 200 nM PDGF in various mesoporous or macroporous materials. The red line in a) and b) indicates a normalized F/Fo of 1.0 (no signal in-crease). Response of c) ATP concatemer with 0 – 3 mM ATP or d) PDGF concatemer with 0 – 300 nM PDGF in Meso or Macro 40% MTMS.

Signal responses of monomeric and concatemeric ATP (Figure 3.3A) or PDGF (Figure 3.3B) aptamers entrapped in the three macroporous materials were compared with those from their mesoporous counterparts (formed with no porogen). In mesoporous materials, both monomeric and concatemeric versions of the ATP aptamer showed a similar response to ATP (~8–10-fold increase in signal) while addition of PDGF to entrapped monomeric and concatemeric PDGF aptamers produced no increase in fluorescence, indicating that the PDGF was unable to enter the mesoporous material, as expected. However, macroporous materials containing entrapped concatemeric aptamers demonstrated substantial fluorescence enhancements, with an 8-fold enhancement for the ATP aptamer and up to a 3-fold enhancement for the PDGF aptamer. In stark contrast, addition of cognate targets to macroporous materials containing monomeric forms of the ATP or PDGF aptamer produced much less fluorescence enhancement, consistent with loss of the entrapped aptamers via leaching. Taken together, these results conclusively demonstrate that entrapment of long-chain DNA aptamers in suitable macroporous materials (such as Macro 40% MTMS) allows detection of a wide range of targets, spanning small molecules to proteins.

We also examined concentration-dependent signal responses of concatemeric ATP (Figure 3C) and PDGF (Figure 3D) aptamers entrapped in Meso and Macro 40% MTMS. While ATP could induce a concentration-dependent fluorescence enhancement in both mesoporous and macroporous systems, PDGF was only able to cause a signal change in the macroporous system, further confirming that large targets such as the PDGF proteins cannot penetrate the pores of mesoporous materials to access the entrapped aptamers.

As a practical demonstration of the potential utility of the newly engineered macroporous bio/inorganic hybrid materials, we produced aptamer-doped monolithic columns within fused silica capillaries using the 40% MTMS material (see Supporting Information for details on column fabrication) for use as flow-through biosensors. The columns could withstand flow rates up to 30 µL/min, though at very high backpressures, but were typically utilized at a flow rate of 1 µL/min, which allowed operation at a low backpressure (Figure S3.4). Scanning electron microscopy (SEM) was used without a conductive metal coating to image the structure of mono-lithic columns with and without entrapped concatemeric aptamers (Figure 3.4). The macroporous nature of the un-doped columns is evident, and shows that the macropores are on the order of 1 – 2 µm in diameter. Columns with entrapped concatemeric aptamers show a substantially different structure, with the appearance of roughly spherical DNA structures coating the silica particles.

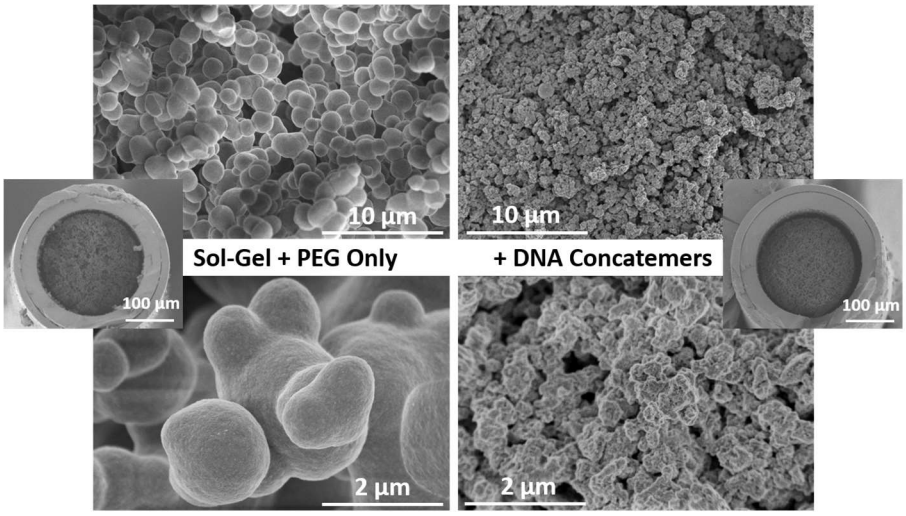

Figure 3.4. SEM images of sol-gel derived monolithic columns. Magnified images of a monolithic columns with or without entrapped concatemeric aptamers formed in a 250 µm i.d. capillary using environmental SEM analysis of non-conductive materials.

Energy dispersive x-ray spectroscopy (EDX) was also used to com-pare the elemental composition of columns with or without entrapped concatemers (Figure S3.5). In columns containing concatemeric aptamers, the decreased contribution from silicon with increased carbon and nitrogen content further support the conclusion that the nanostructures observed using SEM are in fact long-chain DNA aptamers adsorbed and/or entrapped in the silica skeleton.

To convert the structure-switching concatemeric aptamers to a format for flow-through fluorescence sensing, the original QDNA strand sequence was modified by removing the quencher and replacing it with a fluorophore to produce F′DNA, and the original FDNA was not included. In this configuration, the F′DNA is released upon target binding and can elute from the column to produce a fluorescence spike (Figure 3.5A). Following column conditioning to remove any free PEG using 8 bed volumes of buffer, target molecules were introduced and the intensity of the column eluate was measured (Figure S3.6). Inclusion of the target resulted in a significant increase in the fluorescence intensity of the eluate for both the ATP (Figure 3.5B) and PDGF (Figure 3.5C) systems in a concentration-dependent manner, while addition of targets to columns with entrapped monomers or F′DNA alone resulted in no fluorescence in the eluate (Figure 3.5B and 3.5C, insets). Hence, the entrapment of concatemeric aptamers into macroporous columns provides a method to produce flow-based fluorescence sensors for a range of targets, and should also be amenable to affinity based purification of such species from mixtures, or evaluation of aptamer-target binding constants using well known chromatographic methods.[35-38]

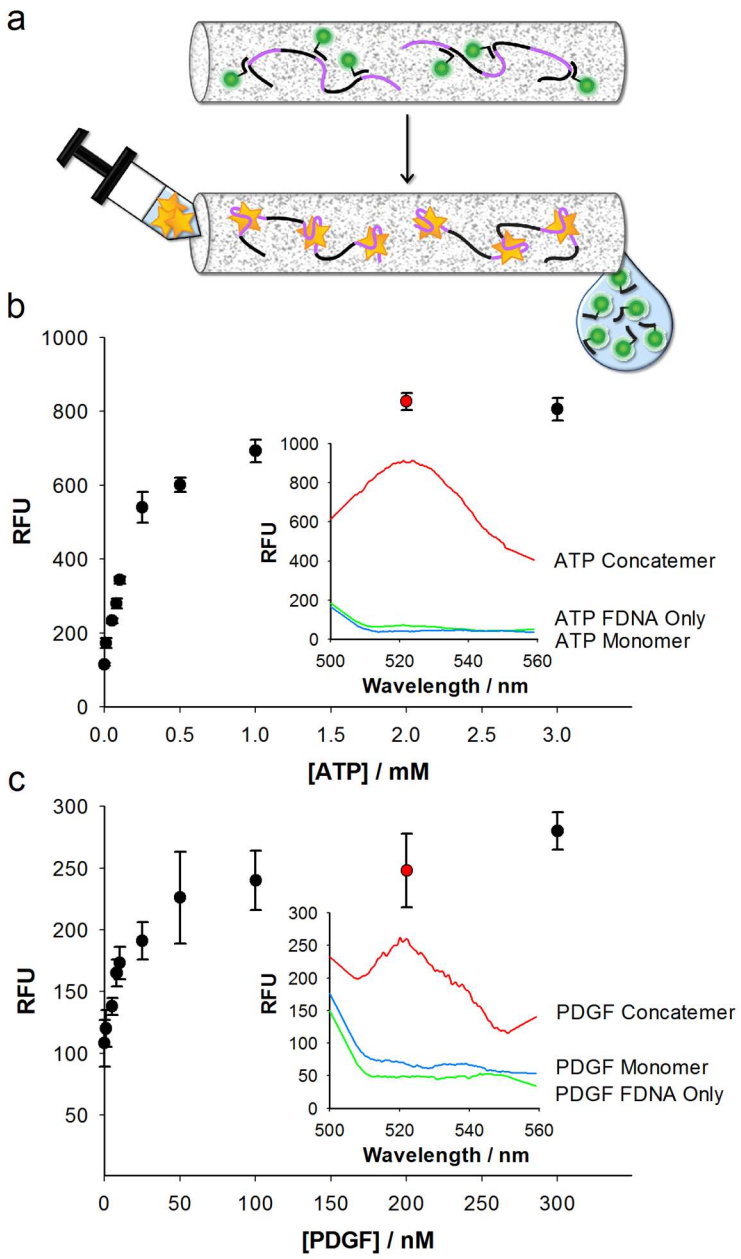

Figure 3.5. Target-detection response of biohybrid monolithic column. A) Schematic of macroporous sol-gel derived monolith containing entrapped concatemeric aptamers and the target binding-induced release of F′DNA. B) ATP concatemer column response to 0 – 3 mM ATP or c) PDGF concatemer column response to 0 – 300 nM PDGF. Insets: representative fluorescence scans of eluate fractions upon target addition – b) 2 mM ATP or c) 200 nM PDGF.

3.4 Conclusions

In conclusion, we have been able to show that concatemeric DNA aptamers can be entrapped and retained within macroporous sol-gel derived materials with minimal leaching, high activity and the ability to bind a wide range of targets of varying size. Our findings demonstrate another advantage of aptamers, as it is fair to provide large concatemeric species using simple biochemical techniques such as RCA. We further show that screening of sol-gel derived materials offers an efficient way to identify a macroporous material with a suitable environment for aptamer functionality and the ability to form monolithic capillary columns. These novel biomaterials were suitable for use as flow-based biorecognition columns. This work expands the use of sol-gel entrapped biomolecules beyond small molecule targets to large macromolecular proteins, providing a method to develop multiple new applications using sol-gel derived bio/inorganic hybrid materials.

3.5 Experimental

3.5.1 Materials. Standard and functionalized DNA oligonucleotides were synthesized and purified by HPLC by Integrated DNA Technologies (Coralville, IA). Adenosine 5′-triphosphate (ATP), cytidine 5′-triphosphate (CTP), guanosine 5′-triphosphate (GTP), uridine 5′-triphosphate (UTP), T4 polynucleotide kinase (PNK; with 10× reaction buffer A), T4 DNA ligase (with 10× T4 DNA ligase buffer), 10 mM dNTPs, ϕ29 DNA polymerase (with 10× ϕ29 DNA polymerase buffer), GeneRuler^{TM} 1 kb Plus DNA ladder and 10,000× SYBR Safe DNA gel stain were purchased from Fermentas Life Sciences

(Burlington, ON). Recombinant human platelet derived growth factor (PDGF), epidermal growth factor (EGF) and insulin-like growth factor I (IGF-I) were purchased from Cedarlane (Burlington, ON). Sodium silicate solution (SS solution, ultrapure grade, ~14% Na_2O, ~29% silica) was purchased from Fischer Scientific (Pittsburgh, PA). Bovine serum albumin (BSA), poly(ethylene) glycol (PEG, 600 – 10,000 Da), tetramethylorthosilicate (TMOS), methyltrimethoxysilane (MTMS), and Dowex 50x8–100 cation exchange resin and all other analytical grade chemicals and solvents were purchased from Sigma-Aldrich (Oakville, ON). Water was purified prior to use with a Millipore Milli-Q Synthesis A10 water purification system.

3.5.2 Methods.

Preparation of Concatemeric DNA Aptamers and Reporter Complexes. Concatemer constructs of each structure-switching aptamer and the fluorescence-signaling aptamer reporter complexes for ATP and PDGF binding were prepared using the sequences given in Table S3.1 as described elsewhere[19] and briefly below. The linear circular templates were first phosphorylated using 10 U of T4 PNK and 100 nmol ATP at 37 °C for 30 min followed by heating at 90 °C for 5 min and cooling to room temperature. These were then ligated using 15 U of T4 DNA ligase at room temperature for 12 h in 1× ligase buffer. The circularized templates were ethanol precipitated before purifying on a 10% polyacrylamide gel, ethanol precipitated and resuspended in water.

The RCA reaction of each aptamer sequences was carried out by heating 10 pmol of circular template with 10 pmol of primer and 5 μL of 10× ϕ29 polymerase buffer (36.5 μL

total volume) at 90 °C for 1 min. Following cooling, 2.5 μL of 10 μM dNTPs and 10 U of ϕ29 polymerase were added to the reaction mixture and allowed to incubate at 30 °C for 1 h. The reaction was followed by a 5-fold dilution with water before heating at 90 °C for 5 min to deactivate the enzyme. The concatemeric aptamers from the reaction mixture were purified by centrifugation using a 100 kDa Nanosep® spin column and quantified using a NanoVue spectrophotomer (absorbance at 260 nm). As the exact size of the concatemer construct is unknown, its approximate molar concentration was obtained based on one repeat of the monomeric aptamer sequence.

Tripartite reporter complexes were prepared by combining either the concatemeric or monomeric aptamer with its FDNA and QDNA in a 1:1:6 molar ratio (100 nM final concentration of FDNA), respectively, in assay buffer (40 mM Tris·HCl, 200 mM NaCl, 4 mM $MgCl_2$ at pH 7.8). Our previous work determined that using a 1:1 aptamer/FDNA ratio with 6× QDNA greatest amount of quenching for low initial background fluorescence prior to target binding and a sensitivity and selectivity similar to the monomeric aptamer reporter systems.[19] These solutions were then heated at 90 °C for 5 minutes, cooled and incubated for 30 minutes at room temperature.

Optimization of Concatemer Fluorescence Signaling in Solution. To study the effects of PEG on signaling in solution, the reporter system solutions were prepared at 2× concentration then mixed in a 1:1 ratio with 1.25 – 10% PEG (w/v, final) of 4 – 10 kDa. Baseline fluorescence was measured for 10 min prior to the addition of target. Target

analyte for each aptamer was then added at a final concentration of 2 mM ATP or 200 nM PDGF to the appropriate system and fluorescence measurements were continued.

Preparation of Sols and Monolithic Silica Disks. The silane and organosilane precursors: SS, TMOS and MTMS, were used to prepare the sols for aptamer entrapment studies as described elsewhere.[25] Sodium silicate sols were prepared by diluting 2.59 g of a stock SS solution to 10 mL with water, mixing the solution with 5.5 g DOWEX for 2 min to bring the pH to ~4, and then vacuum filtering this solution through a Büchner funnel to remove the resin followed by further filtration through a 0.2 μm membrane syringe filter to remove any particulates in the solution. Before use, 120 g of the Dowex resin was cleaned with 150 mL 0.1 N HCl and stirring for 1 h, followed by vacuum filtration and washing with water until the filtrate ran clear to ensure that the final pH of the sol solution was close to 4.0 (in order to form consistent final materials). To make TMOS and MTMS sols, 700 μL of water and 50 μL HCl (0.1 N) were added to 2.25 mL TMOS or MTMS and then sonicated for 20 min in ice-cold water. The 60 % TMOS – 40 % MTMS mixture were prepared by proportionally dividing the 2.25 mL of silane to 1350 μL TMOS and 900 μL MTMS, mixing with water and acid and co-hydrolyzing in an ultrasonic bath, as described above. All prepared sols were stored on ice until use (and used within the hour).

Monoliths for opacity screening were prepared by combining one of these four sols with 2× PEG-doped assay buffer in a 1:1 (v/v) ratio, depositing 50 μL of the mixtures in a 96-well plate and allowing to gel for 3 h prior to absorbance measurements at 400 nm (using a Tecan M1000). Poly(ethylene) glycol with various molecular weight, 0.6 – 10

kDa, was used at five final concentrations from 0 – 10 % (w/v). Kinetic opacity analysis of the 60 % TMOS – 40 % MTMS mixture with 0 – 10 % (w/v) of 0.6 – 10 kDa PEG was performed in a 96 well-plate by measuring absorbance at 400 nm every 5 min for 12 h.

Entrapment of Concatemeric Aptamer Complexes in Sol-Gel Derived Disks. Tripartite aptamer complexes (in a 1:1:6 Aptamer/FDNA/QDNA molar ratio) for entrapment were prepared at 2× final concentration in 2× PEG-doped assay buffer, heated at 90 °C for 5 min, cooled at room temperature and mixed in a 1:1 volume ratio with a freshly-prepared sol at room temperature. The aptamer-sol mixtures were deposited into a 96-well plate at a volume of 50 μL per well and allowed to gel and age for at least 3 h and then overlaid with assay buffer prior to washing and analysis.

The various sol-gel derived materials containing the reporter complexes were washed three times with 50 μL buffer at room temperature to remove any un-encapsulated DNA from the material surface. Leaching of entrapped aptamers from the materials was determined by comparing the total fluorescence intensity prior to any washing to that of washed materials, as well as the fluorescence intensity of the combined wash solutions for all three washes. Fluorescence anisotropy of the wash solutions were also measured. Following washing, materials were incubated at 25 °C for 10 min in the plate reader prior to target addition to the overlay buffer solution and fluorescence measurements. This experiment was also repeated with the monomeric versions of each aptamer, complexed in the same 1:1:6 ratio.

To test the sensitivity of the aptamer complexes in materials, following incubation and washing, ATP was then added to the ATP-binding concatemer at final concentrations of 0

– 3 mM, while PDGF was added to the PDGF-binding concatemer at a final concentration range of 0 – 300 nM (2 μL of each analyte solution at the appropriate concentration).

Preparation of Monolithic Chromatography Columns. Both monomeric and concatemeric aptamers were entrapped in monolithic columns, where the original QDNA quencher moiety was replaced with a fluorescein-labelled strand with an identical sequence to produce F′DNA. The aptamers were combined with F′DNA in a 1:6 molar ratio at 2× final concentration in 2× PEG-doped assay buffer, heated at 90 °C for 5 min, and cooled at room temperature to anneal the F′DNA to the aptamer.

Monolithic columns were prepared by mixing the 60 % TMOS – 40 % MTMS sol in a 1:1 volume ratio with the 2× PEG-doped assay buffer and immediately loaded into 2 m of 250 μm i.d. fused-silica capillary. The final composition of the solution was 5 % PEG (6 kDa) containing either no DNA molecules, 600 nM FDNA only, or 100 nM aptamer (concatemeric or monomeric aptamer) complexed with 600 nM FDNA in 1× assay buffer. Columns were laid flat at room temperature in air for 3 h for gelation and preliminary aging to occur. Then, the ends of the capillaries were immersed in Eppendorf tubes containing 1× assay buffer and covered with Parafilm™ to prevent evaporation. The monoliths were further aged for at least 3 – 14 days at 4 °C. Columns were then cut into 10-cm pieces (discarding the initial and last 10 cm) and attached to an Eksigent 2D nanoLC pump with autosampler (Dublin, CA) using standard Upchurch Scientific fittings. Assay buffer was delivered to the column at a flow rate of 1 – 30 μL/min and compare to empty capillaries in order to measure backpressure and column robustness. For flow-through sensor assays,

buffer was introduced to the column at a flow rate of 1 µL/min and four 20 µL fractions were collected in Eppendorf tubes. four 20 µL fractions were collected in Eppendorf tubes. Columns were conditioned using 8 bed volumes of buffer and the first two pre-wash fractions were collected. Either ATP or PDGF were then added to the column using the autosampler at final concentrations of 0 – 3 mM or 0 – 300 nM, respectively and a third 20 µL fraction was collected, after which buffer was introduced and a final fourth fraction of 20 µL volume was collected.

Fluorescence Intensity and Anisotropy Measurements. All fluorescence measurements were performed using a Tecan Infinite® M1000 platereader in fluorescence mode. Excitation was set at 490 nm (5-nm bandpass) and emission was measured at 520 nm (5-nm bandpass) with a 20 µs integration time using the bottom-read setting. Fluorescence scans were performed using an excitation wavelength of 490 nm (5-nm bandpass) and measuring emission from 500 – 560 nm (5-nm bandpass) using bottom-read mode. Fluorescence anisotropy measurements were performed using a 470 nm excitation wavelength and 520 nm emission wavelength (5-nm bandpass) in top-read mode. All assays were carried out in triplicate with background fluorescence subtraction at 25 °C.

Kinetic measurements in solution and monolithic disks were performed to assess signal response upon addition of a given target using fluorescence intensity reads every 1 min for both baseline (before target addition; 10 min) and assay (after addition of target; 1 h) measurements, with orbital shaking of 2.5 mm amplitude for 5 s between each measurement to ensure proper mixing. Raw fluorescence intensity measurements were

normalized to F/F_o where F is the endpoint fluorescence intensity and F_o is the initial fluorescence intensity prior to target addition.

DLS Measurements. DNA sizing was performed using a Malvern Instruments Zatasizer Nano ZS to measure light scattering intensity. Samples were placed in a plastic cuvette and three separate samples of each DNA construct at 1 μM were measured using 10 runs in automatic mode at 20 °C.

SEM Imaging. Samples for SEM imaging were aged for at least 5 days at room temperature before being cut to expose a fresh surface for mounting. Scanning electron microscopy imaging was performed using a FEI Magellan XHR 400 at 1 kV. Energy dispersive x-ray spectroscopy was performed using the same scanning electron microscope with a 5 keV beam.

3.6 Acknowledgements

The authors thank the Natural Sciences and Engineering Research Council of Canada for financial support of this work. The EM research described in this paper was performed at the Canadian Centre for Electron Microscopy at McMaster University, which is supported by NSERC and other government agencies. Y.L. holds the Canada Research Chair in Directed Evolution of Nucleic Acids. J.D.B. holds the Canada Research Chair in Bioanalytical Chemistry and Biointerfaces.

3.7 References

(1) Avnir, D.; Braun, S.; Lev, O.; Ottolenghi, M. *Chem. Mater.* **1994**, *6*, 1605-14.

(2) Bhatia, R. B.; Brinker, C. J.; Gupta, A. K.; Singh, A. K. *Chem. Mater.* **2000**, *12*, 2434-41.

(3) Kandimalla, V. B.; Tripathi, V. S.; Ju, H. *Crit. Rev. Anal. Chem.* **2006**, *36*, 73-106.

(4) Avnir, D.; Coradin, T.; Lev, O.; Livage, J. *J. Mater. Chem.* **2006**, *16*, 1013-30.

(5) Brennan, J. D. *Acc. Chem. Res.* **2007**, *40*, 827-35.

(6) Monton, M. R. N.; Forsberg, E. M.; Brennan, J. D. *Chem. Mater.* **2011**, *24*, 796-811.

(7) Forsberg, E. M.; Sicard, C.; Brennan, J. D. *Annu. Rev. Anal. Chem.* **2014**, *7*, 337-59.

(8) Cruz-Aguado, J. A.; Chen, Y.; Zhang, Z.; Brook, M. A.; Brennan, J. D. *Anal. Chem.* **2004**, *76*, 4182-8.

(9) Hodgson, R. J.; Chen, Y.; Zhang, Z.; Tleugabulova, D.; Long, H.; Zhao, X. M.; Organ, M.; Brook, M. A.; Brennan, J. D. *Anal. Chem.* **2004**, *76*, 2780-90.

(10) Rupcich, N.; Nutiu, R.; Li, Y.; Brennan, J. D. *Anal. Chem.* **2005**, *77*, 4300-7.

(11) Besanger, T. R.; Hodgson, R. J.; Guillon, D.; Brennan, J. D. *Anal. Chim. Acta* **2006**, *561*, 107-18.

(12) Besanger, T. R.; Hodgson, R. J.; Green, J. R.; Brennan, J. D. *Anal. Chim. Acta* **2006**, *564*, 106-15.

(13) Shen, Y. T.; Mackey, G.; Rupcich, N.; Gloster, D.; Chiuman, W.; Li, Y. F.; Brennan, J. D. *Anal. Chem.* **2007**, *79*, 3494-503.

(14) Forsberg, E. M.; Green, J. R. A.; Brennan, J. D. *Anal. Chem.* **2011**, *83*, 5230-6.

(15) Carrasquilla, C.; Lau, P. S.; Li, Y.; Brennan, J. D. *J. Am. Chem. Soc.* **2012**, *134*, 10998-1005.

(16) Zhao, Q.; Li, X.-F.; Le, X. C. *Anal. Chem.* **2008**, *80*, 3915-20.

(17) Zhao, Q.; Li, X.-F.; Shao, Y.; Le, X. C. *Anal. Chem.* **2008**, *80*, 7586-93.

(18) Deng, N.; Liang, Z.; Liang, Y.; Sui, Z.; Zhang, L.; Wu, Q.; Yang, K.; Zhang, L.; Zhang, Y. *Anal. Chem.* **2012**, *84*, 10186-90.

(19) Forsberg, E. M.; Brennan, J. D. *Anal. Chem.* **2014**, *86*, 8457-65.

(20) Wang, Z.; Zhao, J.-c.; Lian, H.-z.; Chen, H.-y. *Talanta* **2015**, *138*, 52-8.

(21) Fire, A.; Xu, S. Q. *Proc. Natl. Acad. Sci. U.S.A.* **1995**, *92*, 4641-5.

(22) Liu, D. Y.; Daubendiek, S. L.; Zillman, M. A.; Ryan, K.; Kool, E. T. *J. Am. Chem. Soc.* **1996**, *118*, 1587-94.

(23) Zhu, G.; Hu, R.; Zhao, Z.; Chen, Z.; Zhang, X.; Tan, W. *J. Am. Chem. Soc.* **2013**, *135*, 16438-45.

(24) Hu, R.; Zhang, X.; Zhao, Z.; Zhu, G.; Chen, T.; Fu, T.; Tan, W. *Angew. Chem. Int. Ed.* **2014**, *53*, 5821-6.
(25) Carrasquilla, C.; Little, J. R. L.; Li, Y.; Brennan, J. D. *Chem. Eur. J.* **2015**, *21*, 7369-73.
(26) Smith, A. M. E.; Fortuna, J.; Forsberg, E. M.; Brennan, J. D. *RSC Advances* **2014**, *4*, 15952-60.
(27) Carrasquilla, C.; Brennan, J. D. *Methods* **2013**, *63*, 255-65.
(28) Huizenga, D. E.; Szostak, J. W. *Biochemistry* **1995**, *34*, 656-65.
(29) Green, L. S.; Jellinek, D.; Jenison, R.; Ostman, A.; Heldin, C. H.; Janjic, N. *Biochemistry* **1996**, *35*, 14413-24.
(30) Nutiu, R.; Li, Y. *J. Am. Chem. Soc.* **2003**, *125*, 4771-8.
(31) Nutiu, R.; Li, Y. *Chem. Eur. J.* **2004**, *10*, 1868-76.
(32) Nutiu, R.; Li, Y. *Methods* **2005**, *37*, 16-25.
(33) Del Vecchio, P.; Esposito, D.; Ricchi, L.; Barone, G. *Int. J. Biol. Macromol.* **1999**, *24*, 361-9.
(34) Bonner, G.; Klibanov, A. M. *Biotechnol. Bioeng.* **2000**, *68*, 339-44.
(35) Schriemer, D. C.; Bundle, D. R.; Li, L.; Hindsgaul, O. *Angew. Chem. Int. Ed.* **1998**, *37*, 3383-7.
(36) Peyrin, E. *J. Sep. Sci.* **2009**, *32*, 1531-6.
(37) Pichon, V.; Brothier, F.; Combes, A. *Anal. Bioanal. Chem.* **2015**, *407*, 681-98.
(38) Du, F.; Guo, L.; Qin, Q.; Zheng, X.; Ruan, G.; Li, J.; Li, G. *TrAC, Trends Anal. Chem.* **2015**, *67*, 134-46.

3.8 Supplementary Information

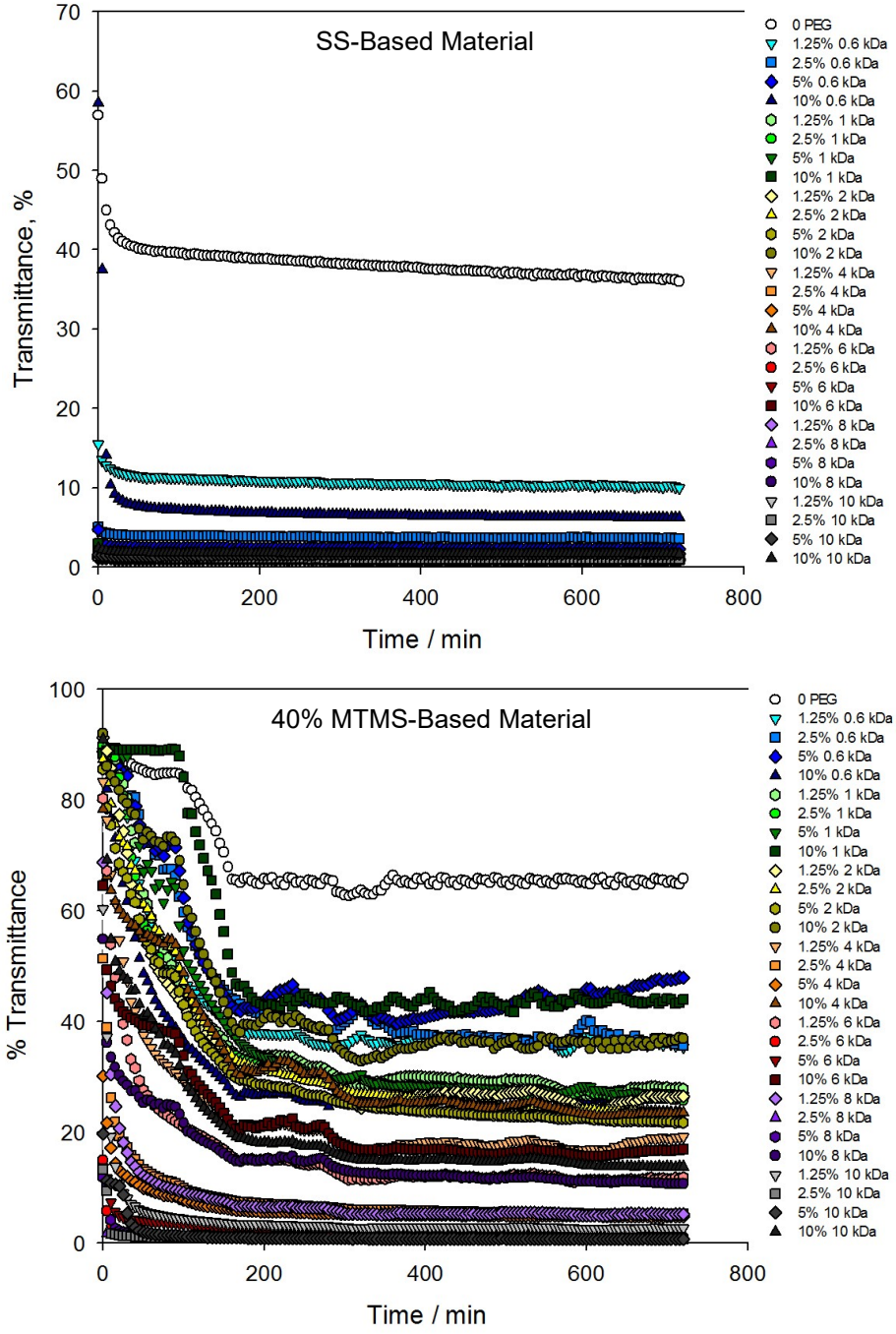

Figure S3.1. Time-resolved changes in transmittance of sol-gel derived materials. Transmittance at 400 nm of SS (top) and 40% MTMS (bottom) mixed in assay buffer with 0 – 10 kDa PEG at various concentrations over 12 h as samples of phase separation evolution over time.

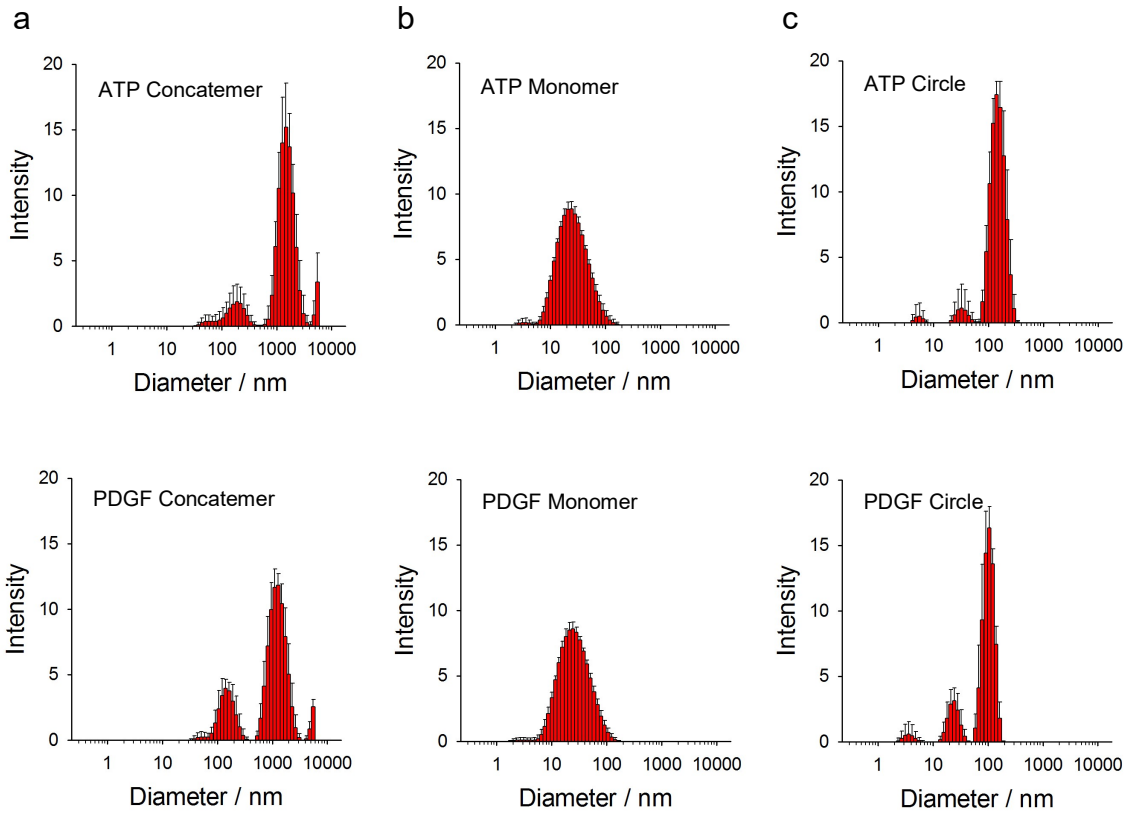

Figure S3.2. DLS measurements of DNA constructs in solution. Hydrodynamic size distributions of a) concatemeric, b) monomeric and c) circular template constructs for the ATP aptamer (top) and PDGF aptamer (bottom) in solution as measured by dynamic light scattering intensity.

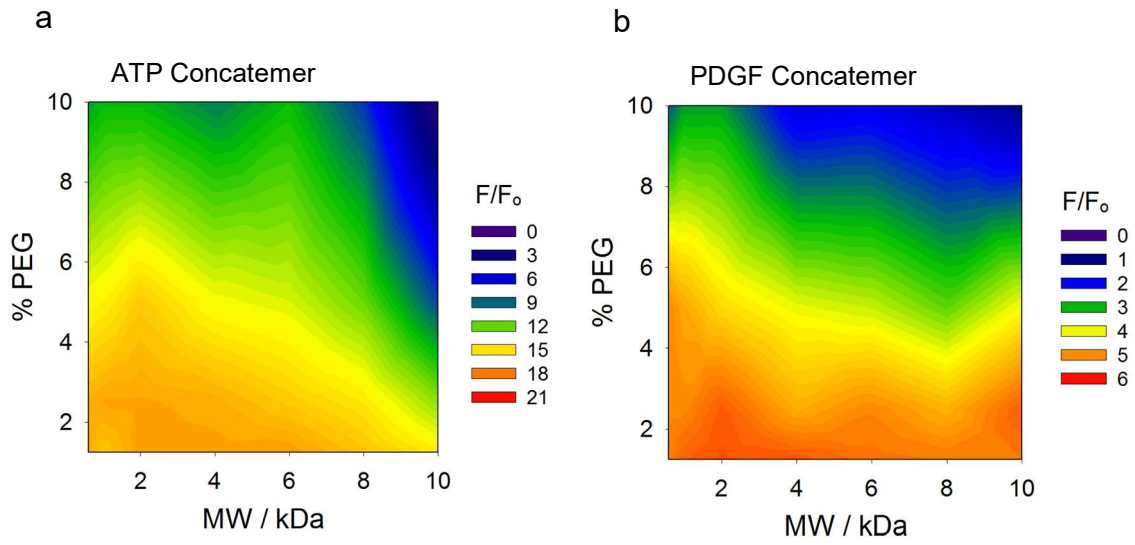

Figure S3.3. Signal enhancement of concatemeric reporters in PEG-doped buffer. Fluorescence signal response of the a) concatemeric ATP aptamer with 2 mM ATP and b) concatemeric PDGF aptamer with 200 nM PDGF, in solution containing increasing concentrations of 1.25 – 10 kDa PEG.

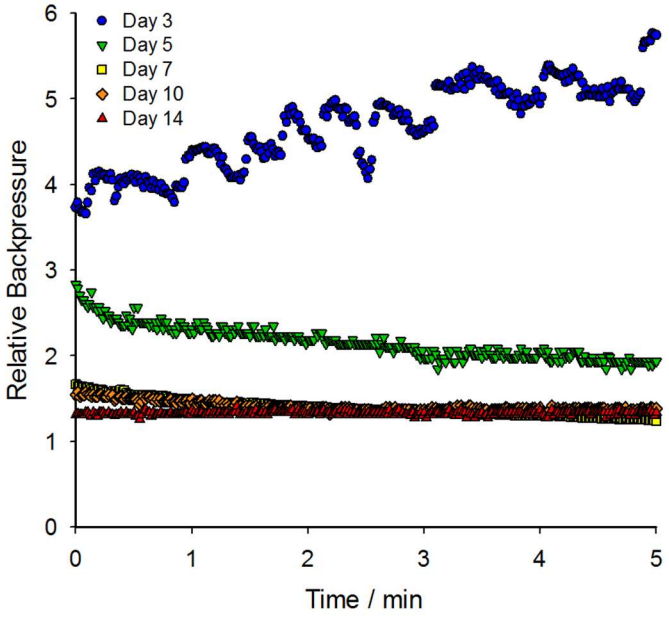

Figure S3.4. Backpressure of monolithic columns upon aging. Backpressure of monolithic columns relative to empty capillaries (indicated by a relative backpressure of 1 at ~15 PSI) after various aging periods at a flow rate of 1 µL/min. Columns were used for target detection assays only after at least 7 days of aging.

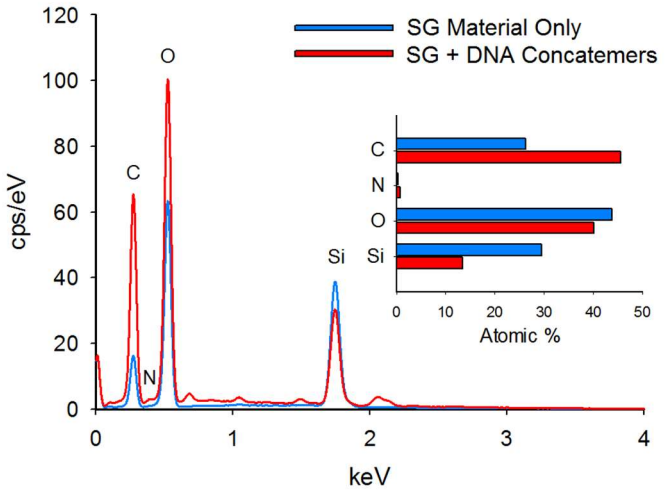

Figure S3.5. EDX analysis of sol-gel derived monolithic columns. A spectral overlay comparing the differences in elemental composition between a monolithic column with versus without entrapped concatemeric aptamers. Inset: the relative atomic contribution from C, N, O and Si for a sol-gel derived monolithic column with or without entrapped concatemeric aptamer amplicons.

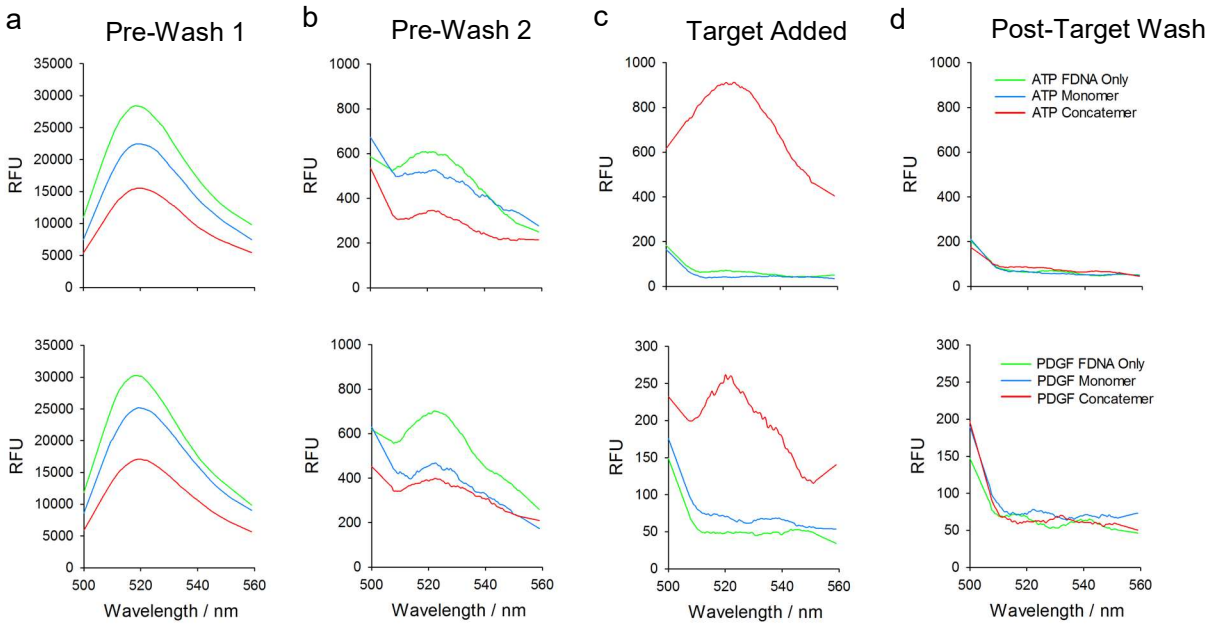

Figure S3.6. Fluorescence Scans of Column Fractions. Scan measurements of eluate from monolithic columns containing various entrapped DNA molecules, divided into four fractions: a) pre-wash 1, b) pre-wash 2, c) elution with target and d) post-target wash. Fractions 1, 2 and 4 serve as wash steps with buffer only and fractions 3 contains either 2 mM ATP (top) or 200 nM PDGF (bottom) for the appropriate column.

Table S3.1. DNA oligonucleotide sequences for aptamer reporter systems.

DNA oligonucleotide	Sequence (5'→3')
Linear ATP Aptamer Circular Template	TGTCT TCGCC TATAG TGAAC CTTCC TCCGC AATAC TCCCC CAGGT ATCTT TCGAC TAAGC ACC
ATP Aptamer Ligation Template	GGCGA AGACA GGTGC TTAGT C
ATP Aptamer Primer	GGGGG AGTAT TGCGG AGGAA
Linear PDGF Aptamer Circular Template	TGCAG CGACT CACAG GATCA TGGTG ATGCT CTACG TGCCG TAGCC TGCCC TTTCG ACTAC C
PDGF Aptamer Ligation Template	GAGTC GCTGC AGGTA GTCGA A
PDGF Aptamer Primer	CGTAG AGCAT CACCA TGATC
ATP aptamer FDNA (ATP-FDNA)	(fluorescein)CGACT AAGCA CCTGT C
ATP aptamer QDNA (ATP-QDNA/F'DNA)	CCCAG GTATC TT(dabcyl/fluorescein)
ATP aptamer monomeric construct (ATP-Apt)	TCACT ATAGG CGAAG ACAGG TGCTT AGTCG AAAGA TACCT GGGGG AGTAT TGCGG AGGAA GGT
PDGF aptamer FDNA (PDGF-FDNA)	(fluorescein)GACTA CCTGC AGCGA
PDGF aptamer QDNA (PDGF-QDNA/F'DNA)	AGCCT GCCCT TT(dabcyl/fluorescein)
PDGF aptamer monomeric construct (PDGF-Apt)	TGAGT CGCTG CAGGT AGTCG AAAGG GCAGG CTACG GCACG TAGAG CATCA CCATG ATCCT G

Table S3.2. Composition of the 24 macroporous sol-gel derived materials chosen for aptamer entrapment.

Precursor	PEG MW (kDa)	[PEG] (%)
SS	0.6	1.25
SS	0.6	2.5
SS	0.6	5
SS	1	1.25
SS	1	2.5
SS	1	5
TMOS	4	1.25
TMOS	4	2.5
TMOS	4	5
TMOS	6	1.25
TMOS	6	2.5
TMOS	6	5
TMOS	8	1.25
TMOS	8	2.5
TMOS	8	5
40% MTMS	4	1.25
40% MTMS	4	2.5
40% MTMS	4	5
40% MTMS	6	1.25
40% MTMS	6	2.5
40% MTMS	6	5
40% MTMS	8	1.25
40% MTMS	8	2.5
40% MTMS	8	5

Table S3.3. Fluorescence polarization from ATP or PDGF concatemer, monomer and FDNA in solution or leached from materials.

	Solution (mP)	Leached (mP)
ATP Concatemer	110 ± 2	70 ± 4
ATP Monomer	105 ± 1	107 ± 6
ATP FDNA only	61 ± 2	66 ± 3
PDGF Concatemer	122 ± 1	81 ± 9
PDGF Monomer	111 ± 1	116 ± 7
PDGF FDNA only	69 ± 1	76 ± 4

CHAPTER 4.

PATTERNED PAPER SENSORS PRINTED WITH LONG-CHAIN DNA APTAMERS

Author's Preface:

The following chapter was published in *Chemistry – A European Journal* under the citation:

Carrasquilla C, Little JRL, Li Y and Brennan JD. Patterned Paper Sensors Printed with Long-Chain DNA Aptamers. *Chem. Eur. J.* **2015** 21: 7369-7373.

I was responsible for the design, performance and analysis of experiments pertaining to printed long-chain DNA aptamers and final solution-based optimization. The initial optimization of long-chain DNA aptamers in solution was performed by Jessamyn R. L. Little, an undergraduate thesis student under my direct supervision. I wrote the first draft of the manuscript with helpful suggestions from Dr. Li. Both Dr. Brennan and Dr. Li provided editorial input to generate the final draft.

4.1 Abstract

There is growing interest in developing printable paper sensors to enable rapid testing of analytes for environmental, food safety, and clinical applications. A major challenge is to find suitable bioinks that are amenable to high-speed printing and remain functional after printing. We report on a simple and effective approach wherein an aqueous ink composed of megadalton-sized tandem repeating structure-switching DNA aptamers (concatemeric aptamers) is used to rapidly create patterned paper sensors on filter paper via inkjet printing. These concatemeric aptamer reporters remain immobilized at the point of printing through strong adsorption but retain sufficient segmental mobility to undergo structure switching and fluorescence signaling to provide both qualitative and quantitative detection of small molecules and protein targets. The convenience of inkjet printing allows for the patterning of internally referenced sensors with multiplexed detection, and provides a generic platform for on-demand printing of sensors even in remote locations.

4.2 Introduction

Due to its portability, abundance and low cost, paper has drawn increasing interest as a platform for sensing devices, particularly in the field of point-of-care (POC) diagnostics and disease screening applications for the developing world.[1-5] Currently, the main techniques to fabricate paper-based biosensors involve either conjugating the biological sensing elements to the paper surface by chemical modification of the paper fibers,[6-11] entrapping these biomolecules within sol-gel derived inks,[12-15] or localizing adsorbed biomolecules using hydrophobic barriers to define channels created by photolithography, etching, plasma treatment, flexographic or screen printing methods.[16-23] However, such approaches can be laborious, prone to non-specific binding, and may require many complex reactions, which can make fabrication inconvenient and increase cost. Herein, we report a simple technique for creating an "all inkjet-printed" paper-based aptamer biosensor that does not require printing of hydrophobic barriers or complicated functionalization steps to immobilize the sensing elements on the paper surface, and allows high-speed printing of patterns that can be used to provide a rapid readout of analyte presence or concentration.

DNA aptamers have become important sensing elements due to their thermal and chemical stability, versatility in target recognition (from small molecules to whole cells), high affinity and specificity, and ease of synthesis and manipulation[24-28] – all inherent advantages over conventional antibody and enzyme-based sensors.[29-34] However, aptamers have rarely been explored for paper-based diagnostics since they suffer from some of the same issues as proteins in their need for complex immobilization strategies or conjugation

to species such as nanoparticles or microbeads for localization on paper.[35-39] Thus, methods that allow for facile immobilization of DNA aptamers on paper, preferably using printers, are urgently needed to generate a versatile diagnostic platform.

We hypothesized that a simple solution to the above challenge is the printing of megadalton-sized aptamer species onto a paper surface. Such species should be too large to undergo global motion after adsorption but still allow the recognition chemistry and signaling to occur. Extremely long, tandem repeating DNA molecules can easily be produced by a biochemical technique known as rolling circle amplification (RCA) – an isothermal process in which a special DNA polymerase, such as ϕ29 DNA polymerase, extends a short DNA primer by making round-by-round copies of a circular DNA template[40-42] – and have been extensively explored for bioanalytical applications to detect a variety of targets,[43-50] and for various nanotechnology applications.[51-54] As we will show below, RCA products containing tandem repeating structure-switching DNA aptamers (referred to as long-chain or concatemeric aptamers) can be inkjet-printed as patterns directly onto unmodified paper surfaces, remain immobilized at their initial locations after flow of liquids over the sensing area, and retain sufficient local and segmental motion required for structure-switching and signaling to occur after introduction of target analytes. Figure 4.1 schematically illustrates our approach wherein concatemeric DNA aptamers are allowed to hybridize with two short DNA strands – FDNA and QDNA – labeled respectively with a fluorophore and matching quencher in order to function as optical structure-switching reporters[55-57] on paper.

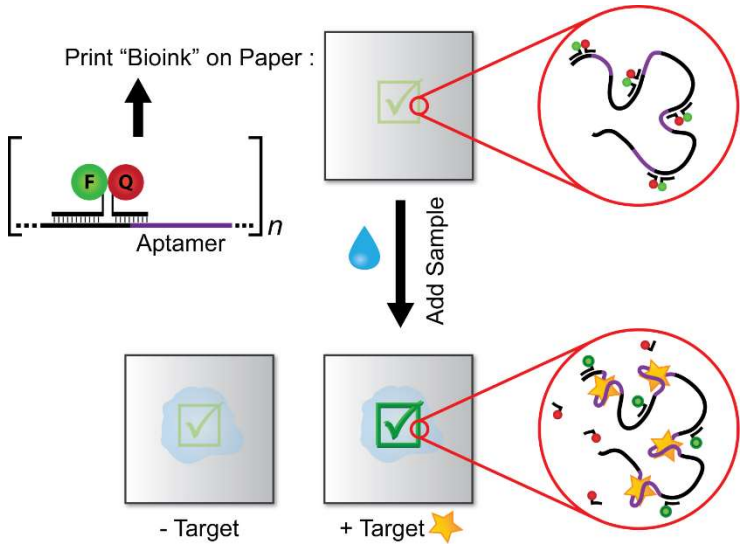

Figure 4.1. Schematic representation of paper sensors inkjet-printed with concatemeric fluorescence-signaling aptamers. A "bioink" consisting of tandem repeating units of a fluorophore-quenched structure-switching DNA aptamer reporter is inkjet-printed on paper in a desired pattern. Upon spotting or flowing a target-containing sample over the paper surface, the reporters bind the target to release the quencher and produce a fluorescence signal.

4.3 Results and Discussion

Two different concatemeric structure-switching aptamer reporters were produced, using model aptamers for adenosine triphosphate (ATP) and platelet-derived growth factor (PDGF), respectively.[58,59] These aptamers were not only chosen for the ability to bind their cognate targets at biologically relevant levels[60,61] but also as well-characterized representative aptamers for small molecule and protein detection. The complementary sequence for each aptamer is encoded into a circular template designed to generate two different sequence elements: the DNA aptamer that partially binds the QDNA, and a spacer that binds FDNA. Successful preparation of both concatemers was confirmed by agarose

gel electrophoresis (Figure S4.1), with a band for each sequence above the 20,000 base-pair marker, corresponding to several megadaltons in size or hundreds to thousands of aptamer repeats in tandem.

To create the reporter systems, the molar ratios of FDNA and QDNA to bind to the concatemers were optimized in order to construct the pre-quenched duplex. In the original tripartite monomeric reporter, a 2:1:3 ratio of aptamer/FDNA/QDNA was used to ensure that the majority of FDNA would anneal to the aptamer and also engage QDNA for proper quenching and low background signal levels prior to target binding.[11a] However, it was found that using a 1:1 aptamer/FDNA ratio with excess QDNA (6× FDNA concentration) provided the greatest amount of quenching (Figure S4.2). Constructs using QDNA and FDNA alone in solution (without the aptamer unit) or a scrambled QDNA with no complementarity to either aptamer were unable to generate any signal reduction, indicating that quenching was the result of proper hybridization to the concatemeric aptamers.

We then evaluated whether the concatemeric aptamer constructs could undergo structure switching while maintaining the sensitivity and selectivity of the original monomers. The results, shown in Figure 4.2, revealed that each concatemeric reporter provided a target concentration-dependent response similar to that of the monomeric reporter, but with a greater relative signal enhancement, particularly at higher target concentrations. Fluorescence lifetime measurements (Table S4.1) showed that the enhanced signal generation arose from dynamic quenching of FDNA in the concatemer, which would be expected from bringing quenchers non-adjacent to a given fluorophore closer in space if the concatemer folds upon itself, adding to the static quenching obtained

in both the monomeric and concatemeric constructs. Importantly, the concatemeric aptamers also retained their expected selectivity and did not produce any measurable change in signal with similar but non-intended targets (Figure S4.3).

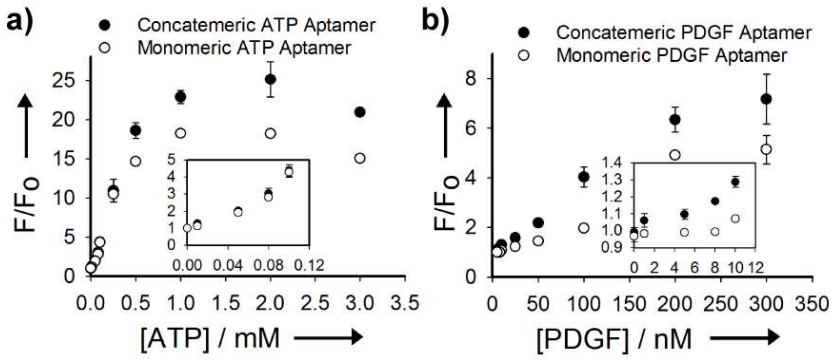

Figure 4.2. Fluorescence response of (A) ATP aptamers and (B) PDGF aptamers with cognate target added in solution.

Preliminary studies involved pipetting the concatemeric aptamers on paper by hand (Figure S4.4), but this proved to be too slow and irreproducible. To address these issues, the aptamer reporters were printed on paper using a Canon office inkjet printer (thermal printhead) by replacing the content of the black ink cartridge with the aptamer bioink. Although the printed bioinks are invisible, the color cartridge is available to print cut lines and labels for precise fabrication – examples are shown in Figure S4.5. A consumer thermal inkjet printer was chosen for this study since it is generally cheaper and more accessible than piezoelectric inkjet printers. Furthermore, piezoelectric printers require a narrow window of viscosity and surface tension (ex. 3-10 cP and 20-40 mN/m), making it necessary to optimize additives to control these factors, while thermal printers can print

aqueous inks with properties similar to water;[62-66] Table S4.2 provides the viscosity and surface tension of the aptamer bioinks.

For the paper adsorption assays, the movement of "+" shapes printed using the concatemeric ATP aptamer/FDNA reporter (denoted "RCA" in Figure 4.3) was compared to that of the monomeric aptamer/FDNA ("Tri" in Figure 4.3) following lateral flow using three assay solutions: buffer alone ("Buffer"), buffer with 0.1 % Triton-X 100 ("0.1Trix") and with 1 % BSA ("1BSA"). As seen in Figure 4.3, increasing the number of passes through the printer to make multiple layers of each bioink resulted in better signal intensity. After washing by wicking different buffer solutions, the monomeric construct was either highly smeared or completely delocalized from its initial position, whereas the concatemers remained in place. Buffer solutions containing either Triton-X 100 or BSA were chosen to demonstrate the strength of adsorption despite the use of standard washing or blocking agents. Figure S4.6 also shows that the effects of lateral flow on a bipartite version of the monomeric construct, in which the fluorophore is covalently bound (to avoid dehybridization and elution of FDNA alone), are similar to the tripartite version of the monomeric aptamer, indicating the delocalization of the entire aptamer unit on paper.

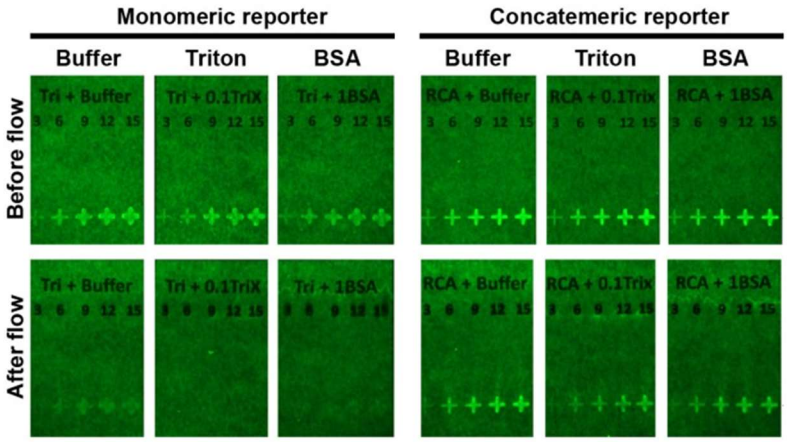

Figure 4.3. Fluorescence images of paper devices before and after lateral flow. Each paper device was printed with 3, 6, 9, 12, and 15 layers of either monomeric or concatemeric ATP aptamer reporter ("+"). Lateral flow was done in pure buffer, buffer containing 0.1% Triton-X 100, and buffer with 1% BSA. Dark letters on paper were printed with the ink-jet printer using cyan toner during sensor fabrication.

To confirm the fluorescence response of printed concatemers on paper and aid in sensor design, the full reporter system (aptamer/FDNA/QDNA) for ATP detection was printed using a boxed "✓", while the construct with the aptamer/FDNA only, acting as the positive control, was printed with a boxed "×". Since the Canon printer can only print a limited amount of ink per pass and printing 15 layers provided the highest fluorescence signal in the lateral flow tests, 15-layer printing was used for all subsequent assays allowing us to produce 160 sensors per hour per printer (32 sensors per page). Industrial inkjet printers can deposit far more material per pass, which may allow single pass printing once the method is scaled up. It can be observed in Figure 4.4 that the concatemeric aptamer reporter appears less diffuse after printing and drying when compared to the monomeric version. After spotting either the assay buffer alone or that containing 2 mM ATP onto the printed

areas, signal enhancement of the full complex was only observed in the concatemeric aptamer checkmark, whereas the monomeric aptamer checkmark became delocalized. While the signal response assay also functioned in a lateral flow format (data not shown), it was found that the method of spotting sample on the paper decreased both the assay time (flow and drying) and the sample volume required, and was thus adopted in subsequent assay designs.

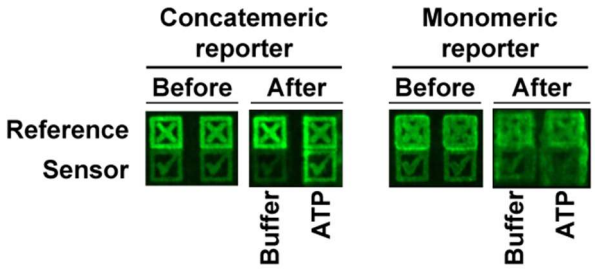

Figure 4.4. Fluorescence images of the concatemeric ATP aptamer reporter and monomeric ATP aptamer reporter before and after addition of buffer or 2 mM ATP.

Continuing with the boxed "×" and "✓" format, the response upon adding a concentration gradient of ATP to the printed concatemer reporter was assessed. Figure 4.5 demonstrates the relative emission intensity after spotting target with increasing concentrations from left to right. Visualization of the fluorescence output demonstrated increasing fluorescence intensity of the checkmarks with increasing ATP concentrations, while quantitative pixel intensity analysis revealed a detection limit and dynamic range consistent with that observed in solution. We conducted the same experiment with the PDGF aptamer reporters printed on paper, and as shown in Figure S4.7, the concatemeric

PDGF reporter system behaved very similarly to the ATP reporter. These results indicate that our approach is generally applicable to both small molecule and protein-binding DNA aptamers.

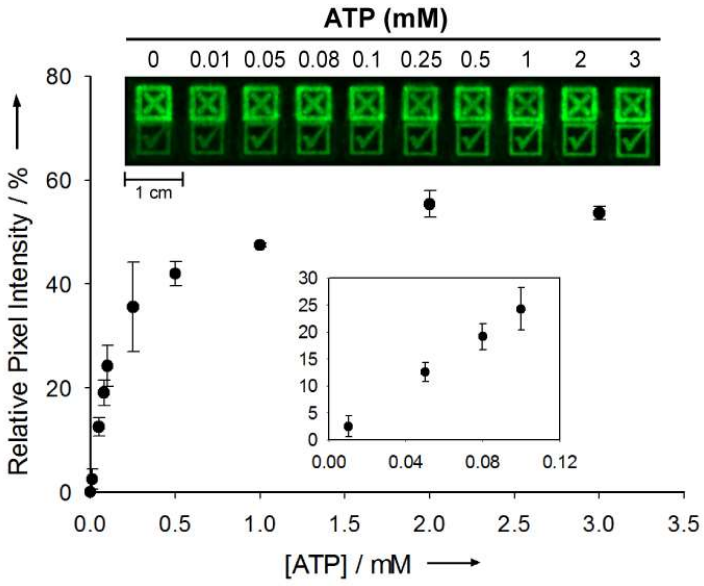

Figure 4.5. Signal response of the concatemeric reporter with increasing concentrations of ATP. ☑: aptamer/FDNA/QDNA; ☒: aptamer/FDNA.

The design versatility offered by combining the control of specific deposition from inkjet printing and the direct immobilization of our concatemeric bioinks on paper was also tested by creating a multiplexing assay with internal references for quantification. Since the patterning of letters allows for the simplest signal readout with results presented as text,[67] multiplexing was achieved by printing the letters "A" and "P" to differentially denote the ATP reporter and PDGF reporter, respectively. Reference guides, which consisted of increasing numbers of layers of the ATP concatemer/FDNA only, depicting

signal intensities expected for different levels of each target, were printed bordering the letters using "0", "Lo", 'Med" and "Hi". After spotting either 2 mM ATP or 200 nM PDGF to the printed area, only the appropriate letter displays a signal enhancement similar to the adjacent reference guide, while no signaling occurs with buffer alone (Figure 4.6).

Figure 4.6. Fluorescence response of binary letter sensors (A: ATP and P: PDGF concatemeric aptamer reporter - aptamer/FDNA/QDNA) treated with buffer, 2 mM ATP or 200 nM PDGF. Signal intensity references of "0", "Lo", "Med" and "Hi" consist of increasing print layers of the concatemeric ATP aptamer/FDNA duplex.

4.4 Conclusions

In conclusion, we have shown that concatemeric DNA aptamers, which can be easily produced by RCA, can be used as printer-friendly bioinks for the production of highly functional paper sensors using standard office inkjet printers. The large molecular size of concatemers holds the key to the effectiveness of the method as monomeric aptamers are completely nonfunctional. The described strategy is extremely easy and efficient, as it does not require complex coupling steps or hydrophobic barriers and channels in order to immobilize the biological sensing elements. We have also shown that simple inkjet printing allows for the design of patterned sensors with necessary controls to meet any customized need: multiplexing, quantitative detection, and reporting results in written text. Successful

conversion of two different DNA aptamers – one for a small molecule and one for a protein – to functional paper sensors, demonstrates the generality of the approach. Given the fact that many aptamers are available for wide-ranging targets and new aptamers can be easily developed by the SELEX technique, we believe the featured methodology opens new opportunities for developing diverse paper-based biosensing devices for field applications.

4.5 Experimental

4.5.1 Materials. Standard and functionalized DNA oligonucleotides were synthesized and purified by HPLC by Integrated DNA Technologies (Coralville, IA). Adenosine 5′-triphosphate (ATP), cytidine 5′-triphosphate (CTP), guanosine 5′-triphosphate (GTP), uridine 5′-triphosphate (UTP), T4 polynucleotide kinase (PNK; with 10× reaction buffer A: 500 mM Tris·HCl, 100 mM $MgCl_2$, 50 mM dithiothreitol (DTT), 1 mM spermidine at pH 7.6), T4 DNA ligase (with 10× T4 DNA ligase buffer: 400 mM Tris·HCl, 100 mM $MgCl_2$, 100 mM DTT, 5 mM ATP at pH 7.8), 10 mM dNTPs, ϕ29 DNA polymerase (with 10× ϕ29 DNA polymerase buffer: 330 mM Tris·acetate, 100 mM Mg·acetate, 660 mM K·acetate, 1 % (v/v) Tween 20, 10 mM DTT at pH 7.9), GeneRuler^{TM} 1 kb Plus DNA ladder and 10,000× SYBR Safe DNA gel stain were purchased from Fermentas Life Sciences (Burlington, ON). Recombinant human platelet derived growth factor-BB (PDGF), epidermal growth factor (EGF) and insulin-like growth factor I (IGF-I) were purchased from R&D Systems (Minneapolis, MN). All other analytical grade chemicals and solvents were purchased from Sigma-Aldrich (Oakville, ON). Water was purified prior to use with a Millipore Milli-Q Synthesis A10 water purification system.

4.5.2 Methods.

Preparation of Concatemeric Aptamers. Concatemers of each structure-switching aptamer were prepared using the following templates: the linear precursors of the circular templates were first ligated using the appropriate ligation template to generate the circular template, which hybridizes with the primer sequences to initiate the RCA process.

*Linear ATP Aptamer Circular Templat*e: 5′-TGTCT TCGCC TATAG TGAAC CTTCC TCCGC AATAC TCCCC CAGGT ATCTT TCGAC TAAGC ACC-3′

ATP Aptamer Ligation Template: 5′-GGCGA AGACA GGTGC TTAGT C-3′

ATP Aptamer Primer: 5′-GGGGG AGTAT TGCGG AGGAA-3′

Linear PDGF Aptamer Circular Template: 5′-TGCAG CGACT CACAG GATCA TGGTG ATGCT CTACG TGCCG TAGCC TGCCC TTTCG ACTAC C-3′

PDGF Aptamer Ligation Template: 5′-GAGTC GCTGC AGGTA GTCGA A-3′

PDGF Aptamer Primer: 5′-CGTAG AGCAT CACCA TGATC-3′

Circularization of the linear templates to form circular templates for RCA began with phosphorylating 800 pmol of the linear templates in 1× reaction buffer A using 10 U of T4 PNK with 100 nmol of ATP and incubating at 37 °C for 30 min followed by heating at 90 °C for 5 min to inactivate the enzyme and cooling to room temperature. In order to ligate the circle together, 1 nmol of the ligation template was added and then heated at 90 °C for 1 min. Once cooled to room temperature, 15 U of T4 DNA ligase was added to the mixture and incubated at room temperature for 12 h in 1× ligase buffer.

The circularized templates were precipitated with ethanol before purifying by 10% polyacrylamide denaturing (8M urea) gel electrophoresis (dPAGE), from which only the

circular sequences were isolated and eluted from the gel, precipitated with ethanol and resuspended in water for quantification using a NanoVue spectrophotometer (absorbance at 260 nm).

The RCA reaction of each of the aptamer sequences was carried out using 10 pmol of circular template with 10 pmol of primer in water (36.5 μL total volume) and heating this mixture at 90 °C for 1 min. Following cooling, 5 μL of 10× ϕ29 polymerase buffer, 2.5 μL of 10 mM (each) dNTPs and 10 U of ϕ29 polymerase were added to the reaction mixture and allowed to incubate at 30 °C for 1 h. The reaction was followed by a 5-fold dilution with water before heating at 90 °C for 5 min to deactivate the enzyme. Control experiments were also performed without circular template.

Concatemeric aptamers from the reaction mixture were purified by centrifugation using a 100 kDa Nanosep® spin column and quantified using a NanoVue spectrophotomer (absorbance at 260 nm). Visualization of the concatemeric aptamers was performed using a 0.6 % agarose gel (w/v) with a SYBR safe DNA stain. The gel was imaged using a Typhoon Trio+ Variable Mode Imager (488 nm excitation, 526 nm emission, 600 PMT, 3 mm focal plane, medium sensitivity and 200 micron resolution). As the exact size of the concatemeric aptamer is unknown, an approximate molar concentration using the absorbance at 260 nm of the concatemeric aptamer was calculated based on one repeat of the aptamer sequence. Therefore, the concentration of the aptamer sequence units in the concatemer is equivalent to that of the monomeric construct in all subsequent studies.

Preparation of DNA Aptamer Reporter Complexes. The structure-switching, fluorescence-signaling aptamer reporter complexes for ATP- and PDGF-binding were prepared as described below. Fluorophore-labeled oligonucleotides (FDNA) hybridize to the italicized nucleotides for both the monomeric and concatemeric aptamers, while quencher-labeled oligonucleotides (QDNA) hybridize to the nucleotides in bold for both the monomeric and concatemeric aptamers. The 'no hybridization' QDNA (NH-QDNA) lacks complementarity and should not hybridize to any of the aptamer constructs.

FDNA for ATP aptamer (ATP-FDNA): 5′-(fluorescein)CGACT AAGCA CCTGT C-3′

QDNA for ATP aptamer (ATP-QDNA): 5′-CCCAG GTATC TT(dabcyl)-3′

Monomeric ATP aptamer construct, tripartite version (ATP-Apt-Tri): 5′-TCACT ATAGG CGAA*G ACAGG TGCTT AGTCG* A**AAGA TACCT GGG**GG AGTAT TGCGG AGGAA GGT-3′

Monomeric ATP aptamer construct, bipartite version (ATP-Apt-Bi): 5′- TTTTT TTTTT(fluorescein) TCACT GACCT GGGGG AGTAT TGCGG AGGAA GGT-3′

FDNA for PDGF aptamer (PDGF-FDNA): 5′-(fluorescein)GACTA CCTGC AGCGA-3′

QDNA for PDGF aptamer (PDGF-QDNA): 5′-AGCCT GCCCT TT(dabcyl)-3′

Monomeric PDGF aptamer construct (PDGF-Apt): 5′-TGAG*T CGCTG CAGGT AGTC*G **AAAGG GCAGG C**TACG GCACG TAGAG CATCA CCATG ATCCT G-3′

No hybridization QDNA (NH-QDNA): 5′-GGGTC CGTAG GA(dabcyl)-3′

Optimization of Concatemer Fluorescence Signaling in Solution. To determine the optimal ratios of aptamer/FDNA/QDNA required for maximal signal generation, experiments with increasing molar equivalents of FDNA and QDNA to aptamer were performed. Prior to QDNA addition, each concatemeric aptamer and its cognate FDNA were combined in either a 1:1, 2:1 or 3:1 (aptamer:FDNA) molar ratio in the appropriate assay buffer and heated at 90 °C for 5 min, cooled to room temperature and then incubated for 1 h at 25 °C. After the 1 h incubation period, baseline fluorescence was measured for 10 min prior to the addition of the proper QDNA to achieve a final concentration of 1, 3, 6, or 9× the number of molar equivalents of FDNA (100 nM final concentration of FDNA). Identical experiments were also carried out in the varying ratios with non-hybridizing (NH)-QDNA or without aptamer addition as controls. These studies were performed in ATP assay buffer (20 mM Tris·HCl, 100 mM NaCl, 5 mM $MgCl_2$ at pH 7.8) for the ATP aptamer or PDGF assay buffer (20 mM Tris·HCl, 140 mM NaCl, 5 mM KCl, 1 mM $CaCl_2$, 1 mM $MgCl_2$ at pH 7.8) for the PDGF aptamer.

Sensitivity and Selectivity of Concatemeric Aptamers. To test the sensitivity of the concatemeric aptamers, each concatemer complex was combined in the 1:1:6 molar ratio (aptamer, FDNA and QDNA) in the appropriate buffer, heated at 90 °C for 5 min and cooled. Samples were incubated for 1 h at 25 °C. Following baseline fluorescence measurements, ATP was then added to the ATP-binding concatemer at final concentrations of 0 – 3 mM, while PDGF-BB was added to the PDGF-binding concatemer at a final concentrations of 0 – 300 nM (2 μL at the appropriate concentration). This experiment

was also repeated with the monomeric versions of each aptamer, complexed in the same 1:1:6 ratio. To test the ability of the concatemer reporters to bind their specific target over structurally-related molecules, ATP-binding concatemeric aptamers were incubated with ATP, CTP, GTP or UTP at a final concentration of 1 mM following baseline fluorescence measurements, while the concatemeric PDGF aptamer was incubated with PDGF-BB, IGF-1, EGF or BSA at a final concentration of 100 nM.

Paper-Based Assay Fabrication. In the preliminary paper-based tests using manual deposition of aptamers on paper by pipette, three layers of 0.1 μL were pipetted onto small pieces of Whatman® Grade 1 chromatography paper (7 × 10 cm) using the ATP-binding concatemeric aptamer reporter (aptamer/FDNA with or without QDNA) in a "cross" pattern consisting of 5 spots. The solutions were then dried on the paper for 30 min, followed by lateral flow of 1 mL of ATP assay buffer up to half the vertical length of paper. These pieces of paper were then allowed to dry flat for 2 h on a non-absorbent plastic surface prior to imaging. Increasing concentrations of ATP were then spotted on each "cross" region (5 μL; 0 – 3 mM) and imaged after 5 min of drying.

For the inkjet-printed assays, large sheets of Whatman® Grade 1 chromatography paper were cut to standard letter sheet size (8.5 x 11 inches) in order to be fed into a Canon Pixma MP280 inkjet printer, washed with buffer using vertical flow to decrease background fluorescence and allowed to dry. The black ink cartridge specific for the Canon printer (#210) was opened in order to remove the foam pad with liquid ink, and then the empty reservoir was extensively rinsed with water and dried. The color cartridge

(#211) was used as received to print cut lines and labels (cyan) or sensor area outlines (yellow). Patterned templates for printing of both colors and bioinks (using black) were made with Microsoft PowerPoint and were printed using "high" quality with the "color only" or "black only" ink cartridge setting when using these inks, respectively. A bioink consisted of either the ATP- or PDGF-binding concatemeric reporter complex (aptamer/FDNA with or without QDNA) or the ATP-binding monomeric aptamers (tripartite construct with FDNA and bipartite construct) – up to 600 μL can be added to the cartridge. Following the printing of each different bioink, the black cartridge was extensively rinsed with water and dried (alternatively, different cartridges can be used for the various bioinks). Completed assay pages made by feeding the paper through the printer multiple times (to create 3 – 15 layers) were allowed to dry for 5 min and cut following the printed color lines. In the multiplexing assay, increasing layers of the ATP-binding concatemeric aptamer/FDNA (no QDNA) were printed as reference guides to depict the signal intensities expected for each test reporter upon target addition. Since the PDGF-binding aptamer produces a lower signal enhancement than that of the ATP-binding aptamer (see below), fewer layers were used to produce lower intensity references. The number of print layers used for the signal reference guides are as follows: 3 layers in "0", 6 or 4 layers in "Lo", 10 or 6 layers in "Med" and 12 or 8 layers in "Hi" for indicating the ATP- or PDGF-binding aptamers, respectively.

For the ATP aptamer adsorption comparison test, printed and cut paper pieces were placed in a trough containing 1 mL of assay buffer (alone, with 0.1 % (w/v) Triton-X 100, or 1 % (w/v) BSA) and the solution was allowed to flow to up to half the vertical length of

paper. These pieces of paper were then allowed to dry flat for 2 h on a non-absorbent plastic surface prior to imaging. For signal response assays, the appropriate target or buffer only was added using 5 μL of solution deposited directly on the paper surface where the bioinks were printed and imaged after 5 min of drying. All tests were performed at room temperature (~22 °C).

Surface Tension and Viscosity Measurements. Viscosity was measured for 10 mL samples of each bioink and assay buffer using a Sine-Wave Vibro Viscometer (SV-10) at ~20 °C following calibration with Milli-Q water (viscosity ≈ 1 cP).[68] Dynamic surface tension from drop shape and contour analysis was performed using the Pendant Drop Method using an optical contact angle (OCA) 35 instrument with SCA22 software. Pendant drops were formed by a dosing needle with an outer diameter of 2.41 mm, which was connected to a 1-mL glass syringe, and measured at 22 °C. Milli-Q water with a surface tension of 72.8 – 72.0 mN/m at 20 – 25 °C[69] was used for calibration.

Fluorescence Intensity Measurements. All solution-based fluorescence intensity measurements were performed using a Tecan Infinite® M1000 platereader in fluorescence mode. Samples were excited at 490 nm (5-nm bandpass) and emission measured at 520 nm (5-nm bandpass) with a 20 μs integration time using the bottom-read setting. All measurements were acquired at 25 °C. Kinetic measurements were performed to assess FNA response to addition of a given species (i.e. QDNA, targets, etc.) using fluorescence intensity reads every minute for both baseline measurements (no QDNA/target; 10 min)

and after addition of QDNA for a total of 1 h or target for 30 min, with orbital shaking of 2.5 mm amplitude for 5 s between each measurement to ensure proper mixing. All assays were carried out in triplicate with background fluorescence subtraction. Raw fluorescence measurements were normalized to fluorescence enhancement or F/F_o where F is the endpoint fluorescence intensity and F_o is the initial fluorescence intensity prior to QDNA/target addition.

Fluorescence Lifetime Measurements. All fluorescence lifetime measurements were obtained using a Tecan Ultra Evolution platereader with an FLT attachment. Samples were excited at 440 nm with a pulsed diode laser operating at 40 MHz and emission was measured at 544 nm (25-nm bandwidth) for a 1000 ms acquisition time. Five different types of sample were prepared in triplicate for each aptamer: one sample containing FDNA only, samples with either the concatemeric or monomeric aptamer with only FDNA and those prepared with either concatemeric aptamer or monomeric aptamer combined with both FDNA and QDNA. All samples were prepared in their respective assay buffer, heated at 90 °C for 5 min, cooled to room temperature and then incubated at the appropriate assay temperature for 1 h. Fluorescence lifetime measurements were then obtained at 25 °C (no target). Target analyte for each aptamer was then added (1 mM ATP or 100 nM PDGF-BB final concentration) and the fluorescence lifetimes were measured again after 30 min. These fluorescence intensity decays were analyzed using Magellan software with fitting to a multi-exponential model:[70]

$$I\,(t) = \sum_i \alpha_i \exp(-t/\tau_i) \quad (1)$$

where τ_i are the decay times and α_i are the pre-exponential factors (amplitudes) of the individual components ($\Sigma\alpha_i = 1$). The fractional contribution of each component to the steady state intensity is given by:

$$f_i = \frac{\alpha_i \tau_i}{\sum_j \alpha_j \tau_j} \quad (2)$$

The amplitude-weighted lifetime is given by:

$$\langle \tau \rangle = \sum_i \alpha_i \tau_i \quad (3)$$

and the intensity-weighted average lifetime is given by:

$$\bar{\tau} = \sum_i f_i \tau_i \quad (4)$$

Fluorescence Imaging. All fluorescence images (for paper-based assays) were acquired using a ChemiDoc MP Imaging System with UV trans illumination, a standard filter (filter 1) and 0.1 s exposure time. Image color has been artificially set to SYBR Green. Pixel intensity analysis was performed using the volume tools of the ImageLab software to create rectangles around the printed boxed shapes. The relative pixel intensity was calculated using the average pixel intensity obtained from rectangles around the boxed "×" positive controls as the 100% value and the average pixel intensity obtained from rectangles around the boxed "✓" without target added (negative control) as 0%. It should be noted, however, that the pixel analysis provides a slight undervaluation of the "✓" intensity as it occupies ~80% of the volume of the "×".

4.6 Acknowledgements

The authors thank the Natural Sciences and Engineering Research Council of Canada and Sentinel Bioactive Paper Network for support. Y.L. holds the Canada Research Chair in Directed Evolution of Nucleic Acids. J.D.B. holds the Canada Research Chair in Bioanalytical Chemistry and Biointerfaces.

4.7 References

(1) Martinez, A. W.; Phillips, S. T.; Butte, M. J.; Whitesides, G. M. *Angew. Chem. Int. Ed.* **2007**, *46*, 1318-20.
(2) Pelton, R. *TrAC, Trends Anal. Chem.* **2009**, *28*, 925-42.
(3) Martinez, A. W.; Phillips, S. T.; Whitesides, G. M.; Carrilho, E. *Anal. Chem.* **2010**, *82*, 3-10.
(4) Liana, D. D.; Raguse, B.; Gooding, J. J.; Chow, E. *Sensors* **2012**, *12*, 11505-26.
(5) Yetisen, A. K.; Akram, M. S.; Lowe, C. R. *Lab Chip* **2013**, *13*, 2210-51.
(6) Stollner, D.; Scheller, F. W.; Warsinke, A. *Anal. Biochem.* **2002**, *304*, 157-65.
(7) Su, S.; Nutiu, R.; Filipe, C. D.; Li, Y.; Pelton, R. *Langmuir* **2007**, *23*, 1300-2.
(8) Araujo, A. C.; Song, Y.; Lundeberg, J.; Stahl, P. L.; Brumer, H., 3rd *Anal. Chem.* **2012**, *84*, 3311-7.
(9) Filpponen, I.; Kontturi, E.; Nummelin, S.; Rosilo, H.; Kolehmainen, E.; Ikkala, O.; Laine, J. *Biomacromolecules* **2012**, *13*, 736-42.
(10) Yu, A.; Shang, J.; Cheng, F.; Paik, B. A.; Kaplan, J. M.; Andrade, R. B.; Ratner, D. M. *Langmuir* **2012**, *28*, 11265-73.
(11) Noor, M. O.; Shahmuradyan, A.; Krull, U. J. *Anal. Chem.* **2013**, *85*, 1860-7.
(12) Hossain, S. M. Z.; Luckham, R. E.; Smith, A. M.; Lebert, J. M.; Davies, L. M.; Pelton, R. H.; Filipe, C. D. M.; Brennan, J. D. *Anal. Chem.* **2009**, *81*, 5474-83.
(13) Hossain, S. M. Z.; Brennan, J. D. *Anal. Chem.* **2011**, *83*, 8772-8.
(14) Hossain, S. M. Z.; Ozimok, C.; Sicard, C.; Aguirre, S.; Ali, M. M.; Li, Y.; Brennan, J. *Anal. Bioanal. Chem.* **2012**, *403*, 1567-76.
(15) Wang, J.; Bowie, D.; Zhang, X.; Filipe, C.; Pelton, R.; Brennan, J. D. *Chem. Mater.* **2014**, *26*, 1941-7.
(16) Martinez, A. W.; Phillips, S. T.; Whitesides, G. M. *Proc. Natl. Acad. Sci. U.S.A.* **2008**, *105*, 19606-11.
(17) Klasner, S. A.; Price, A. K.; Hoeman, K. W.; Wilson, R. S.; Bell, K. J.; Culbertson, C. T. *Anal. Bioanal. Chem.* **2010**, *397*, 1821-9.
(18) Abe, K.; Suzuki, K.; Citterio, D. *Anal. Chem.* **2008**, *80*, 6928-34.
(19) Li, X.; Tian, J.; Garnier, G.; Shen, W. *Colloids Surf., B* **2010**, *76*, 564-70.
(20) Li, X.; Tian, J.; Nguyen, T.; Shen, W. *Anal. Chem.* **2008**, *80*, 9131-4.

(21) Olkkonen, J.; Lehtinen, K.; Erho, T. *Anal. Chem.* **2010**, *82*, 10246-50.
(22) Maattanen, A.; Fors, D.; Wang, S.; Valtakari, D.; Ihalainen, P.; Peltonen, J. *Sens. Actuators B* **2011**, *160*, 1404-12.
(23) Dungchai, W.; Chailapakul, O.; Henry, C. S. *Analyst* **2011**, *136*, 77-82.
(24) Ellington, A. D.; Szostak, J. W. *Nature* **1990**, *346*, 818-22.
(25) Tuerk, C.; Gold, L. *Science* **1990**, *249*, 505-10.
(26) Navani, N. K.; Li, Y. F. *Curr. Opin. Chem. Biol.* **2006**, *10*, 272-81.
(27) Shangguan, D.; Li, Y.; Tang, Z.; Cao, Z. C.; Chen, H. W.; Mallikaratchy, P.; Sefah, K.; Yang, C. J.; Tan, W. *Proc. Natl. Acad. Sci. U.S.A.* **2006**, *103*, 11838-43.
(28) Liu, J.; Cao, Z.; Lu, Y. *Chem. Rev.* **2009**, *109*, 1948-98.
(29) Breaker, R. R. *Curr. Opin. Chem. Biol.* **1997**, *1*, 26-31.
(30) Wilson, D. S.; Szostak, J. W. *Annu. Rev. Biochem.* **1999**, *68*, 611-47.
(31) Famulok, M.; Mayer, G.; Blind, M. *Acc. Chem. Res.* **2000**, *33*, 591-9.
(32) Famulok, M.; Hartig, J. S.; Mayer, G. *Chem. Rev.* **2007**, *107*, 3715-43.
(33) Song, S. P.; Wang, L. H.; Li, J.; Zhao, J. L.; Fan, C. H. *Trends Anal. Chem.* **2008**, *27*, 108-17.
(34) Sefah, K.; Phillips, J. A.; Xiong, X.; Meng, L.; Van Simaeys, D.; Chen, H.; Martin, J.; Tan, W. *Analyst* **2009**, *134*, 1765-75.
(35) Su, S.; Ali, M. M.; Filipe, C. D.; Li, Y.; Pelton, R. *Biomacromolecules* **2008**, *9*, 935-41.
(36) Liu, H.; Xiang, Y.; Lu, Y.; Crooks, R. M. *Angew. Chem. Int. Ed.* **2012**, *51*, 6925-8.
(37) Ge, L.; Wang, P.; Ge, S.; Li, N.; Yu, J.; Yan, M.; Huang, J. *Anal. Chem.* **2013**, *85*, 3961-70.
(38) Yan, J.; Yan, M.; Ge, L.; Yu, J.; Ge, S.; Huang, J. *Chem. Commun.* **2013**, *49*, 1383-5.
(39) Evans, E.; Gabriel, E. F.; Benavidez, T. E.; Tomazelli Coltro, W. K.; Garcia, C. D. *Analyst* **2014**, *139*, 5560-7.
(40) Fire, A.; Xu, S. Q. *Proc. Natl. Acad. Sci. U.S.A.* **1995**, *92*, 4641-5.
(41) Liu, D. Y.; Daubendiek, S. L.; Zillman, M. A.; Ryan, K.; Kool, E. T. *J. Am. Chem. Soc.* **1996**, *118*, 1587-94.
(42) Ali, M. M.; Li, F.; Zhang, Z.; Zhang, K.; Kang, D. K.; Ankrum, J. A.; Le, X. C.; Zhao, W. *Chem. Soc. Rev.* **2014**, *43*, 3324-41.
(43) Lizardi, P. M.; Huang, X. H.; Zhu, Z. R.; Bray-Ward, P.; Thomas, D. C.; Ward, D. C. *Nat. Genet.* **1998**, *19*, 225-32.
(44) Di Giusto, D. A.; Wlassoff, W. A.; Gooding, J. J.; Messerle, B. A.; King, G. C. *Nucleic Acids Res.* **2005**, *33*, e64.
(45) Cho, E. J.; Yang, L. T.; Levy, M.; Ellington, A. D. *J. Am. Chem. Soc.* **2005**, *127*, 2022-3.
(46) Tian, Y.; He, Y.; Mao, C. D. *ChemBioChem* **2006**, *7*, 1862-4.
(47) Cheglakov, Z.; Weizmann, Y.; Basnar, B.; Willner, I. *Org. Biomol. Chem.* **2007**, *5*, 223-5.

(48) Yang, L. T.; Fung, C. W.; Cho, E. J.; Ellington, A. D. *Anal. Chem.* **2007**, *79*, 3320-9.
(49) Ali, M. M.; Li, Y. *Angew. Chem. Int. Ed.* **2009**, *48*, 3512-5.
(50) Zhao, W.; Cui, C. H.; Bose, S.; Guo, D.; Shen, C.; Wong, W. P.; Halvorsen, K.; Farokhzad, O. C.; Teo, G. S.; Phillips, J. A.; Dorfman, D. M.; Karnik, R.; Karp, J. M. *Proc. Natl. Acad. Sci. U.S.A.* **2012**, *109*, 19626-31.
(51) Zhao, W.; Gao, Y.; Kandadai, S. A.; Brook, M. A.; Li, Y. *Angew. Chem. Int. Ed.* **2006**, *45*, 2409-2413.
(52) Zhao, W.; Gao, Y.; Brook, M. A.; Li, Y. *Chem. Commun.* **2006**, 3582-4.
(53) Cheglakov, Z.; Weizmann, Y.; Braunschweig, A. B.; Wilner, O. I.; Willner, I. *Angew. Chem. Int. Ed.* **2008**, *47*, 126-30.
(54) Zhang, Z.; Eckert, M. A.; Ali, M. M.; Liu, L.; Kang, D. K.; Chang, E.; Pone, E. J.; Sender, L. S.; Fruman, D. A.; Zhao, W. *ChemBioChem* **2014**, *15*, 1268-73.
(55) Nutiu, R.; Li, Y. *J. Am. Chem. Soc.* **2003**, *125*, 4771-8.
(56) Nutiu, R.; Li, Y. *Chem. Eur. J.* **2004**, *10*, 1868-76.
(57) Nutiu, R.; Li, Y. *Methods* **2005**, *37*, 16-25.
(58) Huizenga, D. E.; Szostak, J. W. *Biochemistry* **1995**, *34*, 656-65.
(59) Green, L. S.; Jellinek, D.; Jenison, R.; Ostman, A.; Heldin, C. H.; Janjic, N. *Biochemistry* **1996**, *35*, 14413-24.
(60) Beis, I.; Newsholme, E. A. *Biochem. J.* **1975**, *152*, 23-32.
(61) Huang, J. S.; Huang, S. S.; Deuel, T. F. *J. Cell. Biol.* **1983**, *97*, 383-8.
(62) Calvert, P. *Chem. Mater.* **2001**, *13*, 3299-305.
(63) de Gans, B. J.; Duineveld, P. C.; Schubert, U. S. *Adv. Mater* **2004**, *16*, 203-13.
(64) Di Risio, S.; Yan, N. *Macromol. Rapid Commun.* **2007**, *28*, 1934-40.
(65) Gonzalez-Macia, L.; Morrin, A.; Smyth, M. R.; Killard, A. J. *Analyst* **2010**, *135*, 845-67.
(66) Komuro, N.; Takaki, S.; Suzuki, K.; Citterio, D. *Anal. Bioanal. Chem.* **2013**, *405*, 5785-805.
(67) Li, M.; Tian, J.; Al-Tamimi, M.; Shen, W. *Angew. Chem. Int. Ed.* **2012**, *51*, 5497-501.
(68) Kestin, J.; Sokolov, M.; Wakeham, W. A. *J. Phys. Chem. Ref. Data* **1978**, *7*, 941-8.
(69) Vargaftik, N. B.; Volkov, B. N.; Voljak, L. D. *J. Phys. Chem. Ref. Data* **1983**, *12*, 817-20.
(70) Lakowicz, J. *Principles of Fluorescence Spectroscopy*; Second ed.; Kluwer Academic/Plenum Publishers: New York, 1997.

4.8 Supplementary Information

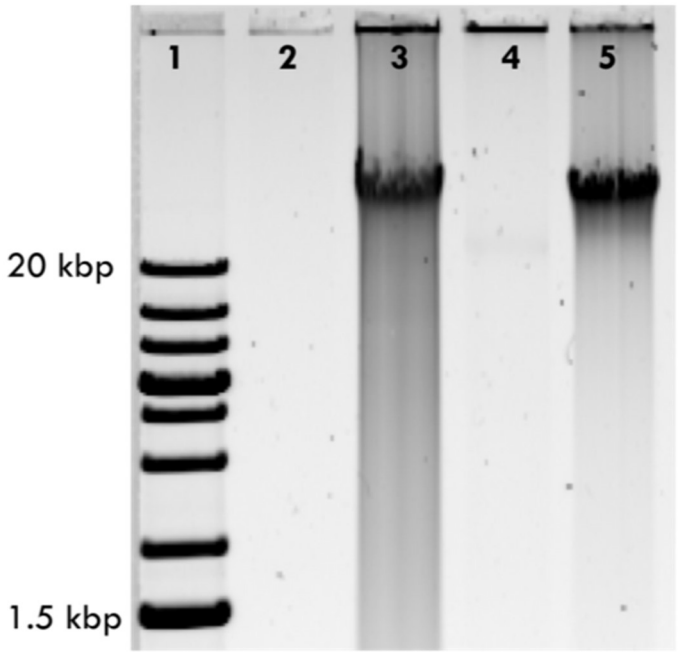

Figure S4.1. Agarose gel containing concatemeric products of RCA reaction. Lane 1, 1 kb Plus DNA ladder as size marker; lane 2, RCA reaction of ATP aptamer sequence without circular template present (control); lane 3, RCA reaction product of ATP aptamer sequence; lane 4, RCA reaction of PDGF aptamer sequence without circular template (control); lane 5, RCA reaction product of PDGF aptamer sequence.

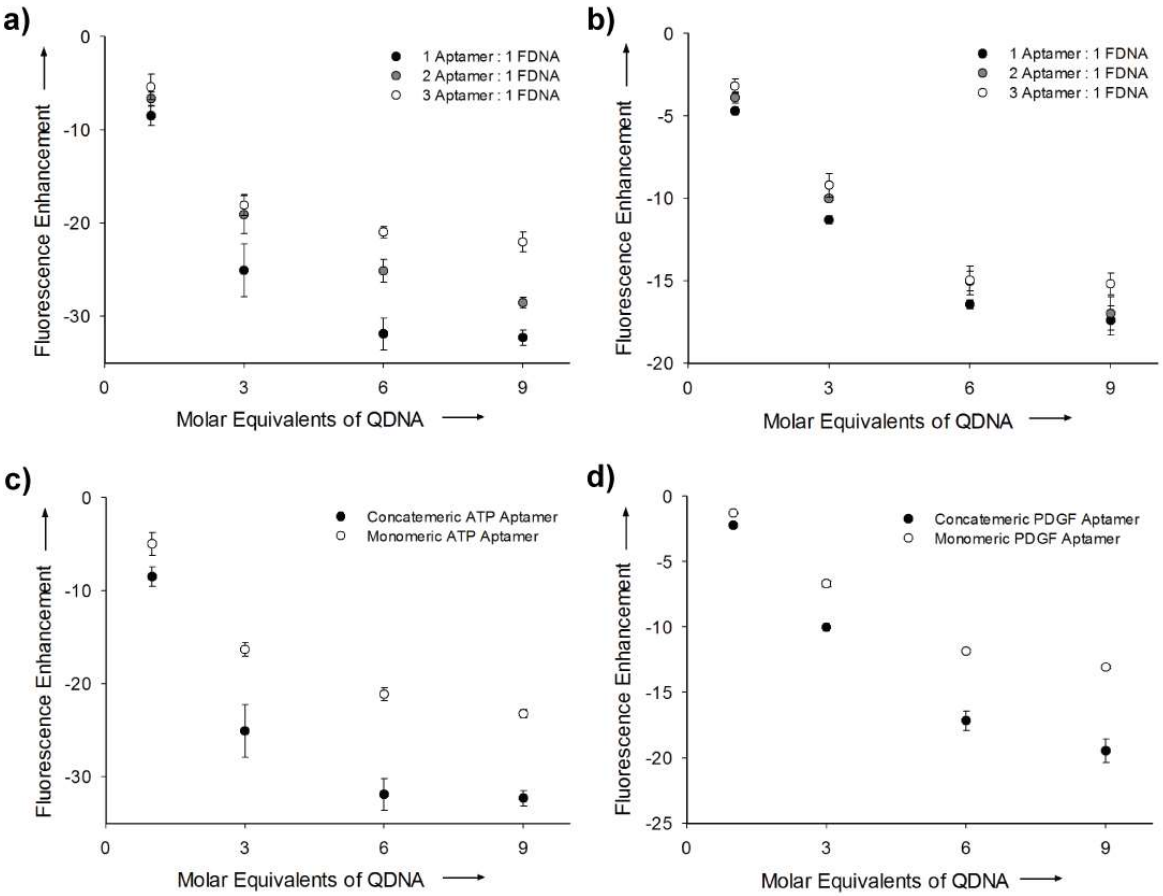

Figure S4.2. Optimization of aptamer reporter quenching using various QDNA molar equivalents. Fluorescence quenching of the concatemeric a) ATP aptamer and b) PDGF aptamer with increasing molar equivalents of both the aptamer unit and QDNA to FDNA. Fluorescence quenching of the c) ATP-binding and d) PDGF-binding concatemeric or monomeric aptamers pre-incubated with FDNA in a 1:1 ratio upon addition of increasing molar equivalents of QDNA.

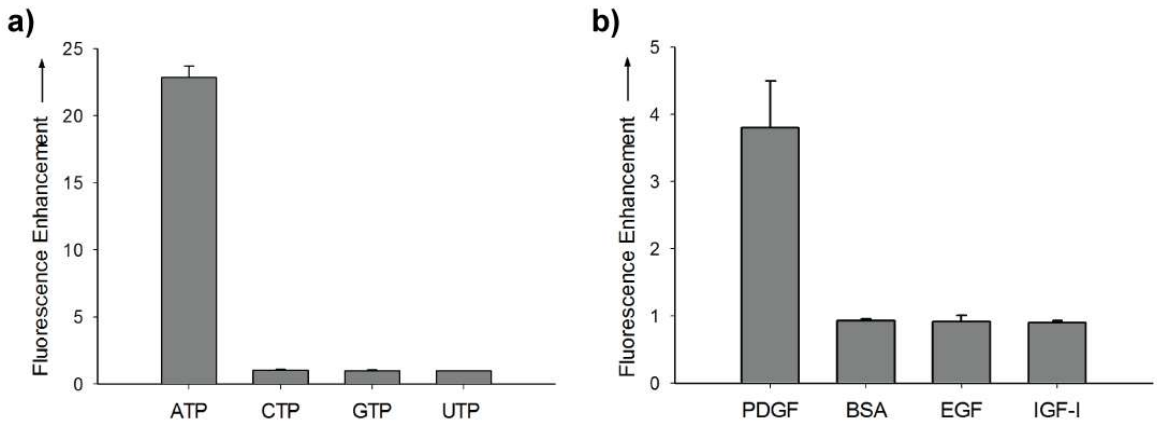

Figure S4.3. Selectivity of concatemeric DNA aptamers in solution. Selectivity of the a) concatemeric ATP aptamer to different nucleotides at 1 mM and b) concatemeric PDGF aptamer to different growth factors and proteins at 100 nM.

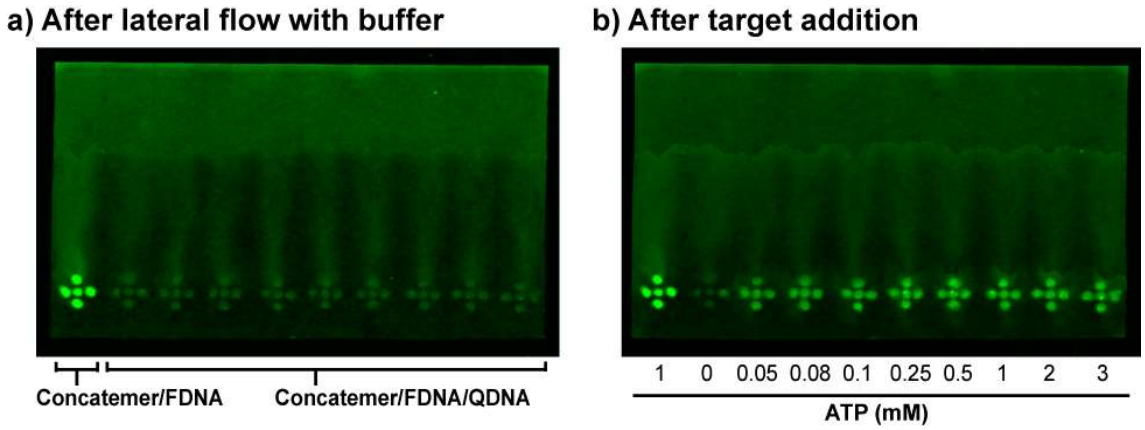

Figure S4.4. Manual deposition assay of concatemeric DNA aptamers on paper. Fluorescence image of the concatemeric ATP aptamer following manual pipette deposition and a) lateral flow with buffer, then b) addition of increasing concentrations of ATP.

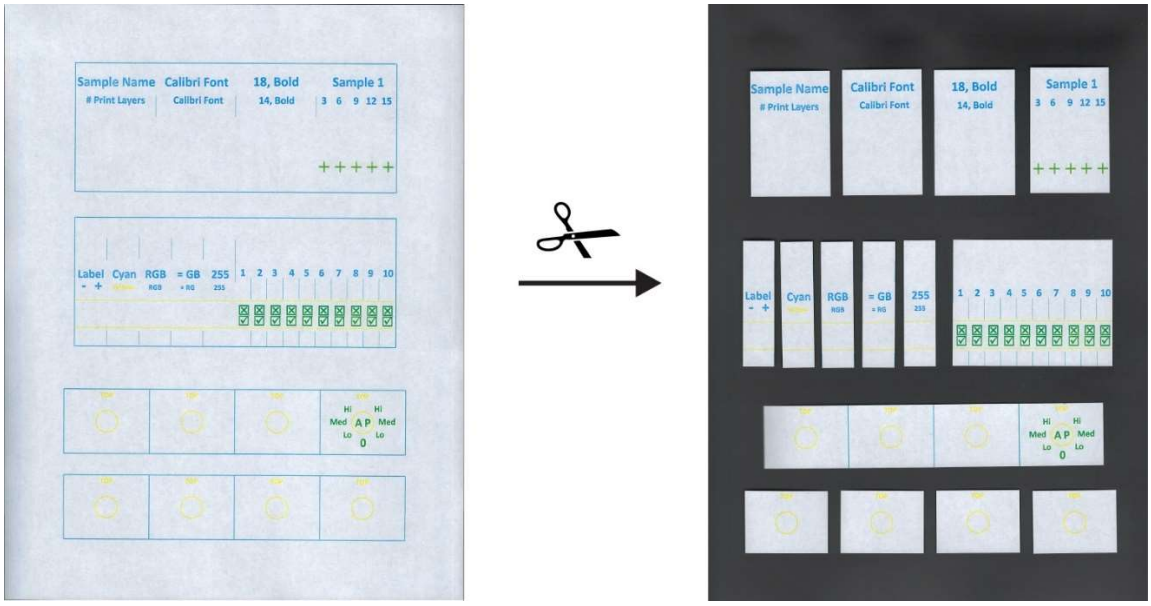

Figure S4.5. Paper printing sample. Example paper with printed color lines and labels for sensor fabrication before and after cutting to sensor size. Cyan was used for cut lines and labels and yellow was used to outline the sensing area (green shows sample "bioink" placement).

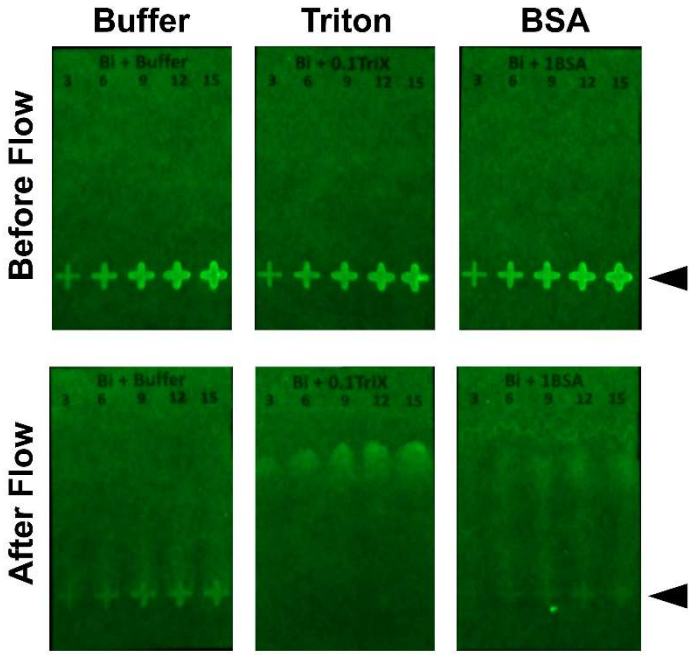

Figure S4.6. Fluorescent images of paper devices before and after lateral flow. Each paper device was printed with 3, 6, 9, 12, and 15 layers of the monomeric bipartite ATP aptamer reporter. Lateral flow was done in pure buffer, buffer containing 0.1 % Triton-X 100, and buffer with 1 % BSA. Arrows indicate where aptamers were printed.

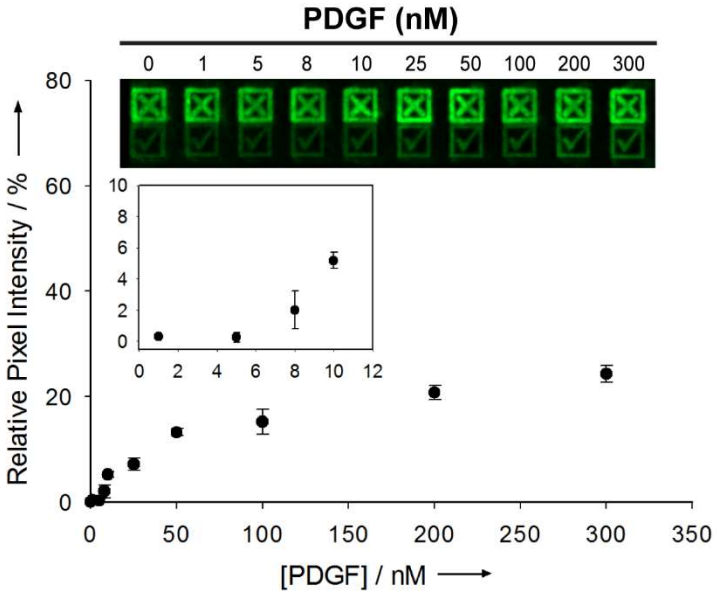

Figure S4.7. Signal response of the concatemeric PDGF aptamer reporter with increasing concentrations of PDGF-BB. Inset shows representative image of the target concentration-dependent curve, wherein ☑: aptamer/FDNA/QDNA; ☒: aptamer/FDNA.

Table S4.1. Intensity-weighted fluorescence lifetimes (ns) of concatemeric and monomeric aptamers in solution.

	ATP Aptamer		PDGF Aptamer	
Sample	- Target	+ Target	- Target	+ Target
FDNA only	4.04 ± 0.04	4.01 ± 0.04	3.78 ± 0.05	3.79 ± 0.05
Monomeric aptamer + FDNA	4.21 ± 0.07	4.19 ± 0.08	3.86 ± 0.05	4.07 ± 0.08
Monomeric aptamer + FDNA + QDNA	3.9 ± 0.1	3.97 ± 0.03	3.6 ± 0.3	3.8 ± 0.1
Concatemeric aptamer + FDNA	4.27 ± 0.06	4.16 ± 0.04	3.73 ± 0.03	3.77 ± 0.05
Concatemeric aptamer + FDNA + QDNA	3.1 ± 0.6	3.9 ± 0.2	2.9 ± 0.1	3.6 ± 0.1

Table S4.2. Viscosities and surface tensions of concatemeric and monomeric aptamers in solution.

	Viscosity (cP)	Surface Tension (mN/m)
ATP Aptamer Buffer	1.07 ± 0.01	70.1 ± 0.8
Monomeric ATP Aptamer Solution	1.07 ± 0.01	70.4 ± 0.6
Concatemeric ATP Aptamer Solution	1.06 ± 0.01	70.6 ± 0.4
PDGF Aptamer Buffer	1.04 ± 0.01	70.2 ± 0.7
Monomeric PDGF Aptamer Solution	1.05	69.9 ± 0.8
Concatemeric ATP Aptamer Solution	1.04 ± 0.01	70.5 ± 0.6
Water[a]	1.00	72.8

[a] International Association for the Properties of Steam (IAPS) values for viscosity and surface tension of water at 20 °C

CHAPTER 5.

CONCLUSIONS

5.1 Summary and Future Outlook

The ultimate goal of this thesis was to develop simple but effective strategies to exploit the advantages of nucleic acid aptamers in solid-phase assay formats, overcome some of their weaknesses when used in such assays and employ these molecules for next-generation solid-phase assay applications. Initial studies focused on entrapment of nucleic acid aptamers in sol-gel derived materials. This method proved particularly useful in stabilizing labile RNA-based aptamers from degradation such that solid-phase assays for small molecule sensing could be developed. The ability to generate very large DNA aptamer amplicons allowed their entrapment into macroporous sol-gel derived materials, which prevented these biorecognition molecules from leaching out of the porous material and allowed detection of protein-sized targets. Finally, these concatemeric DNA aptamers were used as bioinks to print paper-based sensors. The large structure of the long concatemeric aptamer molecules allowed for direct bio-immobilization through adsorption without the need for surface conjugation or entrapment while the simple inkjet printing method facilitated patterning of letters and symbols to create internally-referenced and multiplexed assay designs.

While this work illustrates the potential of nucleic acid aptamers in solid-phase assays, this is only a starting point for exciting future endeavors using these platforms. For example, RCA can be used to synthesize DNA amplicons containing different

functionalities such as catalytically-active DNAzymes. Applying concatemeric DNAzymes to both paper and sol-gel based sensor formats will not only extend the utility of functional nucleic acids but could, for example, be used to generate a colorimetric signal that would significantly enhance the practicality of paper-based assays by allowing signal detection and interpretation using the naked eye. A few strategies used to produce a colorimetric signal with DNAzymes include color production by a horseradish peroxidase-mimicking DNAzyme,[1] dispersion of AuNPs using a DNAzyme-driven cleavage reaction[2] or coupling DNAzyme reactions with urea hydrolysis and litmus test dyes.[3] Alternatively, sol-gel entrapment of concatemeric aptamers could be extended to produce sol-gel derived aptamer microarrays[4-6] for multi-analyte sensing, enhancing the potential of such DNA amplicons for new applications. In addition, monolithic columns containing concatemeric DNA (either aptamers or DNAzymes) could be utilized in other applications, such as solid-phase extraction of analytes from complex mixtures or assessing aptamer-target affinity constants using common chromatographic detection methods. Finally, the potential exists to develop large RNA amplicons, either by rolling circle transcription (RCT)[7] using T7 RNA polymerase or by reverse transcription of DNA amplicons. This could allow the benefits of RNA aptamer entrapment within sol-gel derived materials, as demonstrated in Chapter 2, to be extended to the various assay formats that were demonstrated for concatemeric DNA aptamers in Chapters 3 and 4.

5.2 References

(1) Cheglakov, Z.; Weizmann, Y.; Basnar, B.; Willner, I. *Org. Biomol. Chem.* **2007**, *5*, 223-5.
(2) Zagorovsky, K.; Chan, W. C. W. *Angew. Chem. Int. Ed.* **2013**, *52*, 3168-71.
(3) Tram, K.; Kanda, P.; Salena, B. J.; Huan, S.; Li, Y. *Angew. Chem. Int. Ed.* **2014**, *53*, 12799-802.
(4) Rupcich, N.; Green, J. R. A.; Brennan, J. D. *Analytical Chemistry* **2005**, *77*, 8013-9.
(5) Monton, M. R. N.; Lebert, J. M.; Little, J. R. L.; Nair, J. J.; McNulty, J.; Brennan, J. D. *Anal. Chem.* **2010**, *82*, 9365-73.
(6) Ge, X.; Lebert, J. M.; Monton, M. R. N.; Lautens, L. L.; Brennan, J. D. *Chem. Mater.* **2011**, *23*, 3685-91.
(7) Lee, J. B.; Hong, J.; Bonner, D. K.; Poon, Z.; Hammond, P. T. *Nat. Mater.* **2012**, *11*, 316-22.